UNIVERSIDADE FEDERAL DO RIO GRANDE DO SUL

Escola de Engenharia

Programa de Pós-Graduação em Engenharia de Minas, Metalúrgica e de Materiais - PPGE3M

DESENVOLVIMENTO DE UM EQUIPAMENTO PARA REALIZAR MEDIDAS DE PERMEABILIDADE GASOSA EM POLÍMEROS E NANOCOMPÓSITOS POLIMÉRICOS

Tese para obtenção do título de Doutor em Engenharia

Gilberto João Pavani

Porto Alegre

2023

UNIVERSIDADE FEDERAL DO RIO GRANDE DO SUL
Escola de Engenharia
Programa de Pós-Graduação em Engenharia de Minas, Metalúrgica e de Materiais - PPGE3M

DESENVOLVIMENTO DE UM EQUIPAMENTO PARA REALIZAR MEDIDAS DE PERMEABILIDADE GASOSA EM POLÍMEROS E NANOCOMPÓSITOS POLIMÉRICOS

Gilberto João Pavani
Engenheiro Mecânico

Trabalho realizado no Departamento de Materiais da Universidade Federal do Rio Grande do Sul, no Programa de Pós-Graduação em Engenharia de Minas, Metalúrgica e de Materiais (PPGE3M) como requisito parcial à obtenção do título de Doutor em Engenharia.

Área de concentração: Ciência e Tecnologia dos Materiais

Orientador: Prof. Dr. Carlos Arthur Ferreira

Porto Alegre

2023

A presente tese foi julgada adequada para a obtenção do título de Doutor em Engenharia na área de concentração de Ciência e Tecnologia dos Materiais e aprovada em sua forma final pelo Orientador e pela Banca Examinadora designada pelo Programa de Pós-Graduação em Engenharia de Minas, Metalúrgica e de Materiais da Universidade Federal do Rio Grande do Sul.

Coordenador: Prof. Dr. Rodrigo de Lemos Peroni

Orientador: Prof. Dr. Carlos Arthur Ferreira

Banca Examinadora:

_____

Drª. Paula Cristina Dartora

_____

Drª. Thais Machado Farias

_____

Prof. Dr. Edson Luis Francisquetti

Pavani, Gilberto Pavani. DESENVOLVIMENTO DE UM EQUIPAMENTO PARA REALIZAR MEDIDAS DE PERMEABILIDADE GASOSA EM POLÍMEROS E NANOCOMPÓSITOS POLIMÉRICOS. Orientador Prof. Dr. Carlos Arthur Ferreira — Tese (Doutorado) — Universidade Federal do Rio Grande do Sul, Escola de Engenharia, Programa de Pós-Graduação em Engenharia de Minas, Metalúrgica e de Materiais, Porto Alegre – RS, 2023, 100 p.

1. Permeabilidade gasosa, 2. Polietileno, 3. Nanocompósito, 4. Permeâmetro.

AGRADECIMENTOS

- Ao Prof. Dr. Carlos Arthur Ferreira pela orientação ao longo do desenvolvimento deste trabalho de pesquisa;
- Aos colegas do Laboratório de Materiais Poliméricos (LAPOL) pelo auxílio na realização dos experimentos deste trabalho de pesquisa;
- À Universidade Federal do Rio Grande do Sul (UFRGS) e aos seus professores pelos ensinamentos ao longo de minha trajetória acadêmica;
- Ao Instituto Federal do Rio Grande do Sul (IFRS) pelo suporte técnico.

DEDICATÓRIA

Dedico o presente trabalho ao meu filho.

TRABALHOS PUBLICADOS

- PAVANI GJ, PAVANI SA, FERREIRA CA (2022) Gas permeameter for polymers and nanocomposites: a new equipment. SN Applied Sciences. https://doi.org/10.1007/s42452-022-05190-x

- PAVANI GJ, PAVANI SA, FERREIRA CA (2021) Gas permeameter in polymer nanocomposite plates: construction and validation. Iran Polym J. https://doi.org/10.1007/s13726-021-00915-y

- PAVANI GJ, PAVANI SA, FERREIRA CA (2015) Application of Polymeric Nanocomposites and Carbon Fiber Composites in the Production of Natural Gas Reservoirs. J Nanomaterials. http://dx.doi.org/10.1155/2015/658727

- PAVANI GJ, PAVANI SA, FERREIRA CA (2020) Recycling of Polymer Nanocomposites of Carbon Fiber Reinforced Compressed Natural Gas Reservoirs In: Keka Talukdar (ed.) Nanomaterials-Based Composites for Energy Applications: Emerging Technology and Trends, 1 ed, Apple Academic Press, ISBN 978- 1771888066

- PAVANI GJ, PAVANI SA, FERREIRA CA. Carbon Fiber Recycling of Carbon Fiber Reinforced Polymeric Reservoirs for Compressed Natural Gas. In: International Conference Sustainable Materials Science and Technology, 2015, Paris, France. International Conference Sustainable Materials Science and Technology - Abstracts Book. Badajoz, Spain: ScienceKNOW Conferences C.B., 2015. v. 1. p. 1-238

- PAVANI GJ, AMICO SC, FERREIRA CA. Ampliação do mercado de biocombustíveis: eficiência energética no armazenamento de gás natural veicular. In: 1st International Congress on Bioenergy, 2013, Portalegre - Portugal. Complete Communications - 1st International Congress on Bioenergy, 2013

- PAVANI GJ, FERREIRA CA, AMICO SC. Application of Polymeric Nanocomposites for the Production of Natural Gas Reservoirs for Carbon Fiber Reinforced. In: Asia, 2013, Taipei. Asia-Pacific International Congress on Engineering & Natural Sciences, 2013

RESUMO

A permeabilidade gasosa em materiais semipermeáveis é uma propriedade inerente a sua estrutura e resulta na absorção de fluidos por difusão nos espaços intermoleculares existentes na matriz do material. A capacidade de um gás atravessar uma membrana semipermeável é objeto de pesquisa em várias áreas a indústria de embalagens de alimentos e medicamentos, a indústria química e de prospecção de petróleo e gás natural. Na extração de petróleo bruto, por exemplo, os polímeros minimizam a permeação gasosa, reduzindo o vazamento de gás natural e óleo cru em *risers*, prevenindo acidentes que podem causar graves impactos ambientais. O objetivo deste trabalho de pesquisa foi testar e validar o permeâmetro para gases construído e aprimorado pelo autor, visando verificar a influência da adição de nanoargila ao polietileno de alta densidade (HDPE) na permeabilidade gasosa em relação ao HDPE puro, pois não havia equipamentos disponíveis para sua aferição. O referido equipamento possibilita verificar a permeabilidade de diferentes gases em placas poliméricas e de nanocompósitos poliméricos, sendo testado com nitrogênio a 1 MPa e 69°C (342,15 K) em amostras de HDPE puro e com adição de nanoargila, formando um nanocompósito polimérico. Os resultados foram comparados com dados experimentais obtidos anteriormente e informações contidas na literatura, validando o permeâmetro apresentado, que é capaz de aferir a permeabilidade gasosa nas condições descritas com maior precisão e facilidade de operação do que a versão anterior do equipamento, demonstrando que as melhorias e avanços realizados foram adequados, possibilitando a medição das propriedades de transporte de gases em diferentes materiais.

Palavras-chave: permeabilidade gasosa, permeâmetro, polietileno, nanocompósitos poliméricos, nitrogênio

ABSTRACT

The gas permeability in semipermeable materials is a property inherent to the structure of the material that results in the absorption of fluids by diffusion in the intermolecular spaces existing in its matrix. The ability of a gas to cross a semipermeable membrane is the subject of research in several fields, such as the food and drug packaging industry, the chemical industry and oil and natural gas prospecting. In crude oil extraction, for example, polymers minimize gas permeation, reducing the leakage of natural gas and crude oil in risers, preventing accidents that can cause serious environmental impacts. The objective of this work was to test and validate the gas permeameter built and improved by the authors, aiming to verify the influence of the addition of nanoclay to the high density polyethylene (HDPE) in the reduction of gas permeability in relation to pure HDPE, as there was no equipment available for its measurement. This equipment allows to measure the permeability of different gases in polymeric plates and polymeric nanocomposites, being tested with nitrogen at 1 MPa and 69°C (342.15 K) in samples of pure HDPE and with addition of nanoclay, forming a polymeric nanocomposite. The results were compared with experimental data and information present in the literature, validating the presented permeameter, which is capable of measuring the gas permeability under the described conditions with greater precision and ease of operation than the previous model featured in previous article, demonstrating that the improvements and advances made were suitable, enabling the measurement of gas transport properties in different semi-permeable materials.

Keywords: gas permeability, permeameter, polyethylene, polymeric nanocomposites, nitrogen

SUMÁRIO

LISTA DE FIGURAS

LISTA DE TABELAS

LISTA DE ABREVIATURAS E SÍMBOLOS

ABNT - Associação Brasileira de Normas Técnicas

AISI - *American Iron and Steel Institute*

ASTM - *American Society for Testing and Materials*

CAS - *Chemical Abstracts Service*

CETEA - Centro de Tecnologia de Embalagem

EDS - *Energy-Dispersive X-ray Spectroscopy*

GNV - Gás Natural Veicular

HDPE - *High-Density Polyethylene*

ITAL - Instituto de Tecnologia de Alimentos

PALS - *Positron Annihilation Spectroscopy*

ISO - *International Organization for Standardization*

RTJ - *Ring Type Joint*

Xc: grau de cristalinidade (fração em peso) (%)

ΔHf: entalpia de fusão (J/g)

ΔHfo: calor de fusão do polímero hipoteticamente 100% cristalino (J/g)

ρ: densidade do polímero (g/cm^3)

Tf: temperatura do ponto de fusão (°C)

ΔHf: entalpia de fusão (J/g)

Xc: grau de cristalinidade (fração em peso) (%)

Φa: fração volumétrica da fase amorfa

T: temperatura (°C)

P: coeficiente de permeabilidade (cm^3(STP)/cm·s·MPa)

1. INTRODUÇÃO

O transporte de gases industriais sob pressão, geralmente, ocorre em cilindros e botijões metálicos que são pesados e de difícil manuseio, contribuindo para a ocorrência de acidentes e doenças relacionadas ao trabalho, que podem ser substituídos por contendores poliméricos como os reservatórios recarregáveis para gás natural veicular GNV-4 definidos pela ISO 11439:2013 que apresentam como características leveza, barreira a gases e resistência à pressão de trabalho.

Os polímeros apresentam vantagens sobre outros materiais como baixa densidade, flexibilidade e boa resistência química [1, 2], o que justifica sua crescente utilização nas indústrias automotiva, de embalagens e de óleo e gás. No caso de *risers* flexíveis para transporte de óleo bruto, por exemplo, o polímero entra em contato com diferentes gases a altas pressões e temperaturas que podem formar bolhas nas bainhas internas da tubulação devido à permeação de gases como o dióxido de carbono (CO_2) que devido à mudança de fase do estado supercrítico para o gasoso pode causar descompressão explosiva, bem como, corrosão das armaduras metálicas, requerendo para sua prevenção o conhecimento dos fenômenos de transporte de gases em altas pressões e temperaturas em camadas poliméricas espessas [3], o que é escasso na literatura [4, 5].

A permeação de um gás através de um material polimérico pode ser dividida em três etapas: absorção das moléculas do gás no lado de maior pressão; difusão gasosa dentro de sua matriz; dessorção do gás no lado de menor pressão. Assim, a permeabilidade corresponde ao fluxo de gás através do material, necessitando de técnicas experimentais para determinar com precisão o coeficiente de permeabilidade de determinado gás em cada polímero para diferentes pressões e temperaturas [6].

Para determinar a permeabilidade gasosa de materiais poliméricos sob pressão e temperatura definidas foi necessário construir o permeâmetro em apresentação, a partir da experiência adquirida em protótipos anteriores, de acordo com as práticas para a formulação de um projeto sistemático [7, 8], conforme a metodologia de ensaio definida pela norma ASTM D1434-82 (2015) e1, para obter estimativas quantitativas confiáveis para a permeação de gases puros através de membranas de espessuras variadas.

Como os permeâmetros disponíveis comercialmente [9 - 11] apresentam custo elevado, este trabalho de pesquisa resultou em um permeâmetro de baixo custo para gases, permitindo seu uso em materiais semipermeáveis como polímeros e nanocompósitos poliméricos, apresentando avanços em precisão e operabilidade em relação ao equipamento apresentado anteriormente que foi validado pela literatura.

A precisão do equipamento é aceitável em termos qualitativos, pois indica a permeabilidade gasosa de materiais semipermeáveis e revela a diferença considerável dos coeficientes de permeabilidade entre amostras de polímero puro e de nanocompósito polimérico pesquisados, bem como em termos quantitativos indicados em tabela.

O permeâmetro em apresentação permite a determinação dos coeficientes de transporte de gases a baixas, médias e altas pressões em diversos materiais semipermeáveis, utilizando o procedimento volumétrico conforme a norma ASTM D1434-82 (2015) e1, apresentando vantagens sobre os permeâmetros comerciais como baixo custo de aquisição e flexibilidade devido ao uso de diferentes combinações de gases e materiais poliméricos.

2. OBJETIVOS

2.1 Objetivo geral

Desenvolvimento de um permeâmetro de baixo custo para a determinação da permeabilidade de gases em materiais semipermeáveis como polímeros e nanocompósitos poliméricos.

2.2 Objetivos específicos

- Preparar amostras de nanocompósitos poliméricos de polietileno de alta densidade (PEAD) com diferentes nanoargilas em diferentes teores.
- Realizar medições de permeabilidade ao oxigênio para selecionar a amostra de menor permeabilidade ao oxigênio.
- Preparar amostras de PEAD / montmorilonita para testar sua permeabilidade ao nitrogênio.
- Realizar medições de permeabilidade ao nitrogênio em amostras de PEAD visando validar o permeâmetro junto à literatura.
- Aprimorar o permeâmetro comparando os resultados com os valores obtidos anteriormente e a literatura para verificar se as melhorias e avanços implementados foram adequados.

3. REVISÃO BIBLIOGRÁFICA

O presente capítulo apresenta uma revisão sucinta sobre a análise experimental da permeabilidade gasosa em polímeros e nanocompósitos poliméricos, destacando suas principais características e aplicações, bem como, uma revisão sobre os mecanismos e a cinética de cristalização de polímeros semicristalinos e sua degradação.

3.1 Polietileno de alta densidade

O polietileno é um polímero semicristalino, flexível, cujas propriedades são influenciadas pela quantidade relativa das fases amorfa e cristalina, sendo inerte à maioria dos produtos químicos devido a sua natureza parafínica, massa molecular e estrutura parcialmente cristalina.

Apesar dos polietilenos serem, geralmente, descritos como ramificados ou lineares [12, 13], dependendo das condições reacionais e do sistema catalítico empregado na polimerização, podem ser classificados conforme segue:

- Polietileno de baixa densidade (PEBD ou LDPE);
- Polietileno de alta densidade (PEAD ou HDPE);
- Polietileno linear de baixa densidade (PELBD ou LLDPE);
- Polietileno de ultra alto peso molecular (PEUAPM ou UHMWPE);
- Polietileno de ultrabaixa densidade (PEUBD ou ULDPE).

3.1.1 Propriedades

O polietileno de alta densidade (HDPE) apresenta cadeias lineares e maior densidade do que o LDPE, fazendo com que a orientação, o alinhamento e o empacotamento das cadeias sejam mais eficientes e que as forças intermoleculares (Van der Waals) sejam mais intensas, tornando a cristalinidade maior do que no LDPE e aumentando sua temperatura de fusão [14, 15].

A massa molecular exerce influência devido ao efeito na cinética de cristalização, cristalinidade final e caráter morfológico, bem como, aumenta a resistência ao impacto [16] enquanto o aumento no teor de ramificações reduz a cristalinidade e impacta suas características mecânicas, pois aumenta o alongamento na ruptura e reduz a resistência à tração [17]. A orientação das cadeias poliméricas influencia as propriedades mecânicas do polímero por que aumenta o empacotamento das cadeias e, por consequência, aumenta a rigidez do polímero [18].

O HDPE apresenta baixa reatividade química [19, 20], pois as regiões mais reativas de suas moléculas são as ligações duplas finais e as ligações carbono-carbono (C-C) terciárias em ramificações.

O HDPE à temperatura ambiente não é solúvel em solventes comerciais, apesar de muitos solventes causarem inchamento [21, 22]. Em altas temperaturas, ele se dissolve em alguns hidrocarbonetos alifáticos e aromáticos além de reagir lentamente com soluções concentradas de ácido sulfúrico (H_2SO_4).

Como a maioria dos polímeros sintéticos, o HDPE é sujeito a reações de degradação induzida por calor, radiação ultravioleta e oxigênio. O polímero degradado apresenta alterações no aspecto visual, aumento de densidade e redução da resistência à abrasão, ao impacto e das propriedades de tração [23].

A permeabilidade à água e gases inorgânicos é baixa, sendo menos permeável a gases (CO_2, O_2, N_2) do que o LDPE.

3.1.2 Aplicações

O HDPE é usado em diferentes segmentos da indústria de transformação de polímeros, abrangendo os processos de moldagem por sopro, extrusão e injeção.

No processo de injeção, o HDPE é utilizado para a confecção de baldes, bacias, bandejas, banheiras infantis, brinquedos, potes para alimentos, assentos sanitários, tampas para garrafas e potes, engradados, boias de piscina e caixas d'água, entre outros.

No processo de sopro destaca-se a confecção de bombonas, tanques e tambores ~~tensão~~, bem como, a confecção de frascos que requeiram resistência ao fendilhamento por tensão ambiental como embalagens para detergentes, cosméticos e defensivos agrícolas.

No processo de extrusão, é aplicado em isolamento de fios telefônicos, sacos para congelados, revestimento de tubulações metálicas, tubos para redes de saneamento e de distribuição de gás, emissários de efluentes sanitários e químicos, dutos para mineração e dragagem, embalagens para frutas, sacos para lixo e sacolas de supermercados [24].

Apesar do HDPE e do LDPE terem muitas aplicações em comum, geralmente, o HDPE apresenta maior dureza e resistência enquanto o LDPE é mais flexível e transparente devido à reação de polimerização que os originou. O HDPE é o principal elemento na substituição de materiais industriais devido a sua disponibilidade e propriedades de barreira que podem ser melhoradas com o uso de nanoargilas.

3.2 Nanoargilas

A nanorgila mais empregada em nanocompósitos poliméricos é a argila montmorilonita devido a sua relação de aspecto elevada e suas características de intercalação/esfoliação [25]. A relação de aspecto das camadas (relação entre comprimento e espessura) pode atingir valores superiores a 1000 [26, 27].

A argila montmorilonita é um silicato que possui a estrutura cristalina em camadas. Cada camada consiste em dois tipos de folhas unidas, formando uma lamela. As folhas se mantêm unidas por átomos de oxigênio comuns a ambas. A espessura de uma lamela é de aproximadamente 1nm e suas dimensões laterais variam de 30nm até mícrons, conforme ilustrado na Figura 1. As lamelas são empilhadas devido a forças iônicas e de Van der Waals, possuindo um espaçamento uniforme entre as camadas chamado de espaçamento basal (*d-spacing*) [28].

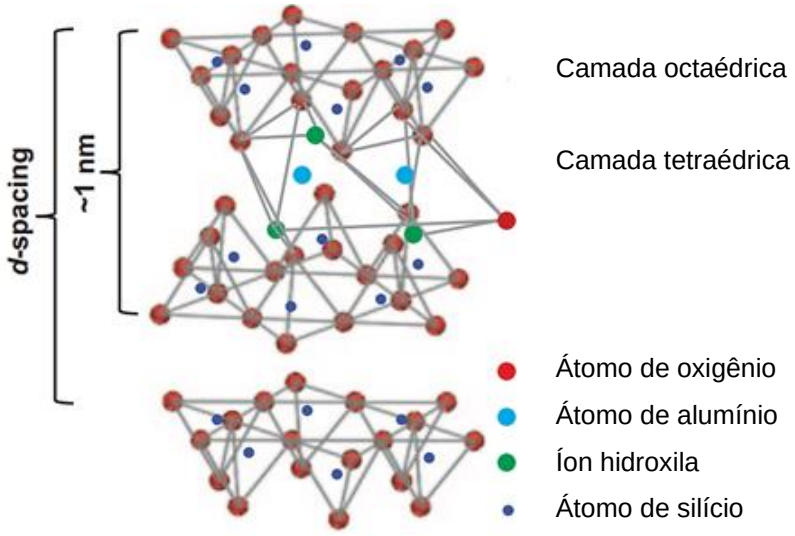

Figura 1 - Estrutura da nanoargila montmorilonita - Shunmugasamy (2015) [29]

A princípio, quanto menor a dimensão da carga, maior o ganho de propriedades no nanocompósito, mas quanto menor a partícula, maior é a tendência de se aglomerar em vez de se dispersar de forma homogênea em uma matriz polimérica [30]. Assim, as camadas de silicato tendem a se organizar para formar pilhas com uma lacuna regular entre elas, chamada de galeria.

A argila montmorilonita possui grande superfície específica e elevada razão de aspecto, apresentando caráter hidrofílico, ou seja, para haver dispersão em matrizes poliméricas é necessário torná-la organofílica através da modificação de sua superfície, trocando os cátions sódio, presentes nas galerias existentes entre as camadas, por cátions de sais quaternários de amônio de cadeias longas, por exemplo, que aumentam o espaço entre as galerias, facilitando a incorporação das cadeias poliméricas [31].

Quando a argila é dispersa no polímero, dependendo da adesão interfacial entre a matriz polimérica e o silicato, pode ocorrer o que segue:

- **Fases separadas**: as cadeias do polímero não intercalam as camadas da argila e o silicato fica disperso na matriz polimérica, levando à formação de uma estrutura com propriedades similares a um compósito convencional;

- **Compósito intercalado**: ocorre quando as cadeias poliméricas intercalam as cadeias do silicato, formando uma estrutura ordenada multicamada que apresenta propriedades superiores ao compósito convencional;
- **Compósito esfoliado**: a argila é completamente dispersa na matriz polimérica, produzindo uma larga interação interfacial, facilitando o reforço pela grande área de contato entre argila e polímero, conferindo significativa melhora nas propriedades barreira [32], por exemplo.

Para a nanoargila tornar-se compatível com polímeros semicristalinos é necessário modificá-la através de reações de troca de íons para a nanoargila tornar-se organofílica [33 - 35]. Os cátions orgânicos reduzem a energia de superfície do silicato e melhoram a molhabilidade com a matriz polimérica.

Além disso, as longas cadeias orgânicas dos agentes surfactantes de carga positiva ligam-se à superfície das camadas de silicato de carga negativa, resultando em um aumento da altura da galeria [36], permitindo que os polímeros se difundam entre as camadas da nanoargila [37].

Algumas vezes, os cátions alquilamônio proporcionam grupos funcionais que podem reagir com o polímero ou iniciar a polimerização de monômeros [38]. Assim, o ambiente nas galerias torna-se apropriado para a intercalação das moléculas poliméricas [39], pois a modificação da superfície aumenta o espaçamento basal das argilas e atua de agente de compatibilização entre a argila hidrofílica e o polímero hidrofóbico.

O excesso de cargas negativas dos silicatos em camadas e sua capacidade de troca de íons podem ser quantificados pela capacidade de permuta catiônica que depende da natureza das substituições isomórficas nas camadas tetraédricas e octaédricas da argila, podendo ser medida pela determinação da quantidade de sal de alquilamônio residual ou por análise química. A distância intralamelar depende do comprimento da cadeia do surfactante e da densidade de carga da argila [40].

A mistura física de um polímero com um silicato não forma, necessariamente, um nanocompósito, pois a pequena atração entre componentes orgânico e inorgânico não resulta em melhora de propriedades, ou seja, quando as cadeias poliméricas não intercalam com as folhas de silicato é obtida uma composição de fases com propriedades similares aos compósitos convencionais [41].

Dependendo do método de preparação e da natureza dos componentes do nanocompósito, incluindo a matriz polimérica e o silicato em camadas, podem ser obtidas estruturas intercaladas e delaminadas ou esfoliadas.

As estruturas intercaladas são formadas quando a cadeia polimérica é alternada com as camadas de silicato da argila, resultando em uma estrutura ordenada de camadas poliméricas e inorgânicas alternadas com uma distância de repetição entre elas [42].

As estruturas delaminadas ou esfoliadas são obtidas quando as camadas de nanoargila são separadas umas das outras e dispersas na matriz polimérica. A delaminação ou esfoliação maximiza a interação entre polímero e nanoargila, levando a mudanças significativas em suas propriedades. Em geral, os sistemas esfoliados resultam em melhores propriedades físicas do que os intercalados [43].

A dispersão completa das nanocamadas de argila em um polímero otimiza os elementos de reforço disponíveis para o transporte de uma carga aplicada. O acoplamento entre a área da superfície da argila e a matriz polimérica facilita a transferência de tensão para a fase de reforço, o que permite a melhoria das propriedades físicas [44].

Porém, não é fácil obter a esfoliação completa das nanoargilas, pois as camadas de silicato são altamente anisotrópicas, além disso, a maioria das cadeias poliméricas é ligada à superfície das camadas de silicato. Assim, mesmo acima da temperatura de fusão dos polímeros constituintes, há uma ordem de longo alcance que é preservada e as camadas de silicato são orientadas em uma direção preferencial [45].

3.3 Nanocompósitos poliméricos

Os nanocompósitos poliméricos resultam da combinação de dois ou mais materiais com propriedades distintas, sendo que a fase dispersa apresenta pelo menos uma de suas dimensões em escala nanométrica, sendo usada em pequena quantidade, tipicamente, 5% em peso [46].

Geralmente, esses materiais apresentam uma fase inorgânica dispersa a nível nanométrico em uma matriz orgânica. A fase inorgânica mais utilizada na preparação de nanocompósitos poliméricos é a argila montmorilonita, pois sua razão de aspecto é elevada, além de apresentar boa capacidade de delaminação, alta resistência a solventes e estabilidade térmica adequada aos processos de polimerização [47].

Os nanocompósitos poliméricos apresentam propriedades superiores aos polímeros convencionais, sendo uma área de grande interesse para a pesquisa e desenvolvimento [48, 49], em especial, em relação à permeabilidade gasosa [50, 51].

O coeficiente de permeabilidade é o principal parâmetro no desenvolvimento de materiais de barreira e a presença de nanopartículas de argila montmorilonita tende a retardar a difusão de gases através de um nanocompósito polimérico que pode ser obtido por diferentes processos [52, 53].

Porém, a dispersão dos silicatos em monocamadas discretas é dificultada pela incompatibilidade dos silicatos hidrofílicos com os polímeros hidrofóbicos. Assim, os silicatos em camadas precisam ser organicamente modificados para se tornarem compatíveis com os polímeros, por exemplo, através da troca dos cátions inorgânicos das galerias da estrutura da argila com agentes surfactantes de alquilamonio para compatibilizar sua química superficial com o polímero [54, 55]. Não basta a interface ser quimicamente adequada, é necessário garantir a homogeneização das nanopartículas na matriz polimérica através de condições de preparação e processamento adequadas [56].

A reduzida dimensão das nanopartículas cria uma grande área interfacial e uma elevada relação de aspecto que levam à melhoria significativa das propriedades do nanocompósito [57, 58], em especial, a redução permeabilidade gasosa que é obtida com a adição de uma pequena quantidade de argila montmorilonita em uma matriz polimérica, indicando os nanocompósitos poliméricos para aplicações que necessitam de propriedades de barreira a gases [59].

As pequenas quantidades de nanoargila não afetam a densidade e a processabilidade do polímero em comparação aos compósitos convencionais, o que compensa o custo das nanopartículas [60].

Considerando as propriedades de barreira aos gases, as camadas impermeáveis da nanoargila tendem a forçar o elemento permeante a percorrer um caminho maior através do nanocompósito, podendo reduzir em até 500 vezes a permeabilidade gasosa, mesmo para baixos teores de argilas [61].

Em polímeros semicristalinos, como o polietileno, o tamanho e a forma dos cristalitos, a estrutura cristalina e o grau de cristalinidade influenciam a permeabilidade gasosa, pois os cristalitos comportam-se como uma fase impermeável para a molécula do gás, ocorrendo difusão somente na fase amorfa.

Como os nanocompósitos são constituídos por uma matriz polimérica semipermeável na qual está dispersa uma fração de nanoplaquetas de argila impermeáveis, há redução na permeabilidade gasosa [62].

Como a matriz polimérica mantém as características do polímero puro e a fração volumétrica da argila é baixa, a redução na solubilidade gasosa no nanocompósito deve-se ao caminho tortuoso para a difusão das moléculas gasosas criado pelas nanoplaquetas devido a sua forma e dispersão, ou seja, ao grau de delaminação da argila [63].

As argilas montmorilonita são frequentemente usadas para preparar nanocompósitos, mas como todo o mineral extraído de jazidas, o teor de contaminantes dependerá do local de extração, da forma de extração e do processo de purificação.

Geralmente, as argilas apresentam contaminação por umidade, óxido de ferro e metais de transição. Assim, para evitar que ocorra uma aceleração dos processos de degradação oxidativos devido à umidade ou contaminações metálicas, é necessário purificar a argila ou aumentar o teor de aditivos antioxidantes no nanocompósito.

No caso das poliolefinas, a preparação de nanocompósitos necessita de agentes de acoplamento, pois as argilas como a montmorilonita possuem grupos químicos polares na superfície da nanopartícula enquanto as poliolefinas são moléculas apolares. Assim, é necessário usar o polietileno modificado com anidrido maleico como compatibilizante para a nanoargila, por exemplo, mas os resíduos do hidroperóxido usado no enxerto do anidrido maleico podem reduzir a estabilidade oxidativa da matriz polimérica [64].

Os principais métodos para a produção de nanocompósitos poliméricos de silicato em camadas são síntese por modelagem, intercalação de polímero a partir de solução, polimerização intercalante *in-situ* e intercalação por fusão [65, 66].

3.3.1 Intercalação do polímero a partir de solução

A intercalação envolve a mistura de uma solução polimérica com a argila, utilizando um solvente no qual o polímero ou pré-polímero é solúvel e o silicato pode ser inchado para separação de suas lamelas.

Após o silicato ser inchado em um solvente, o polímero e os silicatos lamelares são misturados. As cadeias dos polímeros intercalam e deslocam o solvente dos espaços interlamelares do silicato, sendo o solvente removido por vaporização ou precipitação. Então, as folhas são remontadas, ensanduichando o polímero para formar a estrutura do nanocompósito.

A maior vantagem deste método é que os nanocompósitos intercalados podem ser sintetizados com polímeros com baixa ou nenhuma polaridade. Porém, este método envolve a utilização em larga escala de solventes, sendo prejudicial ao ambiente e economicamente proibitivo [67].

3.3.2 Polimerização intercalante in-situ

Na polimerização *in-situ,* o silicato é inchado em uma solução do monômero, permitindo que a formação do polímero ocorra entre as folhas do silicato. A polimerização pode ser iniciada por calor ou radiação, difusão de um iniciador adequado ou por um catalisador fixado nas lamelas antes do inchamento, produzindo polímeros de cadeia longa nas galerias da argila.

A polimerização *in situ* pode ser aplicada para a preparação de nanocompósitos à base de polímeros termoplásticos diferentes, incluindo o polietileno [68, 69]. A polimerização *in situ* apresenta desvantagens como a rota de preparação demorada, esfoliação instável e necessidade de uma linha de produção específica [70].

Portanto, fatores como o efeito catalisador da argila organofílica sobre a reação de cura e a capacidade de penetração do agente de cura facilitam a esfoliação da argila e a obtenção de um nanocompósito polimérico [71].

3.3.3 Intercalação por fusão

A intercalação por fusão consiste em misturar o silicato em camadas com a matriz polimérica em estado fundido. Se as superfícies das camadas são compatíveis com o polímero, ele pode penetrar no espaço interlamelar e formar um nanocompósito esfoliado.

Este é o método mais usado para a preparação de nanocompósitos de polímeros com argilas, tendo aplicação industrial por não utilizar solvente, ser compatível com as técnicas de processamento de polímeros [72].

A síntese por fusão envolve hibridação da mistura de polímero e silicato, acima do ponto de amolecimento do polímero, pois durante o recozimento, as cadeias poliméricas se difundem nas galerias entre as camadas de silicato [73].

A formação de um nanocompósito polimérico de silicato por fusão envolve diversos fatores como as modificações energéticas decorrentes do confinamento do polímero no silicato e a expansão dos espaços entre suas camadas, bem como fatores associados à interação intermolecular entre a superfície de silicato e a cadeia polimérica [74].

A modificação orgânica da argila através da troca de íons nem sempre é suficiente para a formação de um nanocompósito, pois o agente compatibilizante deve combinar componentes incompatíveis em uma única molécula. Os surfactantes cumprem parcialmente esta tarefa, pois sua parte iônica interage com a superfície carregada das folhas das partículas de argila, mas a cauda alquil possui compatibilidade limitada com as cadeias poliméricas [75].

A quantidade de argila incorporada na matriz polimérica desempenha um papel determinante, pois enquanto baixas cargas de argila favorecem a esfoliação, quantidades mais elevadas (acima de 10% *wt*) permitem apenas a intercalação de cadeias de polímero nas galerias de silicato [76].

Porém, as condições de processamento são fundamentais para alcançar altos níveis de esfoliação, por exemplo, os nanocompósitos produzidos em extrusoras de dupla rosca com co-rotação apresentam maior esfoliação e dispersão das camadas de silicato [77].

A condição mais importante para a formação de nanocompósitos por intercalação por fusão é a presença de interações polares, pois a presença de grupos polares ao longo da cadeia aumenta a capacidade do polímero intercalar em argilas montmorilonitas.

Nos polímeros não-polares, como os polietilenos, a preparação de nanocompósitos esfoliados torna-se mais difícil, pois são hidrofóbicos e não possuem interações adequadas com a superfície da argila, mesmo depois de ter sido modificada organicamente [78, 79].

A técnica mais utilizada é adicionar certa quantidade de poliolefina enxertada com anidrido maleico, pois o caráter polar do anidrido maleico tem afinidade com os componentes da argila montmorilonita, fazendo com que a poliolefina com anidrido sirva como um agente compatibilizante [80, 81].

Quanto maior a concentração de poliolefina com anidrido maleico, melhor será a esfoliação e a delaminação da argila, mas é possível utilizar polietilenos funcionalizados com grupos polares e sal de amônio como compatibilizante, pois os sais são utilizados para a organofilização e os cátions orgânicos do sal substituem os cátions de sódio da argila, passando-a de hidrofílica para organofílica [82, 83].

A preparação de nanocompósitos utilizando intercalação por fusão pode causar problemas de degradação do polímero devido à temperatura de processamento. Além disso, se a temperatura de processamento for superior à estabilidade térmica do tratamento químico haverá decomposição. Quando o material é submetido à extrusão, a degradação é detectada como descoloração e redução das propriedades físicas e mecânicas do polímero. Se todo o material extrudado for afetado, a causa mais provável é a temperatura muito elevada para a velocidade de extrusão.

A oxidação também ocorre quando o polímero é aquecido, fazendo com que as ligações moleculares vibrem fortemente até romper e as terminações das ligações rompidas reagirem com o oxigênio.

3.4 Permeabilidade gasosa em polímeros

A unidade de repetição do polietileno possui apenas dois carbonos e quatro hidrogênios, mas algumas de suas propriedades dependem das condições da reação de polimerização que o originou, pois temperatura, pressão e emprego ou não de catalisadores podem levar à formação de ramificações que influenciam as interações entre as moléculas do polietileno, alterando o formato de suas moléculas. Por exemplo, o polietileno de baixa densidade (LDPE) é usado em aplicações que requerem flexibilidade, mas apresenta baixa resistência mecânica enquanto o polietileno de alta densidade (HDPE) apresenta elevada rigidez, resistência mecânica, resistência química e baixa permeabilidade.

Como a permeabilidade indica a facilidade da passagem de um fluido através de um dado material, os chamados materiais de barreira resistem por mais tempo em maiores pressões diferenciais que os materiais comuns. Aplicações como embalagens e contendores para gases industriais requerem materiais de barreira para reduzir sua passagem que definem o seu tempo de prateleira, por exemplo.

Portanto, há necessidade de reduzir este problema que acarreta prejuízos financeiros e ambientais, bem como, acidentes como o vazamento de produtos químicos inflamáveis ou tóxicos que podem resultar em incêndios e explosões.

Neste sentido, a degradação por oxidação está associada à permeabilidade gasosa, pois ocorre após a difusão das moléculas de oxigênio no polímero, causando fragilização e perda de propriedades mecânicas, mas alguns polímeros são mais suscetíveis à oxidação devido à baixa energia de ligação, grande atração dos elétrons pela molécula de oxigênio e à abertura da estrutura polimérica que possibilitam a entrada da molécula de oxigênio, necessitando de antioxidantes para absorver o oxigênio, especialmente, durante o processamento, pois altas temperaturas aceleram a oxidação.

A permeabilidade dos materiais plásticos é definida por propriedades que também determinam sua suscetibilidade a solventes. Por exemplo, se um polímero com grupos polares é sensível a um solvente polar, ele será permeável a um gás polar, bem como um polímero não polar poderá ser barreira para gases polares.

A estrutura do polímero é outro fator importante para a permeabilidade, pois se ela for amorfa com poucas áreas de empacotamento de átomos, as moléculas dos fluidos poderão mover-se facilmente através dela e o material apresentará alta permeabilidade. Assim, entre dois polímeros com polaridades similares, o que apresentar maior densidade e maior cristalinidade será a melhor barreira.

O tamanho da molécula do permeante também é importante, pois moléculas pequenas podem permear a estrutura polimérica mais facilmente do que moléculas maiores, ou seja, o tamanho da molécula pode superar os demais fatores na permeabilidade gasosa.

Os fatores ambientais também influenciam a permeabilidade gasosa, em especial, a temperatura, pois com o aumento da temperatura, o polímero se torna mais flexível, deixando o sistema mais aberto, facilitando a passagem das moléculas gasosas, mas outros fatores como a presença de aditivos químicos também afetam a permeabilidade. Por exemplo, um plastificante pode aumentar significativamente a permeabilidade ao causar inchamento da estrutura polimérica, facilitando a passagem do gás.

3.4.1 Coeficiente de Difusão

A permeabilidade característica de um material em relação a um gás ou líquido em particular pode ser expressa pelo *coeficiente de difusão* ou *constante de difusibilidade*. Por exemplo, se um polímero é sensível a um dado solvente, o coeficiente de difusão será elevado, indicando grande permeabilidade.

O ambiente também pode afetar a difusibilidade, sendo a temperatura o fator ambiental crítico, pois seu aumento torna a estrutura polimérica mais aberta, permitindo que o gás permeie com maior facilidade.

Assim, a temperatura em que a difusibilidade é determinada deve ser indicada e para converter o coeficiente de difusão (D) para uma temperatura específica deve-se utilizar a Equação 1 que é derivada da equação de Arrehnius:

$$D = D_o e^{-(A/RT)} \qquad \text{(Equação 1)}$$

Onde:

D: difusibilidade à temperatura ambiente;

D_o: é a difusibilidade na temperatura tabelada;

e: função exponencial;

A: constante de ativação que indica a energia requerida para o gás ou líquido passar através das moléculas da barreira;

R: constante universal dos gases;

T: temperatura absoluta indicada em Kelvin.

Portanto, a permeabilidade de um gás ou líquido através de um material semipermeável depende do coeficiente de difusão do polímero, da diferença de concentrações ao longo da barreira e da espessura dessa barreira, podendo ser descrita pelas leis da difusão de Fick.

3.4.2 Leis da Difusão de Fick

A permeabilidade de um gás ou líquido depende do coeficiente de difusão do material de barreira, da diferença de concentração do produto em difusão através da barreira e da sua espessura. Caso existam condições de equilíbrio como a concentração em regime permanente em ambos os lados da barreira, esta relação pode ser expressa pela Equação 2, que é chamada de Primeira Lei da Difusibilidade de Fick:

$$J = - D.\delta C/\delta x \qquad \text{(Equação 2)}$$

Onde:

J: fluxo de gás ou líquido através do material de barreira, expresso por unidade de área;

D: coeficiente de difusão do material;

δC: mudança na concentração do gás ou líquido de uma face do material de barreira até o ponto de medição;

δx: distância de uma face do material até o ponto de medição.

O sinal negativo é introduzido porque ***δx*** usualmente se opõe à direção do fluxo, conforme ilustrado na Figura 2 que mostra esquematicamente as variáveis da difusão de moléculas gasosas.

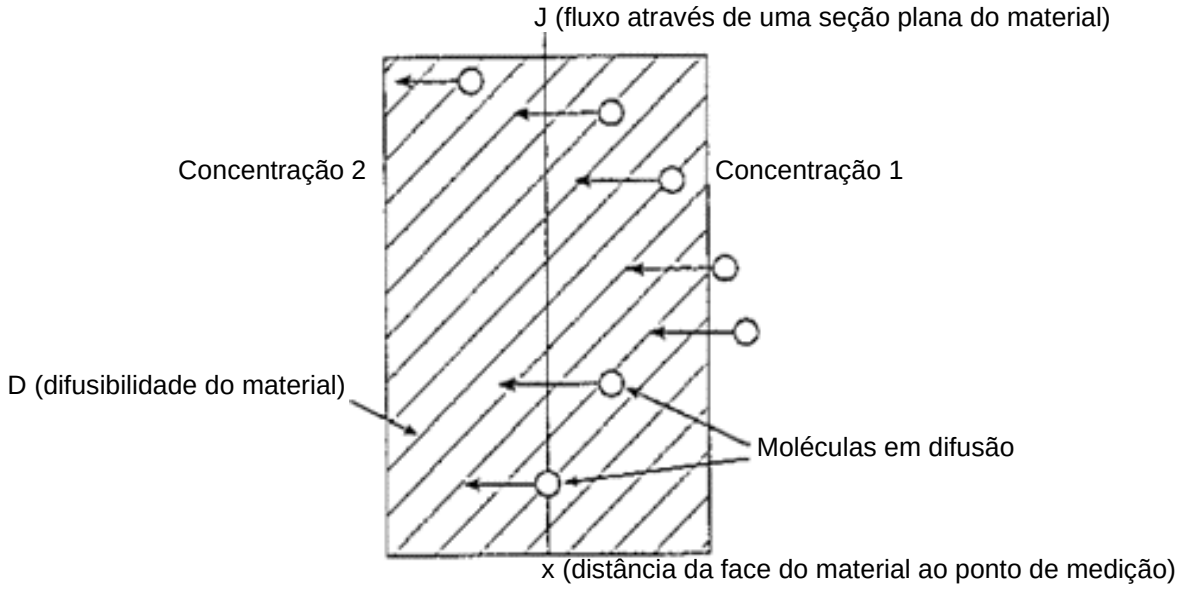

Figura 2 - Variáveis da difusão de moléculas - Strong AB (2005) - Adaptada [84]

Quando a permeabilidade do material varia com o tempo deve-se utilizar a Segunda Lei da Difusibilidade de Fick que pode ser escrita conforme a Equação 3:

$\delta C/\delta t = D.\delta^2 C/\delta x^2$ (Equação 3)

Onde:

C: concentração do gás ou líquido;

t: tempo de permeação;

D: coeficiente de difusão;

x: distância da face do material ao ponto de medição.

As diferenciais parciais indicam que a taxa de mudança da concentração depende da espessura do material de barreira (*x*) e do tempo (*t*).

Portanto, as equações de Fick permitem comparar quantitativamente as propriedades de barreira de diferentes materiais plásticos, além de possibilitar o cálculo da quantidade de um gás ou líquido permeante através de uma dada espessura de um material de barreira conhecido, em determinado tempo, assumindo que a concentração deste gás ou líquido também seja conhecida.

A permeação de gases e vapores ocorre através dos espaços intermoleculares do material de barreira nas seguintes etapas:

i) Sorção e solubilização do permeante na superfície do material;

ii) Difusão do permeante através do material devido ao gradiente de concentração;

iii) Dessorção e evaporação do permeante na outra face do material, conforme mostrado na Figura 3.

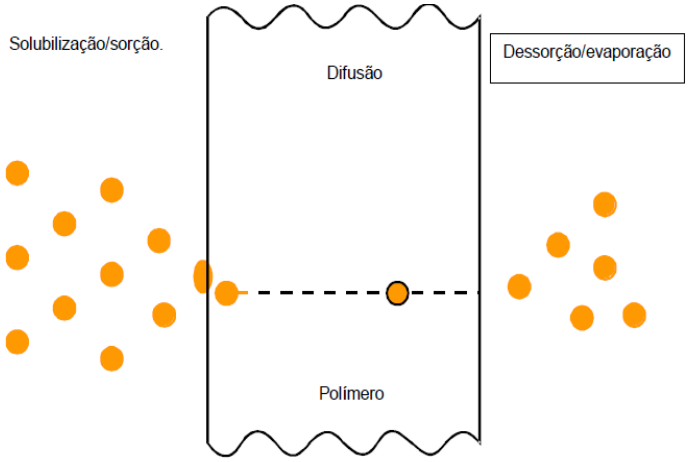

Figura 3 - Processo de permeação de gases - Sarantópulus (2002) [85]

Quando uma face do material é exposta a um gás ou vapor a certa pressão parcial, a primeira (i) e a última (iii) etapas do processo de permeação são mais rápidas que a difusão. Assim, a velocidade da difusão passa a controlar a permeação ou fluxo do permeante através do material.

3.4.3 Permeabilidade em nanocompósitos

Na exploração de petróleo *offshore* são usados *risers* para transporte de óleo bruto e gases, cuja armadura metálica é revestida internamente com polímeros para evitar a corrosão do aço e assegurar sua integridade estrutural.

Porém, o revestimento polimérico tende a permitir a passagem dos gases, pois o gás natural contém dióxido de carbono (CO_2) e sulfeto de hidrogênio (H_2S) em quantidades variadas que podem permear o polímero e permanecer entre o revestimento e a parede de aço do *riser*. O H_2S pode causar corrosão na tubulação enquanto o CO_2 tende a aumentar a pressão entre o revestimento e o tubo, resultando em falha catastrófica.

A incorporação de nanoargila no polímero tende a melhorar as propriedades de barreira em relação ao polímero puro, reduzindo a permeação de gases ácidos através do revestimento, pois a distribuição adequada da nanoargila no polietileno cria caminhos tortuosos que retardam o movimento das moléculas do gás através do polímero, mas isto não ocorre quando as nanopartículas são usadas como carga [86].

As propriedades de barreira podem aumentar significativamente pela adição de pequenas quantidades de nanoargila, tipicamente 5% em peso, desde que se obtenha a dispersão adequada e a esfoliação de nanoplaquetas com alta razão de aspecto. Assim, os nanocompósitos poliméricos apresentam diminuição na permeabilidade gasosa.

A modificação da superfície da nanoargila é outro aspecto importante para melhorar a compatibilidade entre a nanoargila e a matriz polimérica, evitando aglomerados que degradam as propriedades do produto final [87].

As propriedades de transporte como permeabilidade, solubilidade e difusividade em nanocompósitos em comparação com os polímeros puros são relacionadas com o volume livre da matriz polimérica [88]. Por exemplo, a permeabilidade e a solubilidade do metano (CH_4) no HDPE aumentam significativamente com a temperatura, pois o aumento de temperatura aumenta a mobilidade das cadeias do HDPE e das moléculas de gás, reforçando a difusão [89, 90].

Quanto ao efeito da pressão sobre os coeficientes de transporte de gases em polímeros, tanto o aumento quanto a diminuição [91] da permeabilidade do polietileno ao metano (CH_4) têm sido relatadas com o aumento da pressão, dependendo do tipo de polietileno e da faixa de pressão. O aumento da pressão reduz o volume livre disponível para a molécula permear devido à compactação, bem como, a concentração de gás, aumentando a permeabilidade gasosa [92].

Assim, os fatores que afetam a permeação gasosa não estão limitados à plastificação, mas a um processo de sorção/dessorção complexo que depende do compósito, da temperatura e da pressão, bem como da natureza dos aditivos e dos grupos funcionais sobre a superfície desses aditivos, por exemplo, a presença de compatibilizantes tende a aumentar a permeabilidade gasosa [93].

Como os polietilenos não são barreira ao oxigênio, necessita-se da incorporação de argila montmorilonita para reduzir sua permeabilidade gasosa, mas a quantidade de argila, utilização de compatibilizantes e condições de processamento são fundamentais para a esfoliação da argila. As camadas impermeáveis da nanoargila esfoliada forçam o permeante a percorrer um caminho tortuoso através do nanocompósito, podendo reduzir a permeabilidade de gases de 50 a 500 vezes mesmo para baixos teores de nanoargilas.

Em polímeros semicristalinos, o tamanho e a forma dos cristalitos, a estrutura cristalina e o grau de cristalinidade têm grande importância no processo de permeação, considerando-se que a difusão ocorre somente na fase amorfa, pois os cristalitos são impermeáveis à molécula gasosa.

O transporte de gases nos nanocompósitos pode ser comparado ao de um polímero semicristalino que é constituído por uma fase amorfa permeável onde está contida uma fração de nanoplaquetas impermeáveis de argila. Assim, os fatores principais que influenciam a permeabilidade em um nanocompósito são a fração volumétrica, a orientação relativa à difusão do gás e a razão de aspecto das nanoplaquetas.

A redução da permeabilidade gasosa do nanocompósito deve-se à redução do volume da matriz polimérica e à diminuição na difusão das moléculas permeantes devido ao aumento do caminho tortuoso. Como a fração volumétrica da argila é baixa, a diminuição na difusão está ligada à orientação, forma e grau de dispersão de suas nanoplaquetas. Assim, a permeabilidade em uma barreira polimérica pode ser representada por um arranjo regular de nanoplaquetas retangulares com orientação perpendicular ao sentido da difusão gasosa, o que é válido para o processo de injeção, mas não para a rotomoldagem, por exemplo.

O coeficiente de solubilidade dos nanocompósitos pode ser relacionado com o coeficiente de solubilidade do polímero puro e a fração volumétrica das nanoplaquetas dispersas. A solubilidade torna-se independente das características morfológicas das fases e as nanoplaquetas são consideradas barreiras impermeáveis à difusão das moléculas. Então, o coeficiente de difusão é influenciado pela tortuosidade que depende da razão de aspecto, forma e orientação das nanoplaquetas [94].

Portanto, a permeabilidade dos nanocompósitos diminui com o aumento da fração volumétrica e a razão de aspecto das nanoplaquetas que pode ser corrigida por um fator de orientação, inclusive para uma orientação randômica, atendendo a qualquer processo produtivo, inclusive rotomoldagem.

2.4.4 Propriedades de barreira em nanocompósitos

Os nanocompósitos poliméricos com nanoargilas apresentam excelentes propriedades de barreira, pois as moléculas que permeiam o polímero são forçadas a contornar as nanopartículas impermeáveis, difundindo-se por um caminho tortuoso [95].

Variadas técnicas de análise são utilizadas para avaliar a dispersão e o grau de esfoliação da nanoargila como a Difração de Raio X (DRX) que é utilizada para verificar o aumento do espaçamento basal e do estado de delaminação da nanoargila.

A Microscopia Eletrônica de Varredura (MEV) e a Microscopia Eletrônica de Transmissão (MET) caracterizaram a morfologia das amostras. A análise termogravimétrica (TGA) determina a quantidade de fase inorgânica na argila, dado necessário para o cálculo da fração volumétrica da fase impermeável no sistema enquanto o comportamento térmico é caracterizado pela Calorimetria Exploratória Diferencial (DSC) [96].

O aumento do nível de absorção de saturação, geralmente, é atribuído à aglomeração de nanopartículas. Porém, a coexistência de fases com diferentes permeabilidades em nanocompósitos pode levar a fenômenos de transporte complexos [97], inclusive, deve-se considerar a influência da variação da cristalinidade da matriz e a mobilidade da cadeia polimérica induzida pela presença da nanoargila.

Como o coeficiente de permeabilidade define o volume total de um gás que passa por uma barreira no decorrer do tempo, sob um gradiente de pressão parcial, a previsão das propriedades de barreira deve ser baseada na tortuosidade, razão entre a distância que uma molécula penetrante deve percorrer no interior da barreira e a menor distância possível que essa molécula poderia percorrer. Assim, a permeabilidade de um material é diretamente proporcional ao comprimento do caminho que o penetrante deve percorrer, sendo menor quanto maior for o caminho. Os aspectos da morfologia como cristalinidade e orientação molecular são fundamentais na compreensão destas propriedades [98].

Porém, nenhum polímero é barreira absoluta à difusão de moléculas gasosas, pois apresentam espaços vazios entre suas cadeias, permitindo a difusão de moléculas de gases cujo tamanho depende do tipo de polímero e do estado físico em que ele se encontra. Por exemplo, se um polímero amorfo estiver acima de sua temperatura de transição vítrea (Tg), os segmentos moleculares terão considerável mobilidade, aumentando seu volume livre, o que permite maior velocidade de difusão. Abaixo da Tg, esses segmentos têm menor mobilidade, resultando em menor volume livre e menos espaços vazios, o que reduzirá a velocidade de difusão. Como as estruturas cristalinas são praticamente impermeáveis devido ao maior grau de empacotamento molecular, a difusão ocorrerá somente na zona amorfa do polímero [99].

A difusão de gases e vapores através de barreiras poliméricas é caracterizada por um coeficiente, cujo valor depende do permeante, do polímero e da interação entre eles, sendo diretamente proporcional à concentração do permeante na superfície do polímero e ao aumento da temperatura tanto para gases quanto para vapores [100]. Por exemplo, os polímeros não oferecem barreira ao oxigênio como o vidro, mas são chamados pela indústria de *barreira* apesar de estarem sujeitos à degradação induzida pelo oxigênio.

A permeabilidade ao oxigênio depende de fatores como a integridade da barreira, a relação entre as fases amorfas e cristalinas, a taxa de hidrofilicidade e hidrofobocidade, a mobilidade da cadeia polimérica e da interação entre o polímero e o oxigênio.

A taxa de permeabilidade ao oxigênio (TPO_2) é uma característica importante dos materiais com propriedades de barreira, sendo definida como a quantidade de oxigênio que passa através de uma unidade de área paralela à superfície de uma barreira por unidade de tempo sob as condições de ensaio.

A temperatura é um parâmetro crítico que afeta a TPO_2, pois é associada à umidade relativa do ar. Por exemplo, as condições de umidade afetam a TPO_2 de polímeros hidrofílicos como as poliamidas e o EVOH, pois a água absorvida pelos polímeros age como um plastificante, diminuindo a energia de ativação necessária para a difusão do oxigênio, aumentando a taxa de permeabilidade.

A permeação de um gás ou vapor através de um polímero depende do polímero, do permeante e do ambiente (temperatura e umidade). A estrutura do polímero influi na permeabilidade, pois quanto maior a cristalinidade, menor a taxa de permeação, pois os cristalitos são impermeáveis. A solubilidade do permeante no polímero e a relação entre o tamanho de suas moléculas e os espaços intermoleculares da matriz polimérica influem na velocidade de passagem através do polímero.

Portanto, a permeabilidade de uma barreira pode ser definida como a massa de matéria seca do permeante que atravessa uma barreira por unidade de tempo, sendo proporcional à área e à espessura da barreira, bem como à diferença de pressão parcial através da barreira [101].

Como uma única resina não é capaz de apresentar o equilíbrio adequado de propriedades físicas e mecânicas, aparência e economia para todos os tipos de barreiras, geralmente, adota-se a combinação ou modificação de polímeros existentes, através da mistura de polímeros, modificação química ou modificação estrutural.

O principal uso de polímeros de barreira é em embalagens de alimentos, bebidas e medicamentos, mas eles estão se tornando cada vez mais importantes em embalagens de produtos químicos, inseticidas, reservatórios de combustível e de gases industriais, necessitando de materiais poliméricos com propriedades de barreira melhoradas.

O desenvolvimento de nanocompósitos poliméricos com excelentes propriedades de barreira envolve os silicatos naturais em camadas, pois a incorporação de pequenas quantidades de partículas de argila numa matriz polimérica pode resultar em propriedades como a baixa permeabilidade gasosa [102].

4. INTEGRAÇÃO DE ARTIGOS

Os três artigos publicados se baseiam na análise experimental da permeabilidade gasosa em polímeros e nanocompósitos poliméricos, envolvendo a o estudo dos efeitos da adição de nanoargila montmorilonita na redução da permeabilidade gasosa do polietileno de alta densidade que é utilizado em paredes espessas de contendores de gases industriais. Como os equipamentos comerciais para a realização de ensaios de permeabilidade gasosa em materiais semipermeáveis de parede espessa não estavam disponíveis devido ao custo elevado, houve a necessidade de projetar, construir e validar um permeâmetro de baixo custo para aferir o coeficiente de permeabilidade gasosa em amostras de polímeros com precisão, segurança e fácil operação.

O artigo de pesquisa intitulado *Application of Polymeric Nanocomposites and Carbon Fiber Composites in the Production of Natural Gas Reservoirs*, doravante chamado de Artigo 1, trata da análise experimental do comportamento mecânico de reservatórios para armazenamento de gases constituídos por um *liner* em nanocompósito polimérico revestido com fibra de carbono pré-impregnada com resina epoxídica aplicada por enrolamento filamentar, abordando soluções técnicas para otimizar suas propriedades físicas. Assim, entre os produtos incorporados ao polímero visando reduzir a permeabilidade gasosa foi escolhida a nanoargila montmorilonita para ser utilizada nas demais etapas da pesquisa.

O artigo de pesquisa intitulado *Gas Permeameter in Polymer Nanocomposite Plates: construction and validation*, doravante chamado de Artigo 2, aborda a permeabilidade gasosa em materiais homogêneos semipermeáveis.

Como as informações sobre os coeficientes de transporte de gases em condições extremas é escasso na literatura, foi necessário projetar, construir e validar um equipamento capaz de fornecer dados confiáveis sobre essas propriedades. Assim, o objetivo deste trabalho foi descrever um permeâmetro para gases industriais de média pressão para as amostras de materiais semipermeáveis, sendo validado com nitrogênio a 1 MPa e 69ºC (342,15 K) em amostras de polietileno de alta densidade puro e com nanoargila montmorilonita, formando um nanocompósito polimérico, considerando os métodos de obtenção dos coeficientes de transporte estudados na revisão de literatura.

O artigo de pesquisa intitulado *Gas Permeameter for Polymers and Nanocomposites: a new equipment*, doravante chamado de Artigo 3, descreve o novo permeâmetro que apresenta melhorias em relação à precisão e à usabilidade, sendo projetado, construído e validado pelos autores com nitrogênio a 1 MPa e 69°C (342,15 K) permeando amostras de polietileno de alta densidade puro e com adição de nanoargila montmorilonita, refazendo os testes publicados no Artigo 2.

Os resultados foram comparados com os dados obtidos anteriormente e as informações presentes na literatura, validando o permeâmetro apresentado no Artigo 3, que é capaz de avaliar a permeabilidade gasosa, nas condições descritas, com maior precisão e facilidade de operação do que o modelo anterior, demonstrando que as melhorias implementadas foram adequadas, permitindo a medição das propriedades de transporte de gases industriais que permeiam placas poliméricas e de nanocompósitos poliméricos, podendo fornecer informações necessárias para o projeto de *risers* para o transporte de óleo cru e gás natural, por exemplo.

Portanto, os três artigos se baseiam na análise experimental da permeabilidade gasosa em polímeros e nanocompósitos poliméricos, envolvendo o estudo dos efeitos da adição de nanoargila montmorilonita na redução da permeabilidade gasosa do polietileno de alta densidade através do permeâmetro projetado, construído e validado pelos autores.

Apesar do permeâmetro descrito no Artigo 3 apresentar melhorias e avanços em relação ao equipamento descrito no Artigo 2, pois foi projetado e construído aproveitando a experiência adquirida em todos os protótipos anteriores, de acordo com uma metodologia sistemática de projeto, permitindo maior confiabilidade na medição da permeabilidade gasosa do nitrogênio no polietileno de alta densidade puro e com adição de nanoargila montmorilonita em temperatura e pressão definidas, o processo de desenvolvimento de um novo equipamento já foi iniciado, devendo ser concluído em um trabalho futuro.

O permeâmetro em apresentação tem um custo de produção de aproximadamente € 4.850,00 (quatro mil oitocentos e cinquenta euros), permitindo a determinação dos coeficientes de transporte de gases, utilizando o procedimento volumétrico de acordo com a norma ASTM D1434-82 (2015) e1. Trata-se de uma alternativa mais econômica do que os equipamentos comercializados com finalidades semelhantes como o permeâmetro QHV-4 [11] que custa, aproximadamente, € 90.000,00 (noventa mil euros) ou R$ 510.000,00 (quinhentos e dez mil reais) posto fábrica em 10 de fevereiro de 2023.

4.1 Materiais utilizados

No Artigo 1, foi realizado o teste de permeabilidade ao oxigênio em amostras de polietileno de alta densidade com diferentes aditivos, selecionando-se a nanoargila montmorilonita por aumentar significativamente a propriedade de barreira do nanocompósito polimérico estudado.

Nos artigos posteriores, foram utilizadas amostras de polietileno de alta densidade puro e com nanoargila, ambas com 50 mm de diâmetro e 0,6 mm de espessura, verificadas por microscópio óptico quanto a falhas antes de serem colocadas na câmara de permeação.

O polietileno de alta densidade utilizado apresenta densidade de 0,954 g/cm^3, de acordo com a norma ASTM D1505, com índice de fluidez de 0,29 g/10min (190°C/2,16kg), de acordo com a norma ASTM D1238, sendo fabricado pela Dow Chemical Company com o nome comercial de HDPE 35054L [112].

A nanoargila montmorilonita, cujo nome comercial é Cloisite 20A, possui densidade aparente de 350 kg/m³, densidade de 1,80 g/cm³ (20°C), tamanho de partícula D50 < 10 µm, teor de umidade < 2,5 % e espaçamento lamelar (XRD, d001) de 2,7 nm [113], sendo adicionada a 5% em peso (*wt*).

O gás permeante utilizado nos artigos 2 e 3 foi o nitrogênio (N_2) - CAS 7727-37-9 [114] comercialmente puro fornecido em cilindros de 10 m³ a 21,1ºC e 1 atm (0,1 MPa) sob pressão nominal de 200 bar (20 MPa). O nitrogênio foi usado por razões de segurança, pois é um gás inerte e com baixa solubilidade em água [115].

As câmaras de permeação do equipamento apresentado no Artigo 2 foram usinadas em alumínio naval ABNT 5052F [116] devido ao compromisso entre resistência mecânica, resistência à fadiga e resistência à corrosão, enquanto as câmaras de permeação do equipamento apresentado no Artigo 3 foram construídas em aço inoxidável AISI 316 [117] por apresentar elevada resistência à corrosão e excelentes propriedades mecânicas.

4.2 Descrição do equipamento

Nos artigos 2 e 3 foram apresentados permeâmetros que medem a quantidade de gás que passa pela superfície paralela de cada membrana posicionada em sua respectiva câmara de permeação, ao longo do tempo, devido à pressão diferencial existente entre suas faces, conforme o método manométrico, onde um lado da membrana é submetido ao fluxo do gás de teste enquanto o outro lado é evacuado.

O equipamento apresentado em ambos os artigos consiste no que segue:

a) Sistema de fornecimento de gás: nitrogênio, mas poderia operar outros gases;
b) Câmara de permeação: corpo metálico para alojamento das amostras, permitindo a entrada do gás em alta pressão e sua saída em baixa pressão após permeação da amostra, sendo adequadamente vedada;
c) Sistema de vedação;
d) Sistema de controle de temperatura: termostato digital que permite ajuste e leitura da temperatura de teste;
e) Sistema de registro de dados: o gás permeado em cada amostra se acumula em uma pipeta com a face inferior (aberta) imersa em água destilada, cujo nível diminui à medida que o gás é permeado, permitindo o seu monitoramento.

Apesar da norma ASTM D1434-82 (2015) e1 recomendar o uso de mercúrio, o permeâmetro em apresentação utilizou água porque o Brasil é signatário da Convenção de Minamata sobre Mercúrio [118].

O permeâmetro apresentado no Artigo 2 apresenta 5 (cinco) câmaras de permeação em alumínio naval ABNT 5052F vedadas com O-rings em fluoroelastômero (Viton®) enquanto o equipamento descrito no Artigo 3 apresenta 10 (dez) câmaras de permeação em aço inoxidável AISI 316 vedadas com conexões RTJ e um sistema de vedação produzido em borracha de acrilonitrila butadieno (Buna-N) devido às suas adequadas propriedades mecânicas e químicas [119], projetado pelo autor.

O permeâmetro descrito no Artigo 3 apresenta 10 (dez) câmaras de permeação independentes, sendo cada uma delas vedada com uma conexão RTJ para permitir a rápida substituição da amostra, ou seja, o equipamento permite o ensaio simultâneo de 10 (dez) amostras que são inspecionadas quanto a vazamentos individualmente.

As principais diferenças entre as câmaras de permeação dos equipamentos apresentados nos artigos supracitados são mostradas na Figura 4.

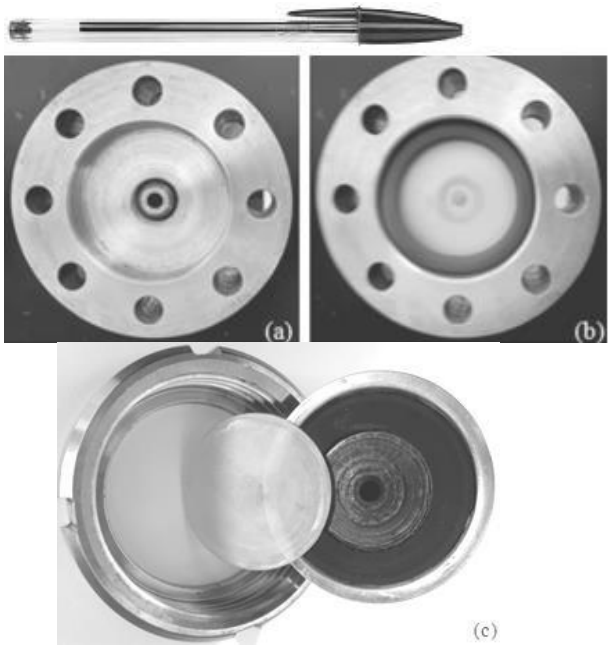

Figura 4 - Sistema de vedação do permeâmetro descrito no Artigo 2 com câmara de permeação aberta e sem amostra (a), com amostra e O-ring para vedação (b) e câmara de permeação do permeâmetro apresentado no Artigo 3 aberta com conexão RTJ, amostra e sistema de vedação (c)

As principais melhorias nas câmaras de permeação em relação ao permeâmetro descrito no Artigo 2 são o novo formato, o novo sistema de vedação com conexões RTJ que dispensam parafusos, o material com que foram construídas, aço inoxidável AISI 316 em vez de alumínio naval ABNT 5052F, e o número de câmaras, ou seja, 10 (dez) em vez de (cinco) câmaras, possibilitando a redução na incerteza de medição [120], sendo mostradas na Figura 5.

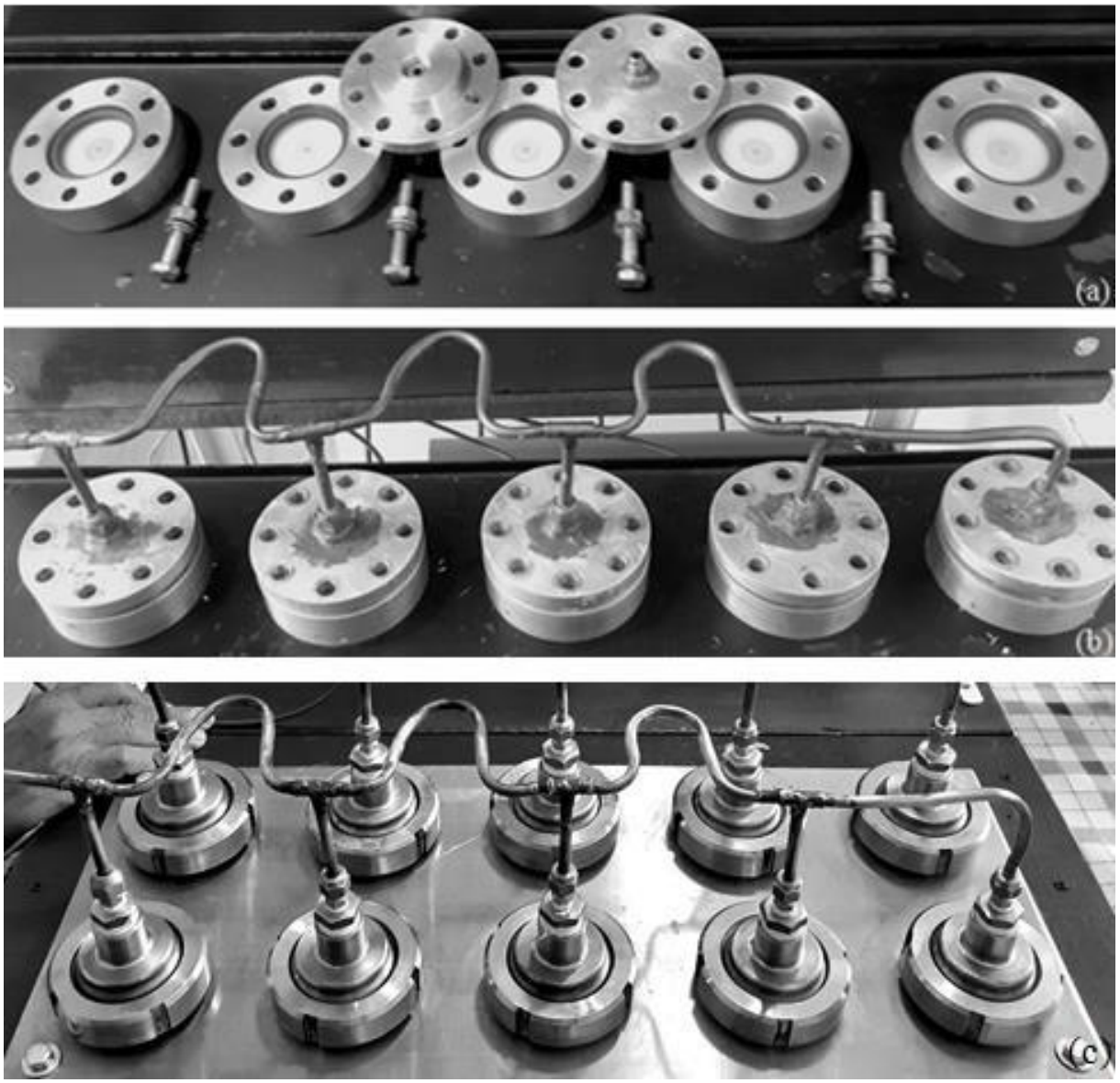

Figura 5 - Câmaras de permeação abertas com amostras e O-rings (a) e câmaras de permeação fechadas (b) do permeâmetro descrito no Artigo 2 e câmaras de permeação do permeâmetro descrito no Artigo 3 (c)

O aço inoxidável AISI 316 foi utilizado nas câmaras de permeação devido a sua elevada resistência à corrosão [121], permitindo realizar experimentos com gases corrosivos como o sulfeto de hidrogênio e amônia [122], além de apresentar excelentes propriedades mecânicas como resistência a altas pressões e temperaturas.

A utilização de conexões RTJ visa reduzir os problemas de vedação decorrentes da utilização de O-rings, pois cada câmara de permeação exigia o aperto de 8 (oito) parafusos para evitar vazamentos, totalizando 80 (oitenta) parafusos por experimento, reduzindo sua operacionalidade. Porém, o torquímetro utilizado para apertar os parafusos apresenta tolerância de ±5%, permitindo diferenças de aperto que possibilitam a formação de microfugas não detectáveis pelos meios convencionais.

O fluoroelastômero (Viton®), utilizado no O-ring do equipamento descrito no Artigo 2, é o material elastomérico mais utilizado para vedação [123], sendo indicado para uso em aplicações de alta temperatura além de apresentar elevada resistência química.

Porém, além do material utilizado, o projeto de vedações com anéis elastoméricos depende de fatores como pressão de vedação, condições operacionais e geometria da peça em que será instalado (ranhura) [124], sendo a extrusão do elemento vedante a principal causa de vazamentos devido a folgas excessivas, alta carga axial e uso de material de baixa dureza, tornando o sistema de vedação uma fonte de vazamentos de difícil medição durante a operação do equipamento.

Portanto, o sistema de vedação RTJ exigiu um projeto específico de anel de vedação para acomodar a amostra de forma adequada, evitando vazamentos sem interferir no fluxo do gás, considerando fatores como o material de vedação, condições de operação, formato e dimensões da amostra a ser testada.

Apesar do permeâmetro apresentado no Artigo 3 ter atingido os objetivos propostos e apresentar avanços em relação ao equipamento descrito no Artigo 2, houve o desenvolvimento de um novo protótipo, cujas principais melhorias pretendidas são mostradas a seguir:

a) O cilindro de gás de teste é conectado a um distribuidor com válvulas e engates rápidos individuais para as mangueiras poliméricas que transportam o gás de teste até cada uma das 10 (dez) câmaras de permeação;

b) A amostra é colocada na câmara de permeação e pressionada contra a base por um O-ring durante o fechamento da câmara de permeação;

c) As câmaras de permeação estão dispostas horizontalmente de modo que cada mangueira polimérica que transporta o gás até cada pipeta tenha o mesmo comprimento;

d) As câmaras de permeação são vedadas por interferência pela ação de um sistema de fechamento hidráulico, facilitando a montagem e eliminando vazamentos interfaciais, sendo o principal diferencial em relação ao equipamento atual;

e) A pressão exercida pelo sistema de fechamento hidráulico não deve ultrapassar o limite de escoamento mínimo do material que constitui a câmara de permeação para que o metal utilizado permaneça em sua zona elástica, que no caso do aço inoxidável AISI 316 é de 290 MPa [125].

A Figura 6 mostra o projeto esquemático do permeâmetro em desenvolvimento:

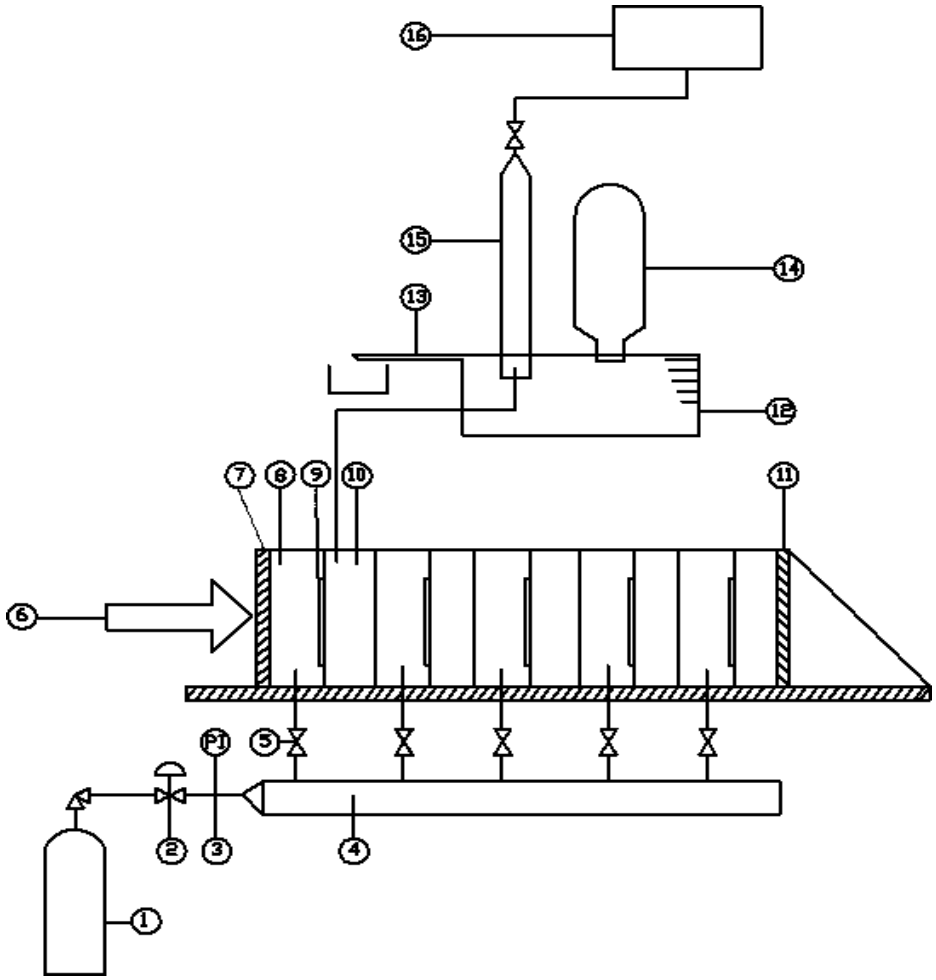

Figura 6 - Desenho esquemático do permeâmetro em desenvolvimento

Notação:

1. Cilindro de alta pressão contendo o gás de teste;
2. Válvula reguladora de pressão;
3. Manômetro de linha;
4. Distribuidor de gás de teste;
5. Válvula de fechamento da câmara de permeação (10x);
6. Sistema hidráulico para fechamento das câmaras de permeação;
7. Placa de aço móvel;
8. Entrada do gás de teste na câmara de permeação a montante (10x);
9. Amostra;
10. Saída do gás de teste na câmara de permeação a jusante (10x);
11. Estrutura de fixação e fechamento das câmaras de permeação;
12. Depósito líquido para o sistema de medição;
13. Saída do excesso de líquido do reservatório;
14. Sistema de reposição de líquido do reservatório;
15. Sistema de medição do gás de teste permeado (10x);
16. Gerador de vácuo.

4.3 Procedimentos operacionais

No Artigo 1 foi realizado o teste de permeabilidade ao oxigênio em amostras de polietileno de alta densidade (HDPE) puro e com nanoargila montmorilonita adicionada a 5% em peso (*wt*), sendo utilizada a norma ASTM F 1927 para placas e a norma ASTM D 3985 para filmes.

No Artigo 2 a validação do equipamento foi realizada com nitrogênio (N_2), com pressão de teste de 10 Bar (1 MPa) e temperatura de 69ºC (342,15 K), em amostras de HDPE puro e com adição de nanoargila montmorilonita a 5% em peso.

O polietileno e a nanoargila foram misturados manualmente e, após secagem em forno a 80ºC (353,15 K) por 24 horas, a mistura foi extrudada a 250 rpm em uma extrusora de rosca simples, sendo os *pellets* obtidos utilizados na preparação das amostras dos experimentos posteriores.

As amostras foram produzidas com diâmetro de 50 mm e espessura de 0,6 mm a partir de *pellets* de HDPE puro previamente desumidificados a 60ºC (333,15 K) por 4 (quatro) horas e moldados em uma prensa hidráulica aquecida a 180°C (453,15 K) com pressão de 0,3 MPa por 5 min. As amostras foram resfriadas na prensa sob pressão e desmoldadas, sendo verificada a espessura de cada amostra com um micrômetro digital 0-25mm e examinadas com microscopia óptica quanto a falhas.

As amostras de nanoargila foram analisadas por microscopia eletrônica de varredura (MEV) para avaliar a homogeneidade de sua dispersão superficial, usando o equipamento de bancada Phenom ProX.

A Figura 7 mostra a imagem de uma região da superfície de uma amostra com um *cluster* formado por um aglomerado de nanoargila não esfoliada (círculo), indicando falha em sua distribuição.

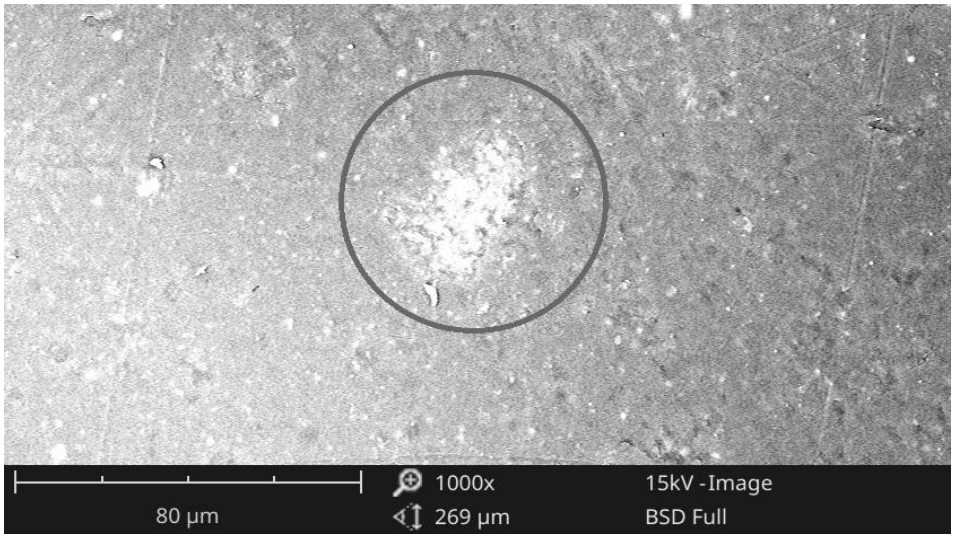

Figura 7 - Imagem MEV de um aglomerado de nanoargila

Antes da realização do experimento, foram feitos testes quanto a vazamentos nas câmaras de pressão com tampa cega de alumínio naval ABNT 5052F, com as mesmas dimensões da amostra, seguindo as diretrizes da norma ABNT NBR 15571:2013.

Para garantir o torque adequado no aperto dos parafusos de cada câmara de pressão do equipamento descrito no Artigo 2, evitando vazamentos e danos aos O-rings, foi utilizado um torquímetro de estalo de ½" de 28 a 210 Nm (± 5%).

Para verificar se as amostras apresentavam características semelhantes às apresentadas na Tabela 2 de Flaconnèche [4], foi realizada a análise de calorimetria exploratória diferencial (DSC) para avaliar sua cristalinidade, considerando as mudanças que ocorreram na microestrutura do polímero devido à história térmica resultante do seu processo de produção. O resultado da análise DSC foi obtido aplicando-se à Equação 4 [126] o calor de fusão (entalpia) do primeiro aquecimento (ΔHf), segundo os dados obtidos com o equipamento Universal V4.5A [127] conforme segue:

$$Xc = (\Delta Hf / \Delta Hfo) \times 100 \qquad \text{(Equação 4)}$$

$$Xc = (196{,}4/293) \times 100 = 67\%$$

Onde:

ΔHf [Calor de fusão da amostra] = 196,4 J/g

ΔHfo [Calor de fusão do polímero hipoteticamente 100% cristalino] = 293 J/g

Como a amostra possui características próximas às apresentadas na Tabela 1 de Flaconnèche [4], permitindo maior assertividade na replicação do experimento e na comparação dos resultados obtidos nesse trabalho com os apresentados pelo referido autor, conforme Tabela 2 [4], os dados referentes ao *Polymer Handbook* [128] servem para a comparação entre os valores apresentados neste trabalho de pesquisa.

No Artigo 3, os procedimentos operacionais foram idênticos aos apresentados no Artigo 2, pois se buscou comparar os resultados atuais com os dados obtidos anteriormente e os disponíveis na literatura.

Portanto, os testes para a validação do equipamento atual foram realizados com nitrogênio, com pressão de teste ajustada para 10 bar (1 MPa) e temperatura de 69°C (342,15 K), conforme Flaconnèche [4], em amostras de polietileno puro de alta densidade (HDPE) puro e com nanoargila.

Antes do experimento, foram realizados testes de estanqueidade em cada câmara de permeação sob a mesma pressão e temperatura utilizadas no teste, com uma tampa

cega de aço inoxidável AISI 316, com as mesmas dimensões da amostra.

4.4 Resultados

Os resultados do Artigo 1 indicaram que a nanoargila montmorilonita aumentou significativamente as propriedades de barreira do nanocompósito polimérico estudado ao oxigênio, indicando seu uso em trabalhos futuros.

A comparação dos resultados apresentados nos artigos 2 e 3 é mostrada na Figura 8 onde o gráfico mostra o valor do coeficiente de permeabilidade obtido a partir de amostras de HDPE colocadas em contato com nitrogênio sob pressão pelo tempo necessário para permear 5 mL de gás, sendo registradas, no primeiro caso, 48 horas (linha grossa) com desvio padrão de 3% para 10 (dez) amostras e, no segundo caso, 46 horas (linha fina) com desvio padrão de 2% para 10 (dez) amostras.

Em ambos os casos, as amostras de nanocompósitos poliméricos estiveram em contato com nitrogênio sob pressão por 48 horas, permeando 2 mL de gás nas condições de teste, indicando a redução da permeabilidade gasosa.

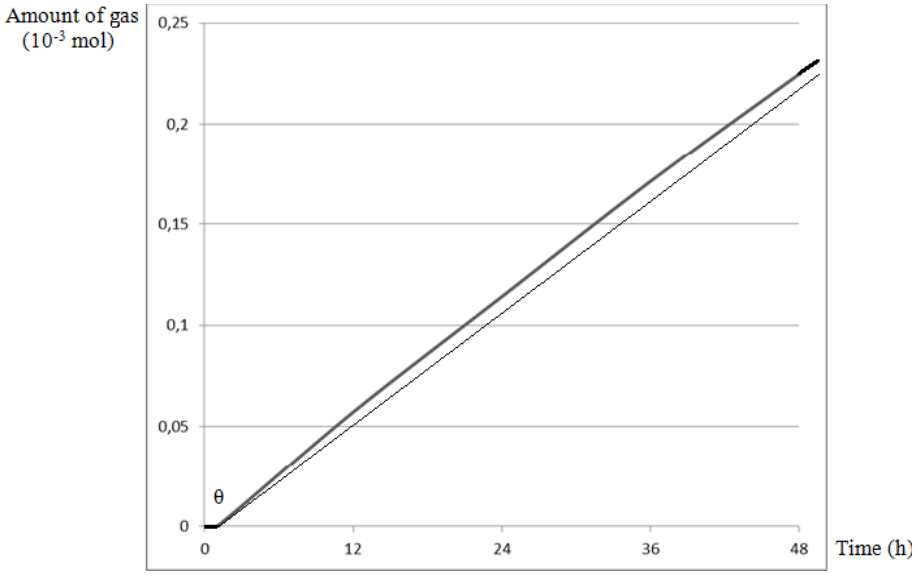

Figura 8 - Gráfico dos resultados de permeação de nitrogênio

Linha grossa: resultado referente ao Artigo 3

Linha fina: resultado referente ao Artigo 2

A Tabela 1 evidencia que a amostra apresenta características semelhantes ao polímero utilizado por Flaconnèche [4], permitindo a comparação dos resultados obtidos.

Tabela 1 - Características dos polímeros antes dos testes de permeação

Polímero	**ρ (g/cm^3)**	**T_f (ºC)**	**ΔHf (J/g)**	**Xc (%)**	**Φa**
Flaconnèche[1]	0.943	136	193	66	0.37

Amostra[2]	0.954[3]	130.96[4]	196.4[4]	67[5]	0.38[6]
Polymer Handbook[7]	0.954				

Notação:

ρ: densidade do polímero (g/cm^3)

Tf: temperatura do ponto de fusão (°C)

∆Hf: entalpia de fusão (J/g)

Xc: grau de cristalinidade (fração em peso) (%)

Φa: fração volumétrica da fase amorfa

Observações:

1. Tabela 2 em [4]
2. Idêntica nos artigos 2 e 3
3. Padrão ASTM D1505
4. Calorimetria exploratória diferencial (DSC) descrita no Artigo 2
5. Obtido de acordo com o software Universal V4.5A da TA Instruments
6. Calculado de acordo com a Equação 3 [4]

   Os valores de *Xc* permitem o cálculo do volume fração da fase amorfa (Φa) para as amostras de polietileno de alta densidade, conforme a equação a seguir:

   $$\Phi a = (1 - Xc) \cdot \rho/\rho a$$

   Onde ρ é a densidade do polímero semicristalino e ρa é a densidade de sua fase amorfa que foi considerada igual a 0,855 g/cm^3 conforme [129].
7. VI/546 - Dados de Permeabilidade e Difusão em [128]

A Tabela 2 apresenta as condições de teste e a comparação dos resultados obtidos por Flaconnèche [4] com os resultados dos experimentos apresentados nos artigos 2 e 3 enquanto os resultados referentes ao *Polymer Handbook* [128] servem como termo de comparação para os valores apresentados.

Tabela 2 - Coeficientes de transporte de nitrogênio em amostras de HDPE puro

Polímero	**Φa**	**T** (°C)	**P** (10^{-7} cm^3(STP)/cm·s·MPa)[5]
Flaconnèche[1]	0.37	69	1.0
Amostra 1[2]	0.37	69	1.4
Amostra 2[3]	0.37	69	1.3
Polymer Handbook[4]		25	1.1

Notação:

Φa: fração de volume da fase amorfa

T: temperatura (°C)

P: coeficiente de permeabilidade (10^{-7} cm^3(STP)/cm·s·MPa)

Observações:

1. Tabela 6 em [4]
2. Tabela 2 do Artigo 2
3. Tabela 2 do Artigo 3
4. VI/546 - Dados de Permeabilidade e Difusão [128]
5. Calculado de acordo com a Equação 1 descrita no Artigo 2

   Assumindo um diferencial de pressão constante que possibilita um fluxo de gás estável através de uma membrana semipermeável, o coeficiente de permeabilidade é calculado pela equação a seguir, onde *P* é o coeficiente de permeabilidade [cm^3.(STP)/cm.s.Mpa], *Q* é a quantidade de gás que permeou o membrana [cm^3], *l* é a espessura da membrana [cm], *t* é o tempo do experimento [s], A é a área da membrana [cm^2] e *p* é a pressão do gás à montante da membrana [Mpa]:

$$P = Q\, l / t\, A\, p$$

Para validar o equipamento com os valores apresentados na literatura, o coeficiente de permeabilidade (P) das amostras foi calculado por meio da Equação 1 do Artigo 3, cujo resultado é apresentado na Tabela 2 para as amostras de HDPE puro.

As medições iniciaram após a vazão entrar em regime permanente com taxa de transmissão de gás constante, sendo mostrado na Tabela 2 o valor da média aritmética da medição feita a partir do nível da água de cada pipeta para 10 (dez) amostras individuais de HDPE puro, com desvio padrão de 10% devido à tolerância das pipetas graduadas.

Para a permeação de nitrogênio em amostras de HDPE puro, o valor de P calculado é de $1{,}3 \times 10^{-7}$ cm^3(STP)/cm s MPa, valor mais próximo aos encontrados na literatura do que o resultado apresentado no Artigo 2, sendo consistente com Flaconnèche [4] cuja diferença de valores se deve, possivelmente, ao uso de amostras com espessuras (l = 0,6 mm) em pressões (p = 1 MPa) inferiores às apresentadas pelo referido autor Flaconnèche.

O valor calculado de P para as amostras de nanocompósitos poliméricos com nanoargila é igual a $0{,}55 \times 10^{-7}$ cm^3 (STP)/cm s MPa, apresentando propriedades de barreira inferiores às apresentadas na literatura [130 - 132], possivelmente, devido à formação de aglomerados dispersos de nanoargila na superfície das amostras não apresentando diferenças significativas em relação ao experimento anterior relatado no Artigo 2.

4.5 Considerações finais

Como o permeâmetro descrito no Artigo *3 indica o* coeficiente de permeabilidade do

HDPE ao nitrogênio com maior precisão do que o equipamento apresentado no Artigo 2, possibilita a realização de testes com outros gases industriais.

As câmaras de permeação em aço inoxidável AISI 316 apresentam maior resistência ao sulfeto de hidrogênio [133], encontrado no óleo cru do que o alumínio naval ABNT 5052F [134] utilizado no equipamento descrito no Artigo 2, por exemplo.

A configuração atual do permeâmetro permite o teste de até 10 (dez) amostras simultaneamente, possibilitando a redução na incerteza de medição na obtenção dos valores dos coeficientes de transporte de gases, tendo maior precisão que o equipamento descrito no Artigo 2, conforme mostrado na Tabela 2, que possuía 5 (cinco) câmaras, exigindo o dobro da quantidade de experimentos para testar o mesmo número de amostras, aumentando o risco de erros inerentes ao processo.

A utilização de conexões RTJ se justifica, pois o equipamento descrito no Artigo 2 apresenta possíveis problemas relacionados à vedação, uma vez que cada câmara de permeação exigia o aperto de 8 (oito) parafusos para prevenir vazamentos, totalizando 80 (oitenta) parafusos para um experimento 10 (dez) amostras, reduzindo sua operacionalidade.

Neste sentido, o torquímetro utilizado para apertar os parafusos apresenta tolerância de ± 5%, permitindo diferenças de aperto que possibilitam a formação fugas de gás não detectáveis por meios convencionais durante sua operação.

No entanto, o sistema de vedação RTJ exige um projeto específico do anel de vedação para acomodar a amostra de forma adequada e permitir o fluxo do gás, evitando vazamentos, conforme as condições de operação, o material de vedação, o formato e as dimensões da câmara de permeação onde será colocada a amostra.

Os resultados diferem da literatura [135 - 137] devido a fatores relacionados às condições de teste como a temperatura, que afeta a mobilidade das cadeias poliméricas, o gás permeante, que influencia o coeficiente de permeabilidade [138], a densidade do polímero, que influencia no volume livre pelo qual o gás pode permear em polímeros semicristalinos [139], e imprecisões inerentes ao método de ensaio.

O fato dos resultados apresentados no Artigo 3 estarem mais próximos dos obtidos por Flaconnèche [4] e aos encontrados no *Polymer Handbook* [128] indica que as melhorias e avanços implementados foram adequados e que o equipamento foi validado.

O permeâmetro apresentado possibilita a medição da permeabilidade gasosa em materiais semipermeáveis com camadas espessas, como os polímeros utilizados em *risers* para transporte de petróleo e gás, pois quanto mais fina a camada, maior a influência dos poros na sua permeabilidade. Além dos vazios intrínsecos à estrutura molecular, os

polímeros também podem apresentar falhas conhecidas como poros, decorrentes do processo de produção, bem como, defeitos decorrentes da utilização como fissuras por estresse ou inchaço químico.

A extrapolação dos valores obtidos em filmes poliméricos pode levar a erros quanto à determinação da permeabilidade gasosa do material, pois em filmes há maior probabilidade de formação de canais que atravessam toda sua espessura, o que impacta a permeação gasosa, mas sua detecção demanda técnicas laboratoriais como espectroscopia de raios X por energia dispersiva (EDS) [140] e espectroscopia de aniquilação de pósitrons (PALS) [141].

O tamanho dos poros em membranas poliméricas pode ser estimado [142], mas o uso de um permeâmetro também pode ser útil. Apesar do coeficiente de permeabilidade ser independente da espessura da amostra para um dado polímero, ele pode sofrer alterações devido ao índice de vazios, ou seja, se a amostra apresentar um coeficiente de permeabilidade muito maior do que uma placa do mesmo material, nas mesmas condições de ensaio, há possibilidade da amostra apresentar um teor de vazios maior do que a placa, causando o aumento da quantidade de gás permeado.

Apesar do permeâmetro apresentado no Artigo 3 ter atingido os objetivos propostos e apresentar avanços em relação ao equipamento descrito no Artigo 2, pois foi projetado e construído aproveitando a experiência adquirida no desenvolvimento de seus antecessores, de acordo com orientações para a formulação de um projeto sistemático, permitindo maior confiabilidade na medição da permeabilidade gasosa do nitrogênio em amostras de polietileno de alta densidade puro e com adição de nanoargila montmorilonita, formando um nanocompósito polimérico, houve continuidade no processo de desenvolvimento de um novo equipamento descrito no referido artigo.

Portanto, a construção do permeâmetro em apresentação justifica-se, pois a medição da permeabilidade gasosa em materiais semipermeáveis com camadas espessas, como as encontradas em *risers* para transporte de óleo cru, não pode ser realizada através da extrapolação dos valores obtidos em filmes do mesmo material porque quanto mais fina a camada, maior a influência dos poros na medição da permeabilidade gasosa [143].

O referido equipamento visa determinar a permeabilidade gasosa do polietileno de alta densidade (HDPE) em determinada pressão e temperatura, a partir da experiência adquirida em protótipos anteriores, de acordo com as práticas para a formulação de um projeto sistemático, conforme a metodologia de ensaio definida pela norma ASTM D1434-82 (2015) e1, para obter estimativas quantitativas confiáveis da permeação de gases puros através de membranas de espessuras variadas.

5. ARTIGOS PUBLICADOS

5.1 Artigo 1

Hindawi Publishing Corporation
Journal of Nanomaterials
Volume 2015, Article ID 658727, 7 pages
http://dx.doi.org/10.1155/2015/658727

Research Article

Application of Polymeric Nanocomposites and Carbon Fiber Composites in the Production of Natural Gas Reservoirs

Gilberto João Pavani,[1] Sérgio Adalberto Pavani,[2] and Carlos Arthur Ferreira[3]

[1]*Instituto Federal de Educação, Ciência e Tecnologia do Rio Grande do Sul, Avenida São Vicente 785, 95180-000 Farroupilha, Brazil*
[2]*Universidade Federal de Santa Maria, Avenida Roraima 1000, Prédio 5, 97105-900 Santa Maria, RS, Brazil*
[3]*LAPOL, Universidade Federal do Rio Grande do Sul, Avenida Bento Gonçalves 9500, 91501-970 Porto Alegre, RS, Brazil*

Correspondence should be addressed to Gilberto João Pavani; gilberto.pavani@farroupilha.ifrs.edu.br

Received 26 May 2015; Revised 4 August 2015; Accepted 11 August 2015

Academic Editor: Sesha Srinivasan

This research work is about the experimental analysis of the mechanical behavior of reservoirs for storage of compressed natural gas (CNG) consisting of a nanopolymeric liner coated with carbon fiber preimpregnated with epoxy resin applied by filament winding (FW). It addresses technical solutions adopted to optimize the reservoir as reinforcement with fiber, the process of healing and thermal analysis, as well as the hydrostatic testing to verify its resistance to the pressure required for CNG storage. Different nanoclays were incorporated to the polymer aiming to increase the strength of the liner and to reduce the thickness of its wall and the final weight of the reservoir as well as decreasing gas permeability. The obtained results were the basis for proposing an adaptation of the equation traditionally used for the dimensioning of the wall thickness of metallic pressure vessels to determine the number of layers needed to endure any internal pressure to which the reservoir is subjected. They indicate that the used methodology enables the production of pressure vessels for the storage of CNG, according to the ISO 11439:2013 Standard.

1. Introduction

Natural gas is considered the fossil fuel with the lowest emissions of carbon dioxide, with low emission of pollutants and waste from the combustion process [1], allowing it to be efficiently used in internal combustion engines [2].

The main disadvantages presented by natural gas as an automotive fuel are the high cost of compression and the weight of the steel reservoir for transport and storage [3].

The use of reservoirs fabricated with nonmetallic material aims to reduce the inert load present in vehicles fueled by compressed natural gas (CNG), allowing fuel saving and the increase of the engine's life, as well as reducing the emission of pollutants.

This type of reservoir consists of a liner, whose primary function is gas impermeability, and reinforcement, whose main function is to resist the pressure of work.

The polymeric liner adds to the reservoir characteristics such as light weight, resistance to pressure and impact, corrosion protection, and durability [4] and is usually made of rotomolded polyethylene (PE) due to the low cost of production. The PE is the most widely used resin for rotational molding due to low cost, chemical inertness, ease of processing, and mechanical properties [5] that can be improved by cross-linking or by the addition of nanoclays.

Rotational molding is suited for production of large and dimensionally stable hollow parts, with superficial finish comparable to injection molding. Additionally, as pointed out by Crawford and Throne [6], it has lower mold costs.

The high pressure of vehicular CNG storage requires the polymeric liner to be coated with carbon fiber, using the process of filament winding (FW) because of its low production cost, high productivity, and high reliability, besides providing nearly isotropic properties to the final product [7].

The liner is used as a mandrel in the FW process, allowing the arrangement of the fibers for structural reinforcement at various angles and patterns in the direction of the main solicitation by overlapping layers composed of nongeodesic winding and circumferential winding.

Based on the concept presented above, the Thiokol company has had success in the storage of hydrogen [8], but the main contribution of this work is the addition of nanoclay to the polyethylene blend, aiming to increase the polymeric liner's resistance to pressure as well as this polymer's gas permeability.

ISO 11439:2013 [9] covers cylinders of any seamless steel, seamless aluminium alloy, or nonmetallic material construction, using any design or method of manufacture suitable for the specified service conditions.

Thus, pressure vessels for CNG must conform to the ISO 11439:2013 Standard's Method, which specifies the requirements for the validation of CNG storage reservoirs for automotive vehicles, including buses and trucks.

The standard classifies as CNG-4 cylinders those produced entirely with nonmetallic materials, using appropriate manufacturing methods for the service conditions for vehicular transport, such as the reservoirs in development.

In order to increase the liner's resistance to pressure, the addition of nanoclays to polyethylene was chosen, adopting the following actions to achieve the standard pressure:

(a) Analysis of possible failure on the existing liner.

(b) Analysis of possible failure in the composite coating.

(c) Adding more carbon fiber layers to satisfy the requirements of the standard.

Aiming to estimate the number of layers needed to endure any internal pressure to which the reservoir is subjected, an adaptation is proposed in the equation presented by Popov [10], having as base the hydrostatic tests' results made on reservoirs with one, two, and three layers of carbon fiber.

The proposed formula indicated that a fourth layer would meet the requirement of this standard, as calculated by linear regression and the equation proposed in this paper for calculating the number of layers for any internal pressure.

The obtained results indicate that the used methodology would allow the production of reservoirs for vehicular use classified as CNG-4, according to ISO 11439:2013, allowing a reduction of at least 60% (sixty percent) of the weight in relation to a steel cylinder.

2. Materials and Methods

2.1. CNG Reservoir. The polymeric liner in real scale (Ø225 × 725 mm), with capacity for 22 liters of water, was manufactured by rotational molding, with a blend of LDPE/HDPE, coated with carbon fiber preimpregnated with epoxy resin, developed in a previous study [11].

2.2. Filament Winding. The simulation of the application of the reinforcement layers by FW was performed with the software CADWind 2007, version 8271 (Material SA).

The liner was used as a mandrel, being coated with in successive layers composed of nongeodesic winding and circumferential winding at a 10° angle which allows variation of the winding angle along a given section of the mandrel.

The layers were applied by a Kuka Roboter GmbH robot, type KR 140 L 100-2, for ensuring reliability and repeatability,

Figure 1: Nongeodesic winding.

shown in Figure 1, necessary characteristics to the reservoir in development that should store CNG.

The carbon fiber was applied at room temperature adopting as the cure cycle heating at < 3°C per minute to 90°C residence for 24 hours and cooling at < 3°C for a minute to 66°C before removal from the oven.

2.3. Reservoir Characterization

2.3.1. Hydrostatic Test. In that test, we used the Flutrol equipment (150 psi) with HBM 50 MPa load cell, Spindler 8, 60 Hz, HBM Interface. The samples were pressurized at 0.1 MPa/s and the data was processed with the Catman 4.0 Professional software.

2.3.2. Differential Exploratory Calorimetric Analysis. The samples were removed from the reservoirs with one, two, and three layers, taking as reference a carbon fiber sample taken from the roll in use, to check whether the cure cycle was adequate.

The samples were heated at a rate of 10°C/min from room temperature to 250°C, with rapid cooling (50°C/min) to room temperature, and again heated to 250°C.

The pieces of equipment used were DSC Q20 (TA Instruments) with nitrogen gas (N_2Up) and graphs generated by Universal Analysis 2000 software, version 4.5 A, build 4.5.0.5, TA Instruments-Waters LLC.

The tensile testing of injection molded and rotomolded samples was carried out in the universal testing machine, aiming to select the best raw materials for the manufacturing of the liner regarding the mechanical strength.

The samples tested were as follows:

(i) Blends of polyethylene.

(ii) Blends of polyethylene with 5 weight% of Brazilian nanoclay.

(iii) Blends of polyethylene with 5 weight% of American nanoclay.

(iv) Blends of polyethylene with 5% of XLPE.

(v) XLPE.

(vi) XLPE with 5 weight% of Brazilian nanoclay.

(vii) XLPE with 5 weight% of American nanoclay.

Remarks are as follows:

(i) XLPE: ICORENE K1502 was from the company ICO Polymers.

(ii) Brazilian nanoclay: montmorillonite clay with granulometry of 74 microns was produced by the company Bentonisa S/A.

(iii) American nanoclay: montmorillonite Cloisite 30B clay was produced by the company Southern Clay Products.

(iv) These products were mixed manually to the blend of polyethylene and extruded in single screw equipment.

The rotomolded samples were ground in a bench mill of the MTC Robotics brand, from the injected mold design, and taken directly from rotomolded parts.

The injected samples were produced in a brand mini-injector, Thermo Scientific, model MiniJet II Haake, with a standardized mold. The samples were injected at 185°C with two tons of pressure, except for the XLPE that was injected at 205°C.

Five samples of each raw material both machined and injected were subjected to a tensile test at 5,000 mm/min.

Tensile testing of carbon fiber preimpregnated with epoxy resin samples was conducted in the EMIC DL20000 brand universal testing machine, with a TRD26 load cell, TRD15 strain gauge, claws for polymeric films, and the MTest version 3.0 software, aiming to find the maximum tensile strength of a single strand of said fiber.

2.3.3. Oxygen Permeability Test. The test intended to measure the permeability of the liner to methane, but due to lack of equipment to measure the permeability, it verified the oxygen permeability which has compatible polarity and molecular diameter.

The test was performed with two groups of samples according to ASTM F 1927 (plates) [12] and ASTM D 3985 (film) [13].

The first group of samples consisted of hot pressed plates in the mold, cut 12 cm in diameter and machined to a thickness of 1 mm in the MTC milling machine.

Three samples were tested as follows:

(i) Blend of polyethylene.

(ii) Blends of polyethylene with 5% weight of Brazilian nanoclay.

(iii) Blends of polyethylene with 5% weight of American nanoclay.

The second group of samples, consisting of films of polyethylene blend with nanoclay, had the pellets extruded at 250 rpm in twin screw corotating MH-Colour-20-32-Lab, after heating in an oven at 80°C for 24 hours for drying.

3. Results and Discussion

Reservoirs with three layers hit the average pressure of 350 bar ± 5% when subjected to hydrostatic test but did not meet the requirements of ISO 11439:2013 that determine the minimum pressure test for a CNG-4 reservoir as 2,25 times the working pressure, which is defined as 200 bar.

Table 1: Relationship between layers, weight, and pressure.

Layers	Weight (kg)	Pressure (bar)
1	1,220 ± 3%	150 bar ± 5%
2	2,240 ± 3%	250 bar ± 5%
3	3,430 ± 3%	350 bar ± 5%

Figure 2: Reservoir destroyed.

3.1. Hydrostatic Testing. Table 1 shows the average weight increase per layer and the average hydrostatic test results of the samples of liner coated with preimpregnated carbon fiber layers.

The calorimetric analysis by Differential Scanning Calorimetry indicates that the cure cycle for the preimpregnated carbon fiber with epoxy resin used in the reservoirs of one, two, and three layers was complete.

3.2. Fracture Liner. The fracture of the liner, in 80% (eighty percent) of the cases, regardless of the number of layers, occurred in the region near the tops due to lower wall thickness resulting from the manufacturing process by rotational molding, shown in Figure 2.

The simulation performed by Velosa et al. [14] indicated that the fracture occurred near the tops, a region of higher stress due to the action of the radial and the longitudinal stress, despite increased wall thickness.

In the case of the reservoir in development, the fracture also occurred near the tops, a region that has the lowest wall thickness, requiring adjustments to the project to increase the mechanical strength of the liner in the hydrostatic test.

However, careful control of the manufacturing process by rotomolding would maintain the continuity of the wall thickness of the polymeric reservoir, eliminating its significant reduction that causes premature rupture during hydrostatic testing. Furthermore, the addition of nanoclay increases the mechanical strength of the polyethylene blend constituting the reservoir and placing preimpregnated carbon fiber strips in the zone of concentration of the radial and longitudinal stresses results in increased resistance to pressure in said test.

3.3. Selection of New Materials for the Liner. In order to increase the liner's mechanical resistance and lower the nominal thickness of its wall, new materials were sought through tensile tests for its selection.

Table 2: Results of tensile testing of candidate materials (N).

Material	Rotomolded	Injected
Blend PE	143,84 ± 32,03	238,70 ± 18,37
Blend PE with 5 wt% of nanoclay, Brazilian	137,80 ± 11,38	205,12 ± 8,24
Blend PE with 5 wt% of nanoclay, American	140,74 ± 6,25	220,27 ± 3,79
Blend PE with 5% XLPE	151,23 ± 8,73	222,46 ± 5,06
XLPE	125,52 ± 4,07	267,44 ± 63,15
XLPE with 5 wt% of nanoclay, Brazilian	85,36 ± 4,25	364,08 ± 30,72
XLPE with 5 wt% of nanoclay, American	60,06 ± 4,74	367,95 ± 50,24

The tensile testing of such materials showed that the injected samples showed higher tensile strength than the rotomolded ones, that the addition of nanoclay increased tensile strength, and that American nanoclay (Cloisite 30B) showed better results than the Brazilian one because of it having more appropriate granulometry as observed in Table 2.

The literature recommends a weight percentage of nanoclay between 1% and 5% [15] for the gas barrier effect, but numerous studies indicate values optimized around 2% [16–18]. We opted for the limit value of 5% [19–21] to verify the influence of the type of nanoclay on the barrier and mechanical behavior of the reservoirs so that later the optimized value of the amount of nanoclay would be deemed appropriate for the purposes of this search.

In the tensile test, we adopted the von Mises criterion for the flow of an ideally plastic material in a triaxial stress state [22, 23]:

$$2(\sigma y)^2 = (\sigma 1 - \sigma 2)^2 + (\sigma 2 - \sigma 3)^2 + (\sigma 3 - \sigma 1)^2, \quad (1)$$

where σy = flow tension at rupture, $\sigma 1$ = circumferential tension: σc, $\sigma 2$ = longitudinal tension: σl, and $\sigma 3$ = radial tension: σr.

Adjusting the equation,

$$2(\sigma y)^2 = (\sigma c - \sigma l)^2 + (\sigma l - \sigma r)^2 + (\sigma r - \sigma c)^2. \quad (2)$$

In cylinders subjected to internal pressure, the expressions for σc, σl, and σr are

$$\sigma c = \frac{p \cdot d}{2} \cdot t,$$
$$\sigma l = \frac{p \cdot d^2}{(D^2 - d^2)}, \quad (3)$$
$$\sigma r = -\frac{p}{2},$$

where p is internal pressure in the cylinder, D is external diameter of the cylinder, d is inner diameter of the cylinder, and t is wall thickness.

Replacing these values in (2) and evidencing "p" we have

$$p = \frac{\left(4 \cdot \sqrt{(3)}\right)}{3} \cdot \sigma y \cdot \frac{\left(t - t^2/D\right)}{\left(D \cdot \sqrt{(1 - 4 \cdot t)}/D\right)}. \quad (4)$$

Equation (4) shows that the cylinder's burst pressure is directly proportional to the flow tension, whose value is close to the tensile resistance limit tension (σrt) obtained in the tensile test.

Thus, the higher the value of σrt, the greater the pressure supported by the cylinder in the hydrostatic test.

For Walters [23], do not use (4) to predict the burst pressure because σy differs from conventional yield stress (σe), obtained in the tensile test.

Therefore, in qualitative terms, it is possible to use the tensile test to select candidate materials for the manufacturing of CNG reservoirs.

3.4. Calculation of the Number of Layers of the Reservoir. The tensile testing of the carbon fiber preimpregnated with epoxy resin samples was carried out to find the maximum tensile strength of a single strand of fiber, allowing the calculation of the number of layers needed for any internal pressure that the reservoir is subjected to during hydrostatic testing.

In a cylindrical shell, there are two major strains:

(i) Longitudinal stress (σl) which tends to break the tops, being supported by the nongeodesic winding.

(ii) Circumferential stress (σc) which tends to break the side wall, being supported by circumferential winding.

For the design of a cylindrical reservoir, circumferential tension is used, because the longitudinal tension corresponds to half of this tension.

The tensile test conducted at IFRS resulted in an average tensile strength of 56.65 kgf/mm^2 ± 15% for one preimpregnated filament of fiber, corresponding to resistance to circumferential tension.

The tensile strength of the nongeodesic winding is calculated by multiplying the value obtained in the tensile test by sin(10°), resulting in an average tensile resistance of 9.84 kgf/mm^2 for one filament.

The value of the layer corresponds to the sum of the values, that is, 66.46 kgf/mm^2.

The number of layers of a cylindrical reservoir can be calculated by tension caused by the internal pressure, according to (5) presented by Popov [10]:

$$\sigma c = \frac{p \cdot r}{t}, \quad (5)$$

where σc is circumferential tension to the layer calculated from the value obtained in the tensile test in IFRS = 66.46 kgf/mm^2, p is internal pressure obtained in the hydrostatic testing for the three layers' reservoir = 3.57 kgf/mm^2, r is radius of the cylinder = 110 mm, and t is layer thickness (mm) = ?

Evidencing "t" in (5), we obtain

$$t = \frac{p \cdot r}{\sigma c}, \quad (*)$$

where $t \sim 5.9$ mm = 6 layers.

However, the experimental results suggest that (∗) must be adapted for coating in a preimpregnated carbon fiber composite as follows:

$$t = \frac{p \cdot r}{k} \cdot \sigma c, \quad (*\text{-}1)$$

where k is the material factor and $k = 1$ for steel and $k = 2$ for preimpregnated carbon fiber.

Recalculating the number of layers of a cylindrical reservoir in preimpregnated carbon fiber ($k = 2$) in (∗-1), we obtain the following result:

$$t = \frac{p \cdot r}{k} \cdot \sigma c, \quad (*\text{-}2)$$

where $t \sim 2.95$ mm = 3 layers, which corresponds to the experimental result.

As the main function of the liner is gas impermeability, its small contribution to resistance to circumferential stress (σc) is disregarded.

Therefore, to calculate the number of layers for the standard pressure of 459 bar (4.59 kgf/mm^2), using (∗-1), we have the following result:

$$t = \frac{p \cdot r}{k} \cdot \sigma c, \quad (*\text{-}3)$$

where p is internal pressure required by international standard = 4.59 kgf/mm^2, r is radius of the cylinder = 110 mm, k is material factor for preimpregnated carbon fiber composite = 2, σc is circumferential tension to the layer calculated from the value obtained in the tensile test in the IFRS = 66.46 kgf/mm^2, and approximately $t = 3.8$ mm corresponding 4 layers.

The value coincides with the calculation by linear regression and the equation proposed for calculating the number of layers for any internal pressure (see (∗-1)), while maintaining the advantage in comparison to the weight of the steel cylinders.

In order to obtain the necessary pressure to halve the volume of the reservoir, at room temperature, (6) is used as follows:

$$P \cdot V = z \cdot n \cdot R \cdot T, \quad (6)$$

where P = pressure [Pa = N/m^2]; V = volume [m^3]; n = number of moles; R (Universal Gas Constant) = 8.3144 Nm/(mol·K); T = absolute temperature [K]; z = compressibility factor (z).

The compressibility factor represents the ratio between the volume occupied by given mass of gas under certain conditions of pressure and temperature and the volume that this mass would occupy at the same conditions as if it was an ideal gas [24].

The compressibility factor varies with the composition, pressure, and temperature of the gas and can be calculated by the equation of state of Dranchuk and Abou-Kassem [25].

As the gas is the same and its temperature remains constant in the compression process, we have

$$n = \frac{P1 \cdot V1}{z1} = \frac{P2 \cdot V2}{z2}, \quad (7)$$

where $P1$ (usual storage pressure) = 220 bar = 22 MPa, $V1$ = volume before compression = 1 m^3, $z1 = 0.73286$ = compressibility factor, $P2$ = ?, $V2$ = volume after compression = 0.5 m^3, $z2 = 1{,}41458$, and $P2$ = 648 kgf/cm^2 = 636 bar.

According to ISO 11439:2013, the hydrostatic test pressure of one CNG-4 reservoir is 2.25 times the working pressure, resulting in a 1.431-bar test pressure.

Calculating the number of layers of a cylindrical reservoir in preimpregnated carbon fiber, using (∗-1), we obtain the following result:

$$t = \frac{p \cdot r}{k} \cdot \sigma c, \quad (*\text{-}4)$$

where p (calculated hydrostatic test pressure) = 1.431 bar = 14.60 kgf/mm^2, r (radius of the cylinder) = 110 mm, k (material factor for preimpregnated carbon fiber composite) = 2, σc (circumferential tension to the layer calculated from the value obtained in the tensile test in the IFRS) = 66.46 kgf/mm^2, and $t = 12{,}13$ mm = 12 layers.

Equation (∗-1) indicates that a fourth layer of carbon fiber will meet the requirements of ISO 11439:2013, resisting the pressure of 495 bar for hydrostatic testing, maintaining the advantage in relation to the weight.

3.5. Gas Permeability. The oxygen permeability test was performed on two groups of samples: rotomolded plates and film, adopted as reference.

The result of the permeability in the tested sheets is as follows:

(i) Polyethylene blend: 13,660 mL (STP/m^2/day) at 1 atm and 23°C.

(ii) Blends of polyethylene with 5% weight of Brazilian nanoclay: 32,829 mL (STP/m^2/day) at 1 atm and 23°C.

(iii) Blends of polyethylene with 5% weight of American nanoclay: 150,000 mL (STP/m^2/day) at 1 atm and 23°C (detection limit of the equipment).

The high permeability shown by rotomolded samples nanoclays is due to the processing in a single screw extruder which did not allow the adequate shear and distribution of the clay particles.

The following samples were analyzed in films:

(i) Sample A: HDPE Blend (95%), LDPE (5%), and sodium nanoclay (no compatibilizer).

Table 3: Oxygen permeability coefficient (PO_2) at 23°C, dry.

Sample	PO_2 (mL (STP)·μm·m^{-2}·day^{-1}·atm^{-1})		
	Average		Individual values
Sample A Nanoclay sodium	295.761	144.332/309.589/433.364	49
Sample B Cloisite 15A	40.258	36.284/44.232	14
Sample C Cloisite 30B	93.236	60.644/63.405/155.659	58

(ii) Sample B: HDPE Blend (95%), LDPE (5%), and Cloisite 15A nanoclay.

(iii) Sample C: HDPE Blend (95%), LDPE (5%), and Cloisite 30B nanoclay.

The rates of oxygen permeability (TPO_2) were determined by coulometric method according to standard D3985-05 (ASTM, 2010), in OXTRAN equipment, model 2/20, from the company Mocon, operating with pure oxygen as permeant gas.

The tests were performed at 23°C with the conditioning of samples at 23°C with no humidity for 46 to 48 hours. The effective permeation area of each sample was 100 cm^2.

The obtained results were corrected to 1 atm of oxygen partial pressure gradient between the two surfaces of the film, since this gradient corresponds to the driving force for permeation of the oxygen through the film.

Although the rate of oxygen permeability is characteristic of the film, the permeability coefficient was used, which characterizes the composite to minimize the effect of variation in thickness of the samples in the comparison.

The material was processed in a twin screw extruder, but the speed of 250 rpm did not allow adequate shear and distribution of the clay particles.

Once TPO_2 was determined, the oxygen permeability coefficient (P) was calculated from the permeability rate as follows:

$$P = \frac{TPO_2 \cdot e}{p}, \quad (8)$$

where Q is oxygen permeability coefficient (mL (STP)·μm·m^{-2} day^{-1} atm^{-1}); TPO_2 is oxygen permeability rate (mL (STP) m^{-2} day^{-1}); e is average thickness of the samples (μm); p is partial pressure of oxygen in the permeating gas chamber of the diffusion cell, because the partial pressure of O_2 in the carrier gas chamber is void.

The results of the oxygen permeability coefficient are presented in Table 3.

Table 3 shows that the sample with nanoclay Cloisite 15A has lower oxygen permeability coefficient, confirming the manufacturer's recommendation that indicates Cloisite 15 compatibilized with maleic acid for polyethylene due to the hydrophobicity of the polymer.

4. Conclusions

It is estimated that a fourth layer of carbon fiber will meet the requirements of ISO 11439:2013, supporting pressure of 495 bar for hydrostatic testing, maintaining the advantage in relation to the weight as calculated by linear regression and (*-1).

It was found that, in 80% (eighty percent) of the reservoirs, the fracture of the liner, regardless of the number of layers, occurred in the region near the tops, due to lower wall thickness resulting from the manufacturing process by rotational molding, corrections being required in the project, change of materials and better control in the process to increase the strength of the liner.

Despite the difference in format between the reservoir in development and the one presented by Velosa et al. [14], there are similarities in the location of fractures resulting from hydrostatic test and the ones found in the simulation that indicated fractures near the tops, the region of highest stress.

In the case of reservoir in development, the region close to the tops has the lowest wall thickness, according to the measurements performed in the liner, requiring adjustments to the project to increase the mechanical strength of the liner in the hydrostatic test.

To increase the mechanical strength of liner and reduce the nominal wall thickness from 10 mm to 7 mm, maximum thickness allowed by rotational molding, we sought new materials with rotomolded and injection molded samples.

The injected samples have higher tensile strength than the rotomolded ones, and the addition of nanoclay increases the tensile strength and the nanoclay Cloisite 30B shows better results than the Brazilian one due to the smaller particle size.

The low results obtained in the rotomolded test bodies with nanoclays are due to processing in a single screw extruder which did not allow adequate shear and distribution of the clay particles, unlike the test samples that were injected at better processing conditions.

Despite the XLPE obtaining the best result in the injected test samples, it showed the worst result as rotomolded samples, being discarded from the process for being permeable to oxygen and, by extension, to methane.

The qualitative method of selection through tensile test to evaluate the mechanical strength of the samples is justified by the application of the von Mises criterion for the flow of an ideally plastic material in a triaxial stress state, adapted to the uniaxial stress state, according to Walters.

The gas permeability is also an essential requirement for the selection of a material for the production of CNG reservoirs, but as it was not feasible to perform testing with methane, the main component of the CNG, we used oxygen which is compatible with it in terms of molecular diameter and polarity.

The high permeability shown by the rotomolded samples with nanoclays is due to processing in a single screw extruder which did not permit good distribution and adequate shearing of the clay particles, demonstrated by the results of permeability which increased with the addition of clay.

The value of the permeability of the blends of polyethylene with nanoclay Cloisite 30B reached the limit of scale equipment, because the smaller the particle is, the greater the tendency it has to be grouped, facilitating the gas passages.

As for the film, the permeability coefficient was used, which characterizes the composite in order to minimize the effect of thickness variation in the comparison of the samples. The permeability coefficient characterizes the barrier of homogeneous materials, not being entirely accurate in this case.

The material was processed in a twin screw extruder, but the speed of 250 rpm did not allow adequate shear and distribution of the clay particles, preventing the samples from becoming homogeneous.

From the data obtained it appears that the sample with nanoclay Cloisite 15A has lower coefficient of oxygen permeability.

As the pressure of the CNG reservoirs is 220 times greater than the gas permeability test performed, the values tend to increase significantly for methane reservoirs.

It was shown that it is possible to halve the volume of vehicular CNG reservoirs, maintaining autonomy equivalent to liquid fuels, by increasing the storage pressure to 636 bar, resulting in a hydrostatic test pressure of 1,431 bar according to ISO 11439:2013, 18 layers of composite to be supported, as calculated according to Formula (∗-1).

Therefore, the use of the reservoir in development is a viable alternative for vehicles fueled by CNG for it reduces the inert load, linking fuel saving to increased engine life, besides adding ecological and economic benefits to society, as well as optimizing the useful volume of the trunk by providing new formats of fuel reservoir to meet the growing range of models due to the internationalization of the car market.

Conflict of Interests

The authors declare that there is no conflict of interests regarding the publication of this paper.

Acknowledgments

The authors are grateful to IFRS, LAMEF/UFRGS, ITAL, UCS, and Xalingo for providing equipment for the testing needed for this research work.

References

[1] V. Chandra, *Fundamentals of Natural Gas: An International Perspective*, Penn Well, Tulsa, Okla, USA, 2006.

[2] V. Ganesan, *Internal Combustion Engines*, McGraw-Hill, New Delhi, India, 3rd edition, 2008.

[3] J. G. Speight, *Natural Gas: A Basic Handbook*, Gulf Publishing, 2007.

[4] Y. Li, J. C. Liang, W. Zhang, W. Qi, M. Su, and C. D. Liu, "Study on processs and impact strength for a rotationally molded truck fender," *Journal of Materials Processing Technology*, vol. 187-188, pp. 492–496, 2007.

[5] R. J. Crawford, *Rotational Molding*, Rapra Technology, 1993.

[6] R. J. Crawford and J. L. Throne, *Rotational Molding Technology*, William Andrew Publishing, 2002.

[7] F. C. Shen, "A filament-wound structure technology overview," *Materials Chemistry and Physics*, vol. 42, no. 2, pp. 96–100, 1995.

[8] T. Propulsion, "High-pressure conformable hydrogen storage for fuel cell vehicles," in *Proceedings of the 2000 Hydrogen Program Review*, San Ramon, Calif, USA, 2000.

[9] ISO 11439:2013 Gas cylinders—High pressure cylinders for the on-board storage of natural gas as a fuel for automotive vehicles, 2015, http://www.iso.org.

[10] E. P. Popov, *Introdução à Mecânica dos Sólidos*, Blucher, São Paulo, Brazil, 1978.

[11] E. S. Barboza Neto, L. A. F. Coelho, M. M. C. Forte, S. C. Amico, and C. A. Ferreira, "Processing of a LLDPE/HDPE pressure vessel liner by rotomolding," *Materials Research*, vol. 17, pp. 236–241, 2013.

[12] ASTM International, *ASTM F1927—Standard Test Method for Determination of Oxygen Gas Transmission Rate, Permeability and Permeance at Controlled Relative Humidity Through Barrier Materials Using a Coulometric Detector*, ASTM International, West Conshohocken, Pa, USA, 2015, http://www.astm.org/Standards/F1927.htm.

[13] ASTM, "Standard test method for oxygen gas transmission rate through plastic film and sheeting using a coulometric sensor," ASTM D3985, 2010, http://www.astm.org/Standards/D3985.htm.

[14] J. C. Velosa, J. P. Nunes, P. J. Antunes, J. F. Silva, and A. T. Marques, "Development of a new generation of filament wound composite pressure cylinders," *Ciência e Tecnologia dos Materiais*, vol. 19, no. 1, pp. 1–9, 2007.

[15] A. L. Brody, "Nano and food packaging technologies converge," *Food Technology*, vol. 60, no. 3, pp. 92–94, 2006.

[16] S. Pavlidou and C. D. Papaspyrides, "A review on polymer—layered silicate nanocomposites," *Progress in Polymer Science*, vol. 33, no. 12, pp. 1119–1198, 2008.

[17] M. N. Khalaf, "Control the discontinuity of the flow curve of the polyethylene by nanoclay and compatabilizer," *Arabian Journal of Chemistry*, 2012.

[18] M. R. Manikantan and N. Varadharaju, "Preparation and properties of linear low density polyethylene based nanocomposite films for food packaging," *Indian Journal of Engineering & Materials Sciences*, vol. 19, no. 1, pp. 54–66, 2012.

[19] T. P. Mohan and K. Kanny, "Melt blend studies of nanoclay-filled polypropylene (PP)—high density polyethylene (HDPE) composites," *Journal of Materials Science*, vol. 48, no. 23, pp. 8292–8301, 2013.

[20] N. Saba, P. M. Tahir, and M. Jawaid, "A review on potentiality of nano filler/natural fiber filled polymer hybrid composites," *Polymers*, vol. 6, no. 8, pp. 2247–2273, 2014.

[21] M. Alexandre and P. Dubois, "Polymer-layered silicate nanocomposites: preparation, properties and uses of a new class of materials," *Materials Science and Engineering R: Reports*, vol. 28, no. 1, pp. 1–63, 2000.

[22] H. Sehitoglu, *Thermomechanical Fatigue Behavior of Materials*, ASTM, 1993.

[23] J. A. Walters, *Hoop-Wrapped Composite, Internally Pressurized Cylinders*, ASME Press, 2003.

[24] C. Borgnakke and R. E. Sonntag, *Fundamentos da Termodinâmica*, Blucher, São Paulo, Brazil, 7th edition, 2009.

[25] Equation, 2015, http://checalc.com/solved/naturalgasZ.html.

5.2 Artigo 2

Iranian Polymer Journal (2021) 30:583–591
https://doi.org/10.1007/s13726-021-00915-y

ORIGINAL RESEARCH

Gas permeameter in polymer nanocomposite plates: construction and validation

Gilberto João Pavani[1] · Sergio Adalberto Pavani[2] · Carlos Arthur Ferreira[3]

Received: 25 May 2020 / Accepted: 8 March 2021 / Published online: 25 March 2021

Abstract
Gas permeability in homogeneous semipermeable materials such as semicrystalline polymers is an inherent property of the material structure that results in the absorption of fluids from diffusion in their matrix. The ability of a gas to cross a semipermeable membrane more or less quickly is the object of research in various fields such as food and drug packaging industry, the chemical industry, and oil and natural gas explorations. In crude oil extraction, polymers minimize permeation and leakage in offshore hoses when materials are in contact with gases at high pressures and temperatures, preventing accidents with serious environmental and human impacts. As information regarding the transport coefficients of gases under extreme conditions is scarce in the literature, it was necessary to experimentally build and validate a device capable of providing reliable data on these properties. Thus, the aim of this paper is to describe a medium pressure gas permeameter in polymer nanocomposite plates, developed by the authors and sought to be validated with nitrogen at 1 MPa and 69 °C (342.15 K) in samples of high-density polyethylene both pure and with nanoclay, forming a polymer nanocomposite, considering the methods of obtaining the transport coefficients studied in the literature review of the standardized experimental techniques. The comparison of the results obtained with the data found in the literature suggests the validity of the equipment in presentation for the analysis of the gas permeability of different polymeric materials.

Keywords Gas permeability · Permeameter · Nanoclay · Polyethylene · Nitrogen

Introduction

Although one of the first papers on gas transport phenomena in polymers was written in 1866 [1], there is still today a need to research and to know the effects of the interaction between the molecules of a gas under pressure with a specific polymeric matrix, aiming to obtain more realistic permeability simulations, in particular for asphyxiating gases, such as nitrogen [2], argon [3] and toxic gases such as ammonia [4] and chlorine [5].

Polymers have advantages over other materials such as low density, flexibility and good chemical resistance, which allow their increasing use in the automotive, packaging, medicine and oil and gas industries. In offshore oil exploration, in the case of flexible crude oil transport raisers, the polymer comes into contact with gases at high pressures and temperatures, present in the petroleum flow, and bubbles may form in the inner sheaths of the piping due to the permeation of gases such as carbon dioxide, which can cause explosive decompression due to gas phase changes in the face of a sudden pressure reduction, from supercritical to gaseous state in addition to the corrosion of metallic reinforcements by gaseous action, requiring knowledge of transport phenomena at high pressures in thick layers [6], which is scarce in the literature [7, 8]. Thus, it is necessary to expand the research of transport phenomena in commodity polymers, allowing their application in a more reliable and safe manner.

The permeation of a gas into a polymeric material can be divided into three stages: (i) absorption of the gas molecules on the side subjected to the highest pressure, (ii) gas diffusion within the polymer matrix and (iii) gas desorption on the lower pressure side. Thus, the permeability

✉ Gilberto João Pavani
gilberto.pavani@restinga.ifrs.edu.br

[1] Instituto Federal do Rio Grande do Sul, Porto Alegre, Brasil

[2] Universidade Federal de Santa Maria, Santa Maria, Brasil

[3] Programa de Pós-Graduação em Engenharia de Minas, Metalúrgica e de Materiais-Universidade Federal do Rio Grande do Sul, Porto Alegre, Brasil

corresponds to the gas flow through the material, requiring experimental techniques to more precisely determine the permeability coefficient in each polymer for different temperatures and pressures [9].

Seeing as gas permeation involves the diffusion of molecules through a semipermeable membrane that allows the permeant to pass from the high concentration zone to the low concentration zone through the material interface, so the permeant molecules are absorbed and desorbed, allowing the permeability of the specific material under certain pressure and temperature conditions to be quantified through experimental methods.

To determine the gas permeability of different polymeric materials under conditions of high temperature and pressure such as those encountered in offshore crude oil extraction, the permeameter in the presentation was built, with its testing methodology being defined by ASTM D1434-82 (2015) e1, providing quantitative estimates for the permeation of individual pure gases across films and membranes.

Assuming a constant pressure differential that allows stable gas flow through a semipermeable membrane, the permeability coefficient is calculated by Eq. 1, where P is the permeability coefficient [cm^3 (STP)/cm s MPa], Q is the amount of gas that permeated the membrane, l is the membrane thickness, t is the time of the experiment, A is the membrane area and p is the gas pressure upstream of the membrane [8].

$$P = \frac{Q\,l}{t\,A\,p} \tag{1}$$

When a gas under pressure comes into contact with the face of a semipermeable membrane, before it reaches a steady state, the flow and concentration of the gas vary overtime at all points of the membrane, with the amount of gas permeating the membrane during time t being defined by Fick's second law [10] and the point where the line intersects the axis being defined by Eq. 2, where θ is called the time lag [11] and D is the diffusion coefficient.

$$\theta = \frac{l^2}{6D} \tag{2}$$

The solubility coefficient S [cm^3 (STP)/cm^3 MPa] is calculated by Eq. 3:

$$S = \frac{P\,6\,\theta}{p} \tag{3}$$

Since the commercial equipment employed to evaluate gas permeability has a high cost, it is difficult to obtain for use in academic and industrial laboratories. The goal of this work was to build a low-cost medium pressure, gas permeameter with results validated by the literature, allowing its use on semipermeable materials such as polymers, polymer nanocomposites, blends and recycled thermoplastics.

Experimental

A low-cost permeameter was developed to determine the transport coefficients of gases in polymers and other semipermeable materials at medium pressures, adopting the volumetric procedure according to ASTM D1434-82 (2015) e1.

In this procedure, the lowest pressure in the permeation chamber was kept close to the atmospheric pressure and gas passage through the semipermeable membrane was indicated by the reduction of water level in the interior of a sealed pipette in which the volume of displaced water was equal to the volume of permeated gas. The search for validation was performed with nitrogen available in high-pressure bottles with pressure reduced to 1 MPa (manometric pressure) and temperatures of 69 °C (342.15 K) on pure high-density polyethylene (HDPE) and HDPE with added nanoclay specimens, constituting a polymer nanocomposite with better gas barrier properties [12–14].

Materials

In the construction of the permeameter in presentation and in the tests for its validation, the following materials were used:

(a) Nitrogen (N_2)—CAS 7727-37-9 [15] commercially pure in 10 m^3 bottles at 21.1 °C and 1 atm (0.1 MPa) under 200 bar (20 MPa) nominal pressure, supplied by Air Liquide Brasil Company. Nitrogen was also used for safety reasons as an inert, colorless and odorless gas with low water solubility [16].
(b) V8 Brasil pressure regulating valve for atmospheric gases, regulated between 0–25 kgf/cm^2 (low pressure) and 0–350 kgf/cm^2 (high pressure), calibrated by the manufacturer according to ABNT NBR 14105-1: 2013, with an inlet pressure of 200 bar (20 MPa) and outlet pressure of 10 bar (1 MPa).
(c) SCAI line pressure gauge, scale 0–60 kgf/cm^2—Class B, calibrated by the manufacturer according to ABNT NBR 14105-1: 2013, allowing the verification of the low-pressure line pressure.
(d) 10 mL graduated glass pipette, heat-sealed at the upper end.
(e) HVAC (heating, ventilating and air conditioning) flexible copper tubing with a nominal diameter of 6.35 mm, a thickness of 0.79 mm and a maximum working pressure of 1649 PSI (11.4 MPa), produced by company Paranapanema in Brazil [17].
(f) 5052F naval aluminum used in the permeameter's pressure chamber, because of the good compromise

between mechanical strength, fatigue resistance and corrosion resistance [18] of material, supplied by company Maxfer in Brazil [19].

The samples were made from high-density polyethylene, some pure and some with added nanoclay, both with 50 mm diameter and 0.6 mm thickness, being tested by optical microscope for production failures before being placed in the pressure chamber. High-density polyethylene (HDPE) has a density of 0.954 g/cm^3, according to standard ASTM D1505, melt mass-flow rate of 0.29 g/10 min (190 °C/2.16 kg), according to standard ASTM D1238, and being manufactured by the Dow Chemical Company with the commercial name of HDPE 35054L [20]. Nanoclay is an organophilic phyllosilicate being used at 5% (wt) in order to improve the barrier properties of HDPE. The nanoclay commercial name is Cloisite 20A, with a bulk density of 350 kg/m^3, density (20 °C) of 1.80 g/cm^3, particle size D50 < 10 µm, moisture content < 2.5% and lamellar spacing (XRD, d001) of 2.7 nm [21].

However, adding nanoclay to the polymer as if it were filler [22], such as in the case of wood-plastic composites [23] would not be enough. That is because the main objective of adding of nanoclays to polymers forming nanocomposites is improving the polymers barrier properties, as it increases the permeant's tortuous path, with reductions of 50–500 times to gas permeability through polymeric films being reported, even with small quantities of nanoclay [24].

Equipment

According to standard ASTM D1434, gas transmission rate (GTR) is the quantity of a given gas passing through a unit of the parallel surfaces of a plastic film in unitary time, being affected by test conditions such as temperature and pressures, as well as by the difference of gas concentration upstream and downstream of the sample. GTR can be quantified by permeameters as follows:

- In the isobaric test, the gas being tested stays on one side of the sample, while the carrier gas stays on the other side, both under the same pressure, usually the atmospheric pressure. Motive power is the partial pressure of the gas being tested or the concentration difference in the film. The continuous flow of the carrier gas takes the molecules of the permeated test gas to a quantification sensor. The most used standards in these test are ASTM D3985 and ASTM F1249;
- In the differential pressure test, also called the manometric method, one side of the sample is submitted to the test gas flow while the other side is usually evacuated. The permeation of the gas through the film is propelled by this difference in pressure, being determined by the change of pressure on the lowest pressure side. The most used standard in this test is ASTM D1434.

The present permeameter, whose schematic diagram is shown in Fig. 1, consists of the following elements:

a) Gas supply system: nitrogen (N_2) under manometric pressure of 10 bar (1 MPa), being able to operate with other atmospheric gases.
b) Pressure chamber: metallic circular body for horizontal positioning of the specimen, allowing the entry of gas at high pressure and its outlet at low pressure after permeating the sample with closing by 8 (eight) hexagon bolts M8 with nut and plain steel washer.
c) Specimen: each sample is individually positioned in the permeation chamber, being sealed with an O-ring.
d) Sealing system: O-ring to prevent gas leakage during the permeability test, manufactured in fluoroelastomer (Viton®), 70 Shore A, which presents good mechanical properties compared to other elastomers, even in high temperatures [25]. Before each experiment, a hermeticity test of the system is done under the same pressure and temperature of the experiment, during 24 h, to investigate leaks.
e) Temperature control system: digital thermostat that allows adjustment and reading of the test temperature.
f) Data recording system: the gas permeated by the test specimen accumulates in a pipette with the underside (open) immersed in distilled water, whose level gradu-

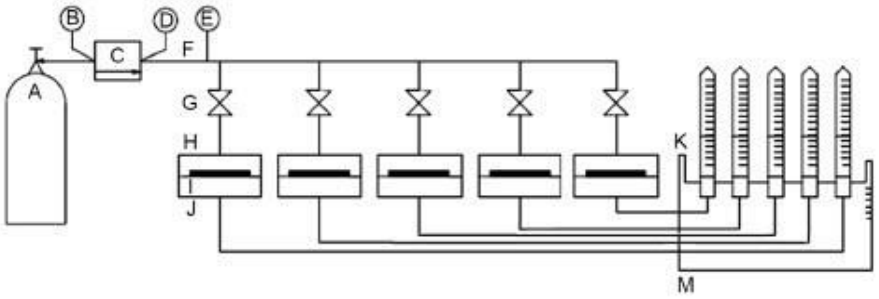

Fig. 1 Permeameter schematic diagram

ally decreases with the inlet of gas, allowing its periodic monitoring.

Where:

A. Gas supply system;
B. High pressure gauge;
C. Pressure regulating valve;
D. Low pressure gauge;
E. Line pressure gauge;
F. Copper tubing;
G. NPT threaded ball valve;
H. Pressure chamber;
I. Sample;
J. Flexible polyurethane hose with an outside diameter of 4.0 mm and an inside diameter of 3.0 mm (low pressure);
K. Pipette (volumetric meter of the permeated gas for samples);
L. Distilled water recipient

The presented permeameter was built based on ASTM D1434-82 (2015) e1 which indicated the use of mercury, but seeing as Brazil is a signatory to the Minamata Convention on Mercury [26, 27] aiming to control the use and releases of mercury until its industrial use is eliminated, using distilled water, eliminating the risk of personal and environmental contamination with mercury.

The pressure chamber was screwed to allow quick replacement of the specimens, without interfering with their mechanical properties, since the applied tensile stress was absorbed entirely by the screw according to ISO 898-1: 2013.

The permeameter had 5 independent pressure chambers, as shown in Fig. 2, allowing to test 5 samples simultaneously, i.e. each sample mounted in its chamber, forming a semipermeable barrier between the high and low-pressure areas.

The sample was positioned in the pressure chamber, sealed with an O-ring (Fig. 3), bolted and leak tested, including the gas pipe fittings.

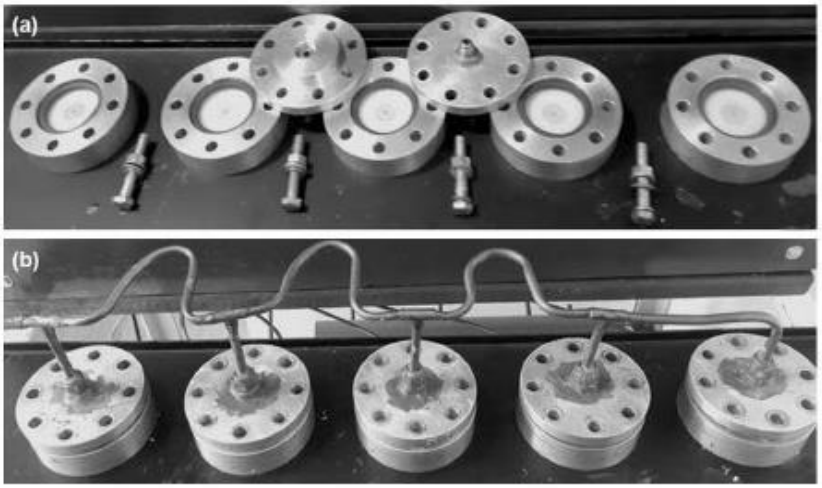

Fig. 2 Pressure chamber open (**a**) and closed with copper tubing (**b**)

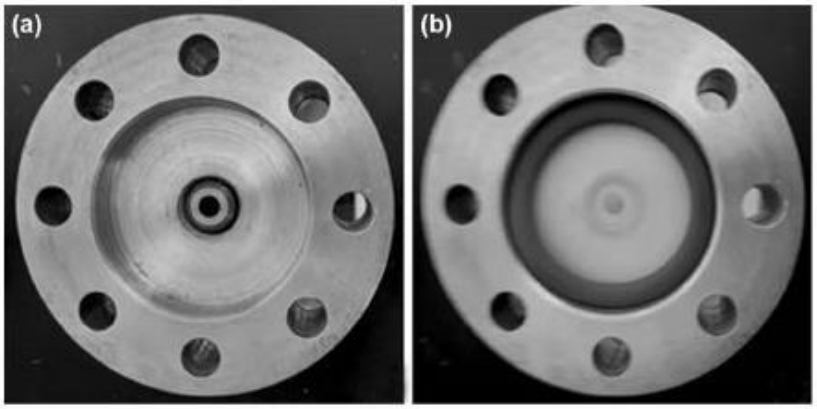

Fig. 3 Pressure chamber top view (**a**) and sample with O-ring (**b**)

Figure 4 summarizes the operation of the presented permeameter by showing the gas supply, comprised of an industrial gas bottle with a pressure regulating valve (Fig. 4a), which generated a high-pressure gas flow downstream of the membrane until it was permeated upstream of the membrane at low pressure and left the pressure chamber (Fig. 4b), being conducted to the data recording system comprised of the graduated pipette (Fig. 4c) that allowed the individual measurement of the gas permeated by each membrane by counting the markings on the pipette every 12 h.

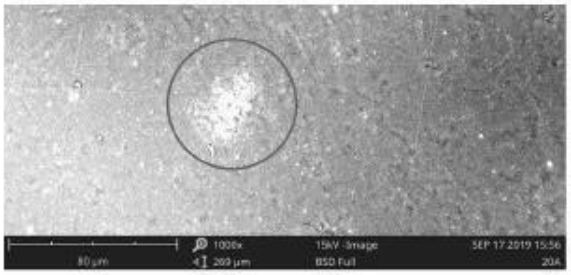

Fig. 5 Microscopic image of a Cloisite 20A nanoclay cluster

Operating procedure

The search for the validation of the equipment was performed with nitrogen (N_2), with test pressure set at 10 bar (1 MPa) and temperatures of 69 °C (342.15 K), in pure high-density polyethylene samples (HDPE) and samples with nanoclay.

Samples with a diameter of 50 mm and a thickness of 0.6 mm were produced from pure HDPE pellets previously dehumidified at 60 °C (333.15 K) for 4 h and molded in a hydraulic press heated to 180 °C (453.15 K) with a pressure of 0.3 MPa for 5 min. The samples were cooled to room temperature in the press under pressure and demolded. After demolding, the thickness of each sample was checked with a 0–25 mm Mitutoyo digital external micrometer, and optical microscopy analysis for faults was done.

The diffusion area was considered as the polymer surface in contact with the gas that was only the hollow area of the disc, discounting the area in contact with the O-ring.

The nanoclay samples were analyzed by scanning electron microscopy (SEM) to evaluate the homogeneity of their surface dispersion, using the Phenom ProX benchtop equipment. Figure 5 shows the image of a surface region of a sample with a cluster of Closite 20A nanoclay in the polymer nanocomposites showing the formation of a nanoclay cluster (circle), indicating a failure in its distribution.

The pressure chambers were placed in an electric oven at 69 °C (342.15 K), in accordance with Flaconnèche [7].

Before the experiment was carried out, leakage tests were done in the pressure chambers with a 5052F naval aluminum blind cover, with the same dimensions as the sample, following the guidelines of the standard ABNT NBR 15571: 2013.

To ensure the adequate torque in the tightening of the screws of the pressure chambers, and to prevent leaks and damages to the O-rings, a torque of 28 Nm was applied to each screw being verified with a ½" click-style torque wrench from 28 to 210 Nm (± 5%), Fortg brand, manufactured in China.

To guarantee the adequate operational conditions a differential scanning calorimetry (DSC) analysis was done to verify the crystallinity of the sample considering the changes that happened to the microstructure of the polymer (HDPE) due to the thermal history resulting from the necessary process to obtain the samples. The result of the DSC analysis is shown in Fig. 3, applying to Eq. 4 the heat of fusion (enthalpy) of the first heating (ΔHf), that is, 196.4 J/g, according to calculations with the Universal V4.5A software by TA Instruments [28].

Applying the equation [29]:

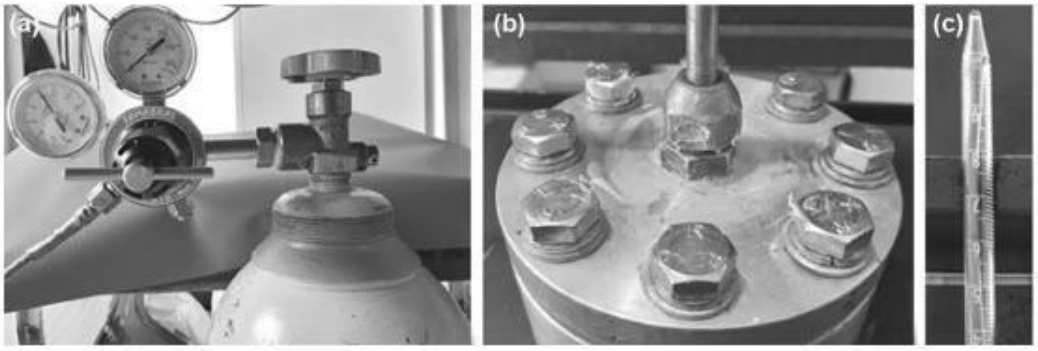

Fig. 4 Permeameter: gas supply (**a**), pressure chamber (**b**) and data record (**c**)

Table 1 Polymers characteristics before permeation tests

Polymer	ρ (g/cm^3)	T_f (°C)	ΔHf (J/g)	Xc (%)	Φa
Flaconnèche[a]	0.943	136	193	66	0.37
Sample	0.954[b]	130.96[c]	196.4[c]	67[d]	0.37[e]
Polymer handbook[f]	0.954				

[a]Table 2 in Flaconnèche B, Martin J, Klopffer MH (2001) Permeability, diffusion and solubility of gases in polyethylene, polyamide 11 and poly (vinylidene fluoride). Oil Gas Sci Technol 56: 261–278

[b]According to standard ASTM D1505

[c]According differential scanning calorimetry (DSC)

[d]Calculated in according Eq. 1

[e]Calculated in according Eq. 3 in Flaconnèche B, Martin J, Klopffer MH (2001) Permeability, diffusion and solubility of gases in polyethylene, polyamide 11 and poly (vinylidene fluoride). Oil Gas Sci Technol 56: 261–278

[f]Brandrup J, Immergut EH, Grulke EA (2003) Polymer handbook, 4th edn

$$Xc = (\Delta Hf/\Delta Hfo) \times 100 \quad (4)$$

$Xc = (196.4/286.18) \times 100 = 67\%$

Where:

ΔHf [Heat of fusion of the sample] = 196.4 J/g.

ΔHfo [Heat of fusion of the hypothetically 100% crystalline polymer] = 293 J/g.

Seeing as the sample presents characteristics close to those shown in Table 2 of Flaconnèche [7] which presents the test conditions explicitly, according to Table 1, allowing greater assertiveness in the replication of the experiment, there is a possibility for the comparison of the obtained results to those presented by the referred author, as seen in Table 2. The data referring to the Polymer Handbook [30] serve as a point of comparison between the presented values.

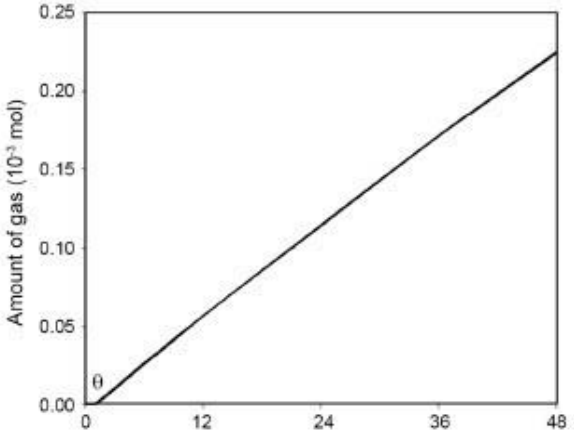

Fig. 6 Graph of nitrogen permeation results

Results

To determine the value of the permeability coefficient, the samples of pure HDPE were placed in contact with nitrogen (N_2) for 48 h (2 days), time required to permeate 5 mL of the gas, as shown in Fig. 6. However, the samples of polymer nanocomposites that were placed in contact with nitrogen (N_2) for 48 h (2 days) permeated 2 mL.

In this search for the validation of the equipment with the values found in the literature, the permeability coefficient (P) and solubility coefficient (S) of the samples was calculated by Eqs. 1 and 3, whose results can be observed in Table 2 for the pure HDPE samples, while Table 3 presents the comparison between the values predicted by Teplyakov [31] and experimental data of the coefficient of diffusion and solubility for the same samples.

Measurements were started after the steady state with constant gas transmission rate was reached and the values shown in Table 2 represent the arithmetic mean of the measurements made at the water level of each pipette, with a standard deviation of 10% due to the use of graduated pipettes, for 10 samples of pure HDPE aiming to reduce the experimental uncertainties originating from factors such as the measuring interval and the parallax effect on the reading of the pipettes.

For N_2 permeated pure HDPE samples, the calculated value of P is 1.40×10^{-7} cm^3 (STP)/cm s MPa, D is 8.3×10^{-7} cm^2/s and S is 0.17 cm^3(STP)/cm^3 MPa while for the polymer nanocomposite samples the calculated value of P is 0.55×10^{-7} cm^3(STP)/cm s MPa, D is 1.7×10^{-7} cm^2/s and S is 0.33 cm^3(STP)/cm^3 MPa.

The results of the pure HDPE samples are coherent with Flaconnèche [7], seeing as the difference of values is probably due to the use of samples with the thickness (l) of 0.6 mm and pressure (P) of 1 MPa lower than those

Table 2 Transport coefficients of nitrogen in pure HDPE samples

Polymer	Φa	T (°C)	P (10^{-7} cm^3(STP)/cm·s·MPa)	D (10^{-7} cm^2/s)	S (cm^3(STP)/cm^3·MPa)
Flaconnèche[a]	0.37	69	1	12	0.09
Sample	0.37	69	1.4	8.3	0.17
Polymer handbook[b]		25	1.1	7.56	0.138

[a]Table 6 in Flaconnèche B, Martin J, Klopffer MH (2001) Permeability, diffusion and solubility of gases in polyethylene, polyamide 11 and poly (vinylidene fluoride). Oil Gas Sci Technol 56: 261–278

[b]Brandrup J, Immergut EH, Grulke EA (2003) Polymer handbook, 4th edn

Table 3 Comparison between expected and experimental values of the diffusion and solubility coefficients

Teplyakov[a]				Flaconnèche[b]		Sample		Pol. Handbook[c]	
Gas	K_1	K_2	logD	D	logD	D	logD	D	logD
N_2	− 8.71	0.25	− 8.73	12E-07	− 5.92	8.3E-07	− 6.07	7.56E-07	− 6.12

K_1 and K_2 to PE ($\rho = 0.914$ g/cm^3)—Table 2—Teplyakov[a]

Def = 0.304 nm to N_2 (T < Tg)—Table 1—Teplyakov[a]

D—Equação 1—Teplyakov[a]

[a]Teplyakov V, Meares P (1990) Correlation aspects of the selective gas permeabilities of polymeric materials and membranes. Gas Sep Purif 4:66–74

[b]Table 6 in Flaconnèche B, Martin J, Klopffer MH (2001) Permeability, diffusion and solubility of gases in polyethylene, polyamide 11 and poly (vinylidene fluoride). Oil Gas Sci Technol 56: 261–278

[c]Brandrup J, Immergut EH, Grulke EA (2003) Polymer handbook, 4th edn

indicated by Flaconnèche, whose thickness and pressure are, respectively, $l = 2.08$ mm and $P = 10$ MPa.

The presented equations do not allow quantifying the influence of the thickness and pressure used in the experiment over the value of P shown in Table 2. The method of estimating coefficients of diffusion (D) was proposed by Teplyakov [31] whose values were calculated with Eq. 5 and presented in Table 3.

$$\log D = K_1 - K_2 . d_{ef}^2 \quad (5)$$

Where D (m^2/s) is the coefficient of diffusion, K_1 and K_2 are the correlation coefficients for the estimation of gas-permeability parameters of polymers at 298 K and d_{ef} (nm) is the effective molecular diameter of the permeating gas.

Table 3 shows that the coefficient of diffusion (D) of N_2 in the sample is within the error band of ± 30%, a prediction considered acceptable by Teplyakov [31], being close to those of Flaconnèche [7] and Polymer Handbook [30] indicating that despite the discrepancies present in the data, the permeameter presented in the paper at hand is valid, allowing the estimation of gas permeability in polymers in the laboratories of schools and small companies.

The results also differ from other authors such as Yasuda [32], Zhu [33] and Mark [34] due to factors related to test conditions such as the test temperature, which affects the mobility of the polymeric chains and of the permeating gas, influencing the permeability coefficient [35] and the density of the polymer, which influences the free volume through which the gas can permeate in semicrystalline polymers [36], the units employed, which affect the representation of numerical values; and imprecisions inherent to the testing method and to the equipment used in the experiment.

Samples with Closite 20A nanoclay presented barrier properties bottom to those indicated in literature [24, 37–39] due to the formation of dispersed clusters on the surface of the samples with nanoclay, as shown in Fig. 5.

Discussion

Although the experiment achieves its goal, testing with only one atmospheric gas (N_2) at medium pressure and at certain temperatures represents a small portion of HDPE applications, as flexible hydrocarbon pipes can work at pressures up to 100 MPa and temperatures above 100 °C (373.15 K), with polymer layers up to 6 mm thick in the presence of gases such as CH_4, CO_2 or H_2S, for example.

The current permeameter configuration allows testing at pressures from 0.1 to 2 MPa and temperatures between 20 °C (293.15 K) and 100 °C (373.15 K), but the use of more expensive building materials such as stainless steel will allow testing at higher pressures and temperatures, as well as any atmospheric gas such as CO_2, O_2, He and CH_4.

To test the permeability of gases at higher pressures or chemically aggressive gases, the permeameter pressure chamber, piping, fittings and valves in contact with the permeant would need to be constructed from AISI 316L stainless steel due to its resistance to corrosive atmospheres [40]. Samples could be made of any semipermeable material, but HDPE was used to validate the equipment as it is one of the most widely used polymers in the industry in general.

Although fluoroelastomer (Viton®) is an excellent elastomer for use in high-temperature applications also exhibits elevated chemical resistance and is the most used elastomeric material for sealing [41], the project of seals with elastomeric rings depends on factors such as operational conditions, the geometry of the part in which it will be installed and sealing material [42], the extrusion of the

sealing element being one of the main causes of leaks due to excessive gaps, high axial load and the usage of low hardness material, making the sealing system a source of leaks of difficult measurement during the operation of the equipment.

The impossibility laboratory validation of the results led to seeking validation through literature such as Flaconneche [7, 8], which suggests the validity of the equipment in presentation for polymers and polymer nanocomposites.

The permeameter being presented will also allow the verification of the permeability in blends and recycled polymers, which generally have additives such as plasticizers that tend to alter the polymer gas permeation [35], phenomena which have scarce information concerning them in literature.

Conclusion

The comparison of the results obtained with the data found in the literature suggests the validity of the medium pressure gas permeameter, indicating that the presented equipment can contribute to a better understanding of the gas transport phenomena in different polymers, as well as in the gas-polymer interactions in regard to its mechanical resistance and long-term chemical stability.

The permeameter being presented can be utilized to qualitatively indicate the gas permeability of different materials, showing the difference in its permeability coefficient (P), as well as to indicate if the use of certain additives such as colorants or plasticizers caused changes to the permeability of the polymer, suggesting whether the product presents differences in relation to the standard as well as indicating if the adequate distribution or exfoliation were present in the case of the addition of nanoclays considering the reduction of the gas permeability of the sample.

The presented permeameter will allow obtaining comparative experimental data that will assist in the production of new polymeric components, the quantification of the influence of parameters such as temperature and pressure that are closer to oil exploration reality on the transport coefficients and the performance of experiments with gases because offshore flexible pipes are generally subject to gas mixtures consisting mainly of methane, carbon dioxide and hydrogen sulfide, for example.

The low-cost equipment, its flexibility in using different combinations of polymers and gases, as well as its ease of operation are the main advantages of the presented permeameter, allowing its use in school laboratories or small production companies that need to check the permeability of their polymeric products.

The presented permeameter allows the acquisition of experimental data necessary for the design, development and testing of polymeric products such as the quantification of the influence of parameters such as pressure and temperature on the transport coefficients of pure gases and gas mixtures in polymers, blends, recycled polymers and polymeric nanocomposites even in conditions closer to the reality of the oil industry, as this information is scarcely available in the literature.

Acknowledgements Acknowledgements to Instituto Federal do Rio Grande do Sul, Universidade Federal de Santa Maria and Universidade Federal do Rio Grande do Sul.

Authors contributions GP: lead author, SP: collaborator, CAF: advisor.

Declarations

Conflict of interests The authors declare that they have no conflict of interest.

References

1. Graham T (1866) On the law of the diffusion of gases. Philos Mag J Sci 32:401–420
2. Nitrogen—Safety Data Sheet P-4631 (2020) https://www.praxair.com/-/media/corporate/praxairus/documents/sds/nitrogen/nitrogen-compressed-safety-data-sheet-sds-p4631.pdf. Accessed 20 Dec 2020
3. Argon—Safety Data Sheet P-4563 (2020) https://www.praxair.com/-/media/corporate/praxairus/documents/sds/argon/argon-gas-ar-safety-data-sheet-sds-p4563.pdf. Accessed 20 Dec 2020
4. Ammonia—Safety Data Sheet P-4562 (2020) https://www.praxair.com/-/media/corporate/praxairus/documents/sds/ammonia-nh3-safety-data-sheet-sds-p4562.pdf. Accessed 20 Dec 2020
5. Chlorine—Safety Data Sheet P-4580 (2020) https://www.praxair.com/-/media/corporate/praxairus/documents/sds/chlorine-cl-2safety-data-sheet-sds-p4580.pdf. Accessed 20 Dec 2020
6. Recommended Practice DNV-RP-J202, April 2010, Det Norske Veritas (2020). https://rules.dnvgl.com/docs/pdf/DNV/codes/docs/2010-04/RP-J202.pdf. Accessed 20 Dec 2020
7. Flaconnèche B, Martin J, Klopffer MH (2001) Permeability, diffusion and solubility of gases in polyethylene, polyamide 11 and poly (vinylidene fluoride). Oil Gas SciTechnol 56:261–278
8. Flaconnèche B, Martin J, Klopffer MH (2001) Transport properties of gases in polymers: experimental methods. Oil Gas SciTechnol 56:245–259
9. Craster B, Jones TG (2019) Permeation of a range of species through polymer layers under varying conditions of temperature and pressure: in situ measurement methods. Polymers 11:1056
10. Beckman IN, Syrtsova DA, Shalygin MG, Kandasamy P, Teplyakov V (2020) Transmembrane gas transfer: mathematics of diffusion and experimental practice. J MembrSci 601:117737
11. Fraga SC, Monteleone M, Lanč M, Esposito E, Fuoco A, Pilnáček K, Friess K, Carta M, Keown NBM, Izák P, Petrusová Z, Crespo JG, Brazinha C, Jansen JC (2018) A novel time lag method for the analysis of mixed gas diffusion in polymeric membranes by on-line mass spectrometry: method development and validation. J MembrSci 561:39–58
12. Verma G (2017) Polymer nanocomposites and coatings: the game changers. Trends App AdvPolym Mater 9:1–22
13. Prasad K, Nikzad M, Sbarski I (2018) Permeability control in polymeric systems: a review. J Polym Res 25:1–20

14. Kumar S, Sarita MN, Dilbaghi N, Tankeshwar K, Kim KH (2018) Recent advances and remaining challenges for polymeric nanocomposites in healthcare applications. ProgPolymSci 80:1–38
15. Chemical Book—CAS DataBase List—Nitrogen (2020) https://www.chemicalbook.com/ChemicalProductProperty_EN_cb2159243.htm. Accessed 20 Dec 2020
16. The Engineering Toolbox (2020) https://www.engineeringtoolbox.com/gases-solubility-water-d_1148.html. Accessed 20 Dec 2020
17. Paranapanema (2020) https://www.paranapanema.com.br/. Accessed 20 Dec 2020
18. Talbot D (2019) Corrosion science and technology. CRC New York
19. Maxfer (2020) https://www.maxfer.com.br/barra-de-aluminio/. Accessed 20 Dec 2020
20. Dow HDPE 35054L, Technical Data Sheet (2020) https://materials.ulprospector.com/pt/profile/default?e=141349. Accessed 20 Dec 2020
21. Cloisite 20A - Technical Data Sheet (2020) https://www.byk.com/en/additives/additives-by-name/cloisite-20-a.php. Accessed 20 Dec 2020
22. Deepthi MV, Sharma M, Sailaja R, Anantha P, Sampathkumaran P, Seetharamu S (2010) Mater Des 31:2051–2060
23. Tufan M, Akbas S, Yurdakul S, Güleç T, Eryılmaz H (2016) Effects of different filler types on decay resistance and thermal, physical, and mechanical properties of recycled high-density polyethylene composites. Iran Polym J 25:615–622
24. Choudalakis G, Gotsis AD (2009) Permeability of polymer/clay nanocomposites: a review. EurPolym J 45:967–984
25. Manufacturer's Rubber and Supply—https://www.manuf-rubber.com/news/buna-vs-viton-seals-whats-the-difference/. Accessed 20 Dec 2020
26. Minamata Convention on Mercury—http://www.mercuryconvention.org. Accessed 20 Dec 2020
27. Decreto 9.470/2018—Promulga a Convenção de Minamata sobre Mercúrio (2020) http://www2.camara.leg.br/legin/fed/decret/2018/decreto-9470-14-agosto-2018-787075-publicacaooriginal-156192-pe.html. Accessed 20 Dec 2020
28. TA Instruments—https://www.tainstruments.com. Accessed 20 Dec 2020
29. Canevarolo SV (2004) Técnicas de caracterização de polímeros. Artliber, São Paulo 430:2004
30. Brandrup J, Immergut EH, Grulke EA (2003) Polymer handbook: permeability and diffusion data, 4th edn. Wiley, New York
31. Teplyakov V, Meares P (1990) Correlation aspects of the selective gas permeabilities of polymeric materials and membranes. Gas Sep Purif 4:66–74
32. Yasuda H, Rosengren KJ (1970) Isobaric measurement of gas permeability of polymers. J ApplPolymSci 14:2839–2877
33. Brandup J, Immergut EH, Grulke EA (1999). In: Zhu L, Chiu FC, Fu Q, Quirk RP, Cheng SZD (eds) Polymer handbook, 4th edn. John Wiley, New York
34. Mark JE (1999) Polymer data handbook. Oxford University Press
35. Comyn J (1985) Polymer permeability. Chapman & Hall, London
36. Sears JK, Darby JR (1982) The technology of plasticizers. Wiley, New York
37. Vasile C (2018) Polymeric nanocomposites and nanocoatings for food packaging: a review. Materials 11:1834
38. Guo F, Aryana S, Han Y, Jiao Y (2018) A review of the synthesis and applications of polymer–nanoclay composites. ApplSci 8:1696
39. Chelladurai V, Jayas DS (2018) Nanoscience and nanotechnology in foods and beverages, 1st edn. CRC, New York
40. Specification sheet—alloy 316/316L (UNS S31600, S31603) W. n. 1.4401, 1.4404 (2020) https://www.sandmeyersteel.com/images/316-316l-317l-spec-sheet.pdf. Accessed 20 Dec 2020
41. The Seak Man's O-Ring Handbook, 1st edn. (2004) Viton ®—EPM, Inc.
42. Martini LJ (1984) Practical seal design. Taylor & Francis, New York

5.3 Artigo 3

Research Article

Gas permeameter for polymers and nanocomposites: a new equipment

Gilberto João Pavani[1] · Sérgio Adalberto Pavani[2] · Carlos Arthur Ferreira[3]

Received: 20 July 2022 / Accepted: 27 September 2022
Published online: 12 October 2022

Abstract
Information on the gas transport coefficients in the permeation of homogeneous semipermeable materials such as semicrystalline polymers under extreme pressures and temperatures is rarely found in the literature. Therefore, the objective of this work is to showcase innovation regarding the accuracy and usability of the medium pressure and temperature gas permeameter suitable for polymeric and polymeric nanocomposite plates built by the authors, which was tested with nitrogen at 1 MPa and 69 °C (342.15 K) permeating pure high density polyethylene samples (HDPE) and HDPE samples with added nanoclay, redoing the tests published in a previous work on the subject. The results were compared against data obtained previously and information present in the literature, validating the permeameter presented in this work, which is capable of analyzing gas permeability under the described conditions with greater accuracy and ease of operation than the previous model for the values of the transport coefficients of nitrogen permeating HDPE, demonstrating that the implemented improvements and advances were adequate, allowing the measurement of the transport properties of gases permeating polymeric and nanocomposite plates, necessary information for the design of risers for the transportation of oil and natural gas, for example.

Article highlights

- Information on gas transport coefficients under extreme pressure and temperature conditions, such as oil and gas prospecting, is still rare in the literature, making it necessary to construct and validate a permeameter adequate to provide valid information about these properties.
- The equipment in the presentation is a low-cost medium-pressure and temperature gas permeameter with results validated by literature, permitting its use on semipermeable materials and presenting improvements and advances in relation to the model presented in previous work.
- The permeameter was validated with nitrogen on pure high density polyethylene (HDPE) samples and with HDPE samples with nanoclay, determining the transport coefficient of nitrogen in HDPE with greater accuracy than the previous model.

Keywords Gas permeability · Polyethylene · Nanocomposite · Permeameter · Innovation

✉ Gilberto João Pavani, gilberto.pavani@restinga.ifrs.edu.br | [1]Instituto Federal do Rio Grande do Sul, Bento Gonçalves, Brazil. [2]Universidade Federal de Santa Maria, Santa Maria, Brazil. [3]Universidade Federal do Rio Grande do Sul, Porto Alegre, Brazil.

SN Applied Sciences (2022) 4:300 | https://doi.org/10.1007/s42452-022-05190-x

SN Applied Sciences
A SPRINGER NATURE journal

1 Introduction

The study of gas transport phenomena needs to be deepened to allow for greater understanding of the interactions between the molecules of a gas under pressure and a certain temperature for a particular polymer, especially for industrial gases such as nitrogen [1] and carbon dioxide [2] and toxic gases such as methane [3] and hydrogen sulfide [4], commonly found in the extraction of oil and natural gas [5], the storage and transportation of which in polymeric containers has been discussed in preceding works [6, 7].

The transportation and storage of industrial gases at high pressure generally occurs in metallic cylinders and gas tanks [8], but these containers are heavy and difficult for workers to handle, causing the occurrence of occupational accidents and work-related illnesses that could be reduced with their replacement by polymeric congeners, such as the CNG-4 vehicular natural gas reservoirs defined by ISO 11439: 2013.

The properties inherent to polymers [9–11] justify their growing use, demanding greater knowledge of transport phenomena at high pressures and temperatures for polymers with thick layers to avoid these issues [12], which is rare in the literature [13, 14]. In the packaging industry, for example, gaseous permeability limits the shelf life of foods, mainly in Meals Ready to Eat (MRE), which must be stored for up to 3 (three) years for military use [15] and up to 5 (five) years for use in space missions [16].

With the intent of determining the gas permeability of distinct polymeric materials under conditions of pressure and temperature similar to those found in oil and gas extraction operations, the current model of the permeameter was manufactured in compliance with the ASTM D1434-82 (2015) e1 standard, which determines quantitative attributes for the permeation of pure gases through membranes of varying thicknesses.

As commercially available permeameter models [17–19] used in permeability tests have a high cost, the objective of this study was to build a new model of a low-cost medium pressure and temperature gas permeameter, permitting its use on semipermeable materials like polymers and polymer nanocomposites, presenting advancements in accuracy and operability in relation to the equipment presented in a previous work [20].

The precision of the current equipment is acceptable in qualitative terms, i.e., indicating the gas permeability of semipermeable materials, and revealing the difference in the permeability coefficients between pure polymer samples and the polymer samples with nanoclay, as well as in quantitative terms, as shows Table 2 presented below.

The permeameter in presentation allows the determination of gas transport coefficients at low and medium pressures in semipermeable materials, using the volumetric procedure according to ASTM D1434, and has some advantages over a commercial permeameter, such as low cost and flexibility in the use of various combinations of gases and polymers or other semipermeable materials.

2 Materials and methods

The current equipment was designed to more accurately determine the gas transport coefficients in polymers and polymer composites at medium pressures and temperatures, adopting the volumetric procedure in accordance with ASTM D1434—82 (2015) e1, in which the gas passage through the sample is shown by the reduction of the water level inside a sealed pipette, that is, the volume of displaced water corresponds to the volume of permeated gas.

The validation experiment was performed with nitrogen, with pressure lowered to 1 MPa (manometric pressure) and a temperature of 69 °C, on pure high density polyethylene (HDPE) samples and HDPE samples with nanoclay, forming a polymer nanocomposite with better gas barrier properties [21–23], replicating the test conditions of the experiment presented in a previous work [20].

2.1 Utilized materials

As in the previous work, the following materials were used for the manufacturing and validation of the current model of the permeameter:

1. Commercially pure nitrogen (N_2) in bottles at 21.1 °C and 1 atm (0.1 MPa) under 200 bar (20 MPa) nominal pressure, chosen due to safety restrictions [24], supplied by the Oxisul company from Brazil;
2. Pressure regulating valve for gases with inlet pressure of 200 bar (20 MPa) and outlet pressure of 10 bar (1 MPa), produced by company V8 Brasil from Brazil;
3. Line pressure gauge, scale 0–60 kgf/cm^2—Class B, allowing the verification of low line pressure, produced by company Metalúrgica SCAI from Brazil;
4. HVAC (heating, ventilating and air conditioning) flexible copper tubing with a nominal diameter of 6.35 mm and a maximum working pressure of 11.4 MPa, produced by company Paranapanema from Brazil;
5. AISI 316 stainless steel was used in the permeation chamber because of its high resistance to corrosion, excellent mechanical properties, resistance to a combination of higher temperatures and higher pressures,

weldability and excellent stability against acids [25], supplied by company Maxfer from Brazil;

6. A 10 ml graduated glass pipette which was heat-sealed at the upper end, produced by company Laborglas from Brazil.

2.2 Equipment description

The current permeameter measures the quantity of gas passing through a unit of the parallel surface of a membrane in a unit of time through the differential pressure test, known as the manometric method, where one side of the membrane is submitted to the test gas flow while the other side is evacuated.

The permeation of the gas through the sample is stimulated by this pressure difference, with its rate being defined by the pressure increase in the evacuated side at a given temperature.

The equipment consists of the following:

1. Gas supply system: nitrogen, capable of operating with different gases;
2. Permeation chamber: metallic body for the positioning of the samples, permitting the entry of the gas at high pressure and its exit at low pressure after permeating the sample, sealed with Ring Type Joints (RTJ), in accordance with standard DIN 11,851, shown in Fig. 1;
3. Sample: each specimen is positioned in a permeation chamber, and sealed with a RTJ;
4. Sealing system: manufactured in acrylonitrile butadiene rubber (Buna-N), 70 Shore A, due to its suitable mechanical and chemical properties [26], designed by the author;
5. Temperature control system: digital thermostat that permits adjustment and reading of the test temperature;
6. Data recording system: the gas permeated in the testing of each sample accumulates in a pipette with the underside (open) immersed in distilled water, the level of which gradually decreases as the gas flows in, allowing its periodic monitoring.

Despite the ASTM D1434—82 (2015) e1 standard recommending the use of mercury, the current permeameter used water in this experiment because Brazil is a signatory to the Minamata Convention on Mercury [27].

The permeation chamber is sealed with a RTJ connection to allow for the quick replacement of the samples, as the permeameter has 10 (ten) independent permeation chambers, which can be seen in Fig. 1c, permitting the testing of up to 10 (ten) samples simultaneously, sealed and inspected for leaks, including the gas pipe fittings.

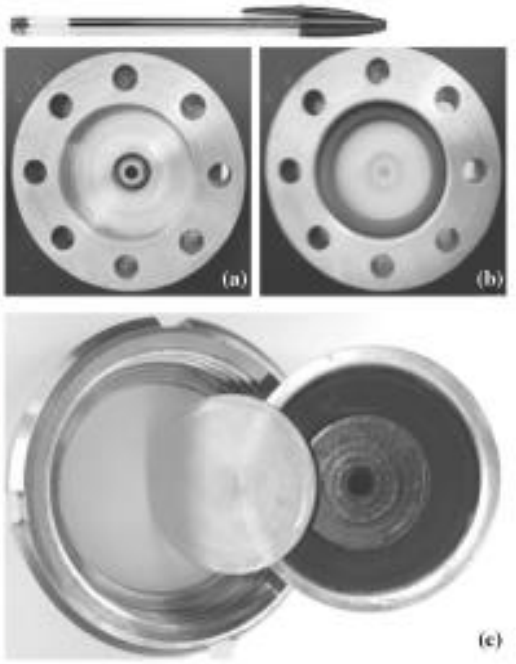

Fig. 1 Sealing system of the previous equipment with permeation chamber open without a sample (**a**), sample with O-ring (**b**) and permeation chamber of the current permeameter open with a sample and its sealing system (**c**)

The main change to the permeation chambers, in relation to the previous work, is their new format, a new sealing system, and the material with which they were built, which is AISI 316 stainless steel instead of 5052F naval aluminum, with 10 (ten) chambers instead of 5 (five), as shown in Fig. 2.

2.3 Operating procedure

The operating procedures were identical to those of the previous work [20], as we sought to compare the new results with the data obtained previously and those found in the literature.

The tests for the validation experiment of the equipment were performed with nitrogen, with the testing pressure set at 10 bar (1 MPa) and a temperature of 69 °C, on pure high density polyethylene samples (HDPE) and on HDPE samples with nanoclay.

Samples were produced from pellets as described in the previous work, and the diffusion area was considered as the only sample surface in contact with the gas, i.e., not considering the area in contact with the O-ring.

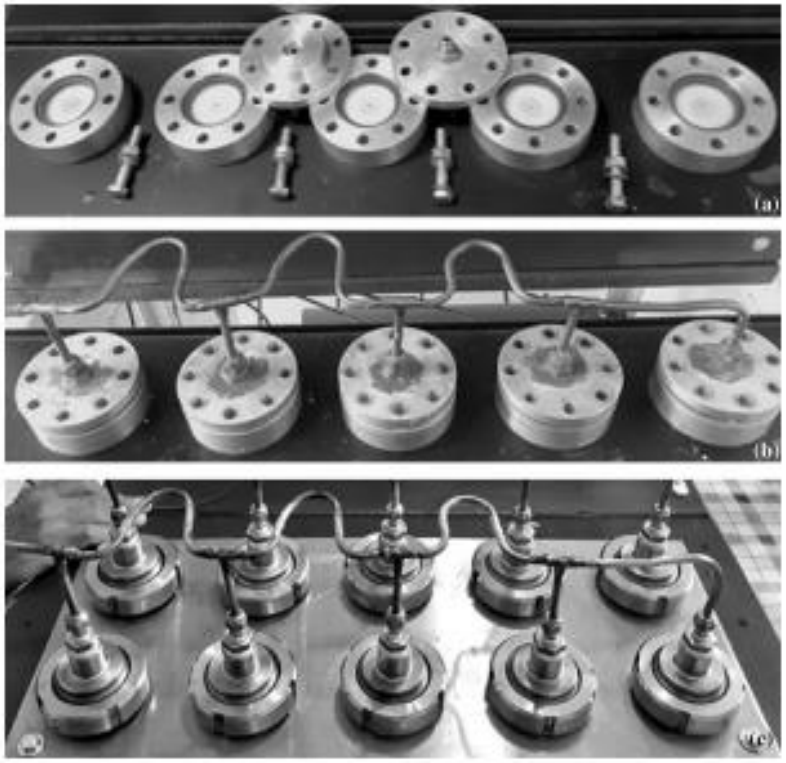

Fig. 2 Permeation chamber in naval aluminium in top view (**a**), sample with O-ring (**b**) of the previous equipment, and top view of the permeation chamber of the current permeameter (**c**)

Before the experiment, leakage tests are performed in each permeation chamber under the same pressure and temperature of the experiment with an AISI 316 stainless steel blind cover, with the same dimensions as the sample.

During the experiment, the permeation chambers remained in an electric oven at 69 °C, in accordance with Flaconnèche [13].

With the intent of evaluating the homogeneity of the dispersion of the nanoclay on the surfaces of the samples, we used scanning electron microscopy (SEM), as described in a previous work [20], whose Fig. 3 showed a cluster of nanoclay on the surface of the polymeric nanocomposite sample, indicating a failure in its distribution, i.e., an absence of the complete exfoliation of the nanoclay that would result in a significant reduction of the material's permeability.

As in the previous work [20], assuming there is a constant pressure differential that permits steady gas flow through a sample, the permeability coefficient is obtained by Eq. 1, where P is the permeability coefficient (cm^3 (STP)/cm s MPa), Q is the amount of gas that permeated the sample, l is the sample thickness, t is the time of the test, A is the sample area and p is the gas pressure upstream from the sample [14].

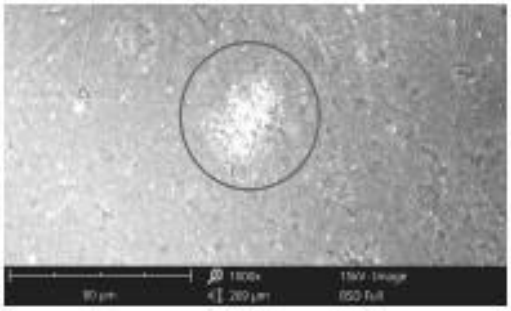

Fig. 3 SEM image of a Cloisite 20A nanoclay cluster

$$P = \frac{Ql}{tAp} \tag{1}$$

The amount of gas permeating the sample during time t is defined by Fick's second law [28], and the point where

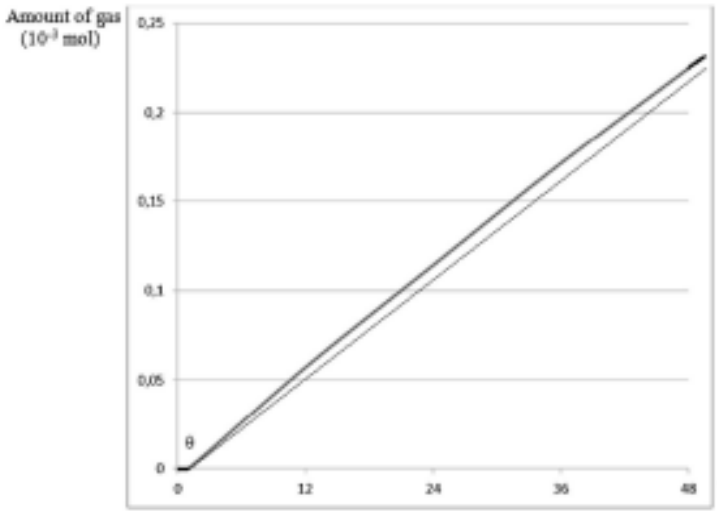

Fig. 4 Graph of nitrogen permeation results

the line intersects the axis is obtained by Eq. 2, where Θ is the time lag [29] and *D* is the diffusion coefficient.

$$\Theta = \frac{l^2}{6D} \quad (2)$$

3 Results

To discover the value of the permeability coefficient, the samples of pure HDPE were placed in contact with nitrogen for the time required to permeate 5 mL of the gas. In this experiment we recorded 46 h (thin line) with a standard deviation of 2% for 10 (ten) samples, less time than the previous experiment, which was 48 h (thick line) with a standard deviation of 3% for 10 (ten) samples [20], as shown in Fig. 4.

The samples of polymer nanocomposites that were in contact with nitrogen for 48 h had a permeation of 2 mL.

Table 1 shows that the sample presents characteristics similar to the polymer used by Flaconnèche [13], allowing comparison to the results obtained by the referred author.

Table 2 presents the testing conditions and the comparison of the results obtained by Flaconnèche [13], with the results of the current and of the previous experiments [20]. The results referring to the Polymer Handbook [30] serve as comparison terms for the presented values.

To validate the equipment using the values presented in the literature, the permeability coefficient (*P*) of the

Table 1 Characteristics of the polymers before permeation tests

Polymer	ρ (g/cm³)	T_f (°C)	ΔHf (J/g)	Xc (%)	Φa
Flaconnèche[a]	0.943	136	193	66	0.37
Sample current[b]	0.954[c]	130.96[d]	196.4[d]	67[e]	0.37[f]
Polymer handbook[g]	0.954				

ρ Density of the polymer (g/cm³), Tf Melting point temperature (°C), ΔHf Enthalpy of fusion (J/g), Xc Degree of crystallinity (weight fraction) (%), Φa Volume fraction of the amorphous phase

[a]Table 2 in [13]

[b]Identical to previous work [20]

[c]Standard ASTM D1505

[d]Differential Scanning Calorimetry (DSC) described ni [20]

[e]Calculated in accordance with Eq. 1 [20]

[f]Calculated in accordance with Eq. 2 [13]

[g]VI/546 Permeability and Diffusion Data in [30]

Table 2 Transport coefficients of nitrogen in pure HDPE samples

Polymer	Φa	*T* (°C)	*P* (10^{-7} cm³(STP)/cm·s·MPa)
Flaconnèche[a]	0.37	69	1.0
Sample current	0.37	69	1.3
Sample previous[b]	0.37	69	1.4
Polymer Handbook[c]		25	1.1

Φa Volume fraction of the amorphous phase, *T* Temperature (°C), P Permeability coefficient (10^{-7} cm³(STP)/cm·s·MPa)

[a]Table 6 in [13]

[b]Table 2 in [20]

[c]VI/546 Permeability and diffusion data [30]

samples was calculated using Eq. 1, the result of which is shown in Table 2 for the pure HDPE samples.

Measurements began to be taken after the steady-state flow with a constant gas transmission rate was attained, and the value shown in Table 2 represents the arithmetic average of the measurement made at the water level of each pipette, with a standard deviation of 10% due to the tolerance of the graduated pipettes, measuring 10 (ten) individual samples of pure HDPE simultaneously, with the objective of reducing experimental uncertainties.

For nitrogen permeation in pure HDPE samples, the calculated value of P is 1.3E-07 cm^3(STP)/cm s MPa, a value closer to those found in the literature than the result obtained in the previous experiment [20], which is consistent with Flaconnèche [13]. The difference in values is possibly because of the use of samples with thicknesses (l = 0.6 mm) at pressures (p = 1 MPa) lower than those presented by Flaconnèche.

The calculated value of P for the polymer nanocomposite samples with nanoclay is equal to 0.55E-07 cm^3 (STP)/cm s MPa and presented barrier properties inferior to those presented in the literature [31–33] because of the formation of dispersed clusters of nanoclay on the surface of these samples not presenting any meaningful differences in relation to the previous experiment [20].

4 Final considerations

Even though the current permeameter determines the transport coefficient of nitrogen in HDPE with greater precision than the previously presented equipment [20], there is room for further testing with a broader range of different gases, pressures and temperatures similar to those found in flexible risers used in the exploration of oil and gas, justifying the construction of the permeation chamber with AISI 316 stainless steel, which presents greater resistance to hydrogen sulphide [34], than the 5052F naval aluminum [35] used in the previously permeameter model.

The current permeameter configuration allows the testing of up to 10 (ten) samples simultaneously, allowing for a reduction in measurement uncertainty [36] when obtaining the values of the transport coefficients of gases, having greater accuracy than the equipment mentioned previously, as shown in the Table 2, which had 5 (five) chambers, requiring double the amount of experiments to test the same number of samples, increasing the risk of errors inherent to the process.

The use of RTJ connections is justified, as the previous equipment presented problems related to sealing, as each permeation chamber demanded the tightening of 8 (eight) screws to prevent leaks, totalling 80 (eighty) screws per experiment, and reducing its operability. However, the torque wrench used to tighten the screws had a tolerance of ± 5%, allowing for tightening differences that allowed the formation of microleaks not detectable through conventional means.

However, the RTJ sealing system demands a specific sealing ring design to allow the gas flow and to accommodate the sample adequately, preventing leaks, because the design of elastomeric seals depends on factors such as operating conditions, the sealing material [37] and the shape and dimensions of the piece in which it will be installed.

The results differ from the literature [38–40] because of factors related to testing conditions such as temperature, which affects the mobility of the polymeric chains and of the permeating gas, influencing the permeability coefficient [41], the density of the polymer, which influences the free volume through which the gas can permeate in semicrystalline polymers [42] and imprecisions inherent to the testing method.

The fact that the results are closer to those of Flaconnèche [13] and those found in the Polymer Handbook [30] indicates that, despite the differences shown in the data, the improvements and advances implemented were meaningful and that the permeameter being presented is valid.

The permeameter allows the measurement of gas permeability in semipermeable materials with thick layers, such as polymers used in risers, as the thinner the layer is, the greater the influence of the pores in the measurement of gas permeability. In addition to the intrinsic voids originating from their molecular structure, the polymers can also present faults known as pores, originating from failures during their processing, such as the inclusion of air, as well as defects occurring during work, such as fissures due to stress or chemical swelling [43].

In polymeric films, the presence of pores is decisive when determining gas permeation, as there is a greater possibility of the formation of channels that traverse through its thickness, but their detection demands advanced laboratory techniques such as energy-dispersive X-ray spectroscopy (EDS) [44] and positron annihilation lifetime spectroscopy (PALS) [45].

However, the size of pores in polymeric membranes can be estimated across equations based on gas permeability in laboratory tests [46], in which the use of permeameters can be helpful. Although the permeability coefficient is independent of the thickness of the sample

for a certain polymer, it can suffer considerable changes due to the material's void ratio, i.e., if the sample presents a permeability coefficient much greater than that of a thick plate of the same material, under the same test conditions, there is a possibility that the sample will show a greater void content than that of the thick plate, which justifies the increase in the amount of permeated gas.

The permeameter in presentation has a low production cost, approximately €4,850.00 (four thousand eight hundred and fifty euros), allowing the determination of the transport coefficients of gases at low and medium pressures in plates of semipermeable materials, using the volumetric procedure in accordance with ASTM D1434, which is a more economical alternative than other commercially available models of this type of equipment with similar purposes, such as the Rapid Helium Permeameter QHV-4 [47], which can cost up to €90,000.00 (ninety thousand euros).

The current permeameter shows improvements and advances, as it was designed and built making use of the experience acquired from previous prototypes, in accord with the norms for the formulation of a systematic project, allowing greater reliability in the measurement of the permeability of different gases through semipermeable materials with temperatures and pressures closer to those found in the reality of oil and gas exploration.

Although the objectives proposed in this work were achieved, the development of a new prototype continued in the process of patenting, whose intended improvements in relation to the permeameter being presented are listed below:

1. The test gas cylinder is connected to a distributor with valves and individual quick couplings for the polymeric hoses that carry the test gas, allowing the same length to be maintained up to each of the 10 (ten) permeation chambers;
2. The sample is placed in the permeation chamber and pressed against the base by an O-ring during the closing of the permeation chamber;
3. The permeation chambers are arranged horizontally on the permeameter so that each polymeric hose that carries the gas to the pipette has the same length;
4. The permeation chambers are sealed by interference by the action of a hydraulic closing system that composes the permeameter, facilitating the assembly and practically eliminating interfacial leaks, being the main difference in relation to the equipment in presentation;
5. The pressure exerted by the hydraulic closing system must not exceed the minimum yield strength of the material that constitutes the permeation chamber so that the metal used remains in its elastic zone, which in the case of AISI 316 stainless steel is 290 MPa [48].

The following figure shows the schematic design of the permeameter under development:

5 Conclusions

The comparison of the obtained results with the data presented in the literature indicates the validity of permeameter presented in this work to contribute to the greater comprehension of gas transport phenomena in different polymers and of gas-polymer interactions in long duration experiments under extreme temperature and pressure conditions.

The current permeameter can be employed to qualitatively indicate the gas permeability of semipermeable materials, for example, reveal the difference in the permeability coefficients between pure polymer samples and the polymer samples with nanoclay, verifying if there was adequate distribution or exfoliation, indicating the void content in the pure material, or even verifying if the use of additives causes changes in the gas permeability of the polymer, contributing to the development of new polymeric products.

The permeameter presented in this work determines the transport coefficient of nitrogen in HDPE with greater precision than the previously presented equipment [20], proving that the implemented improvements were adequate. Despite the small deviance found in the results of the previous experiment, there was a tendency of increased errors with the working pressure and thickness of the sample, which increases the permeation time, in accord with Eq. 1, allowing measurement errors.

This equipment has some advantages over a commercial permeameter, such as low cost and flexibility in the use of various combinations of gases and polymers or other semipermeable materials.

Despite the significant advancements made compared to the previous equipment [20] concerning accuracy and operability, the presented permeameter still requires the use of the torque wrench to close the RTJ system, as well as a sealing ring, the material of which tends to wear over time, allowing leaks. Therefore, the development of a new equipment such as the one shown in Fig. 5 is necessary.

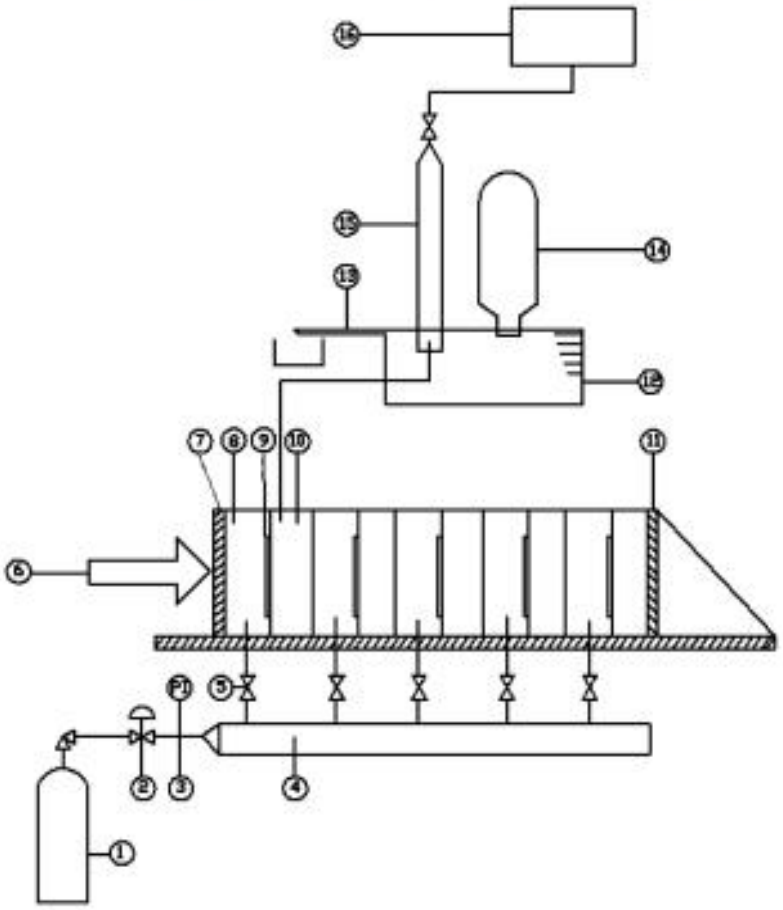

Fig. 5 Schematic drawing of the permeameter under development with accessories. 1. High pressure bottle containing test gas, 2. Pressure regulating valve, 3. Line pressure gauge, 4. Test gas distributor, 5. Permeation chamber shut-off valve (10x), 6. Hydraulic system for closing the permeation chambers, 7. Moving steel plate, 8. Test gas inlet in the permeation chamber—upstream (10x), 9. Sample, 10. Test gas inlet in the permeation chamber—downstream (10x), 11. Fixing and closing structure of the permeation chambers, 12. Liquid deposit for measuring system, 13. Outlet of excess liquid from the reservoir, 14. Reservoir liquid replacement system, 15. Measuring system for the permeate gas test (10x), 16. Vacuum generator

Acknowledgements Acknowledgments to Instituto Federal do Rio Grande do Sul, Universidade Federal de Santa Maria and Universidade Federal do Rio Grande do Sul for technical support.

Author contributions GJP: Lead author; SAP: Collaborator; CAF: Advisor.

Funding This research did not receive any specific grants from funding agencies in the public, commercial or not for-profit sectors.

Declarations

Conflict of interest Conflict of interests are not applicable.

References

1. Nitrogen compressed, Safety Data Sheet 2022. https://www.lindeus.com/-/media/corporate/praxairus/documents/sds/nitrogen/nitrogen-compressed-safety-data-sheet-sds-p4631.pdf?la=en Accessed 25 August 2022
2. Carbon dioxide compressed, Safety Data Sheet 2022. https://www.lindeus.com/-/media/corporate/praxairus/documents/sds/carbon-dioxide/carbon-dioxide-medipure-co2-safety-data-sheet-sds-p4574.pdf?la=en Accessed 25 August 2022
3. Methane compressed, Safety Data Sheet 2022. https://www.lindeus.com/-/media/corporate/praxairus/documents/sds/

methane-ch4-safety-data-sheet-sds-p4618.pdf?la=en Accessed 25 August 2022
4. Hydrogen sulfide compressed, Safety Data Sheet 2022. https://www.lindeus.com/-/media/corporate/praxairus/documents/sds/hydrogen/hydrogen-sulfide-h2s-safety-data-sheet-sds-p4611.pdf?la=en Accessed 25 August 2022
5. Speight JG (2015) Handbook of offshore oil and gas operations. Elsevier. https://doi.org/10.1016/C2009-0-19144-4
6. Pavani GJ, Pavani SA, Ferreira CA (2015) Application of polymeric nanocomposites and carbon fiber composites in the production of natural gas reservoirs. J Nanomater. https://doi.org/10.1155/2015/658727
7. Pavani GJ, Pavani SA, Ferreira CA. Recycling of polymer nanocomposites of carbon fiber reinforced compressed natural gas reservoirs. In: Keka Talukdar (ed) Nanomaterials-based composites for energy applications: emerging technology and trends, 1 ed, Apple Academic Press. 2020. ISBN 978-1771888066
8. MarketsandMarkets 2022. https://www.marketsandmarkets.com/Market-Reports/industrial-gases-metal-fabrication-market Accessed 25 August 2022
9. Mark JE (ed). Physical properties of polymers handbook. Springer. 2007. ISBN 978-0387312354
10. Gunther Hartwig. Polymer properties at room and cryogenic temperatures. Springer. 1995. ISBN 978-0306449871
11. Walter P, Heinemann J, Ebeling H, Mäder D, Trinkle S, Mülhaupt R (2001) Correlations between chain branching, morphology development and polymer properties of polyethenes. In: Blom R, Follestad A, Rytter E, Tilset M, Ystenes M (eds) Organometallic catalysts and olefin polymerization. https://doi.org/10.1007/978-3-642-59465-6_27
12. Det Norske Veritas, Recommended Practice DNV-RP-J202, 2010. 2022. https://rules.dnvgl.com/docs/pdf/DNV/codes/docs/2010-04/RP-J202.pdf Accessed 25 August 2022
13. Flaconnèche B, Martin J, Klopffer MH (2001) Permeability, diffusion and solubility of gases in polyethylene, polyamide 11 and poly (vinylidene fluoride). Oil Gas Sci Technol–Revue d'IFP Energies Nouv. https://doi.org/10.2516/ogst:2001023
14. Flaconnèche B, Martin J, Klopffer MH (2001) Transport Properties of Gases in Polymers: experimental methods. Oil Gas Sci Technol–Revue d'IFP Energies Nouv. https://doi.org/10.2516/ogst:2001022
15. Wornick Foods. 2022. http://wornick.com/militaryrations/military-faq/ Accessed 25 August 2022
16. NASA. 2022. https://www.nasa.gov/content/space-food-systems Accessed 25 August 2022
17. Permeameter GDP-C. Coesfeld material test. 2022. www.coesfeld.com Accessed 25 August 2022
18. Permeameter GP-100A-B. Porous materials Inc. (PMI). 2022. www.pmiapp.com Accessed 25 August 2022
19. Permeameter QHV-4, Vinci technologies. 2022. www.vinci-technologies.com Accessed 25 August 2022
20. Pavani GJ, Pavani SA, Ferreira CA (2021) Gas permeameter in polymer nanocomposite plates: construction and validation. Iran Polym J. https://doi.org/10.1007/s13726-021-00915-y
21 Verma G (2018) Polymer nanocomposites and coatings: the game changers. In: Nayak SK, Mohanty S, Unnikrishnan L (eds) Trends and applications in advanced polymeric materials. Scrivener Publishing LLC. https://doi.org/10.1002/9781119364795
22. Prasad K, Nikzad M, Sbarski I (2018) Permeability control in polymeric systems: a review. J Polym Res. https://doi.org/10.1007/s10965-018-1636-x
23. Kumar S, Sarita MN, Dilbaghi N, Tankeshwar K, Kim KH (2018) Recent advances and remaining challenges for polymeric nanocomposites in healthcare applications. Prog Polym Sci. https://doi.org/10.1016/j.progpolymsci.2018.03.001
24. The Engineering Toolbox. 2022. https://www.engineeringtoolbox.com/gases-solubility-water-d_1148.html Accessed 25 August 2022
25 Talbot DEJ, Talbot JDR (eds) (2018) Corrosion science and technology. CRC. https://doi.org/10.1201/9781351259910
26. Manufacturer's Rubber and Supply. 2022. https://www.manufrubber.com/news/buna-vs-viton-seals-whats-the-difference Accessed 25 August 2022
27. Minamata Convention on Mercury. 2022. http://www.mercuryconvention.org Accessed 25 August 2022
28. Beckman IN, Syrtsova DA, Shalygin MG, Kandasamy P, Teplyakov V (2020) Transmembrane gas transfer: mathematics of diffusion and experimental practice. J Membr Sci. https://doi.org/10.1016/j.memsci.2019.117737
29. Fraga SC, Monteleone M, Lanč M, Esposito E, Fuoco A, Pilnáček FK, Carta M, Keown NBM, Izák P, Petrusová Z, Crespo JG, Brazinha C, Jansen JC (2018) A novel time lag method for the analysis of mixed gas diffusion in polymeric membranes by on-line mass spectrometry: method development and validation. J Membr Sci. https://doi.org/10.1016/j.memsci.2018.04.029
30. Brandrup J, Immergut EH, Grulke EA (ed.) (2003) Polymer Handbook. Wiley. ISBN 978-0-471-47936-9
31. Vasile C (2018) Polymeric nanocomposites and nanocoatings for food packaging: a review. Materials. https://doi.org/10.3390/ma11101834
32. Guo F, Aryana S, Han Y, Jiao Y (2018) A review of the synthesis and applications of polymer-nanoclay composites. Appl Sci. https://doi.org/10.3390/app8091696
33. Chelladurai V, Jayas DS. Nanoscience and nanotechnology in foods and beverages. CRC. 2018. ISBN 978-1498760638
34. Kane RD, Trillo EA, Maligas MN, Coles M, Turbeville E, Operational limits for austenitic stainless steels in h_2s containing environments, Corrosion 2006, NACE-06156, 2006. 2022. https://onepetro.org/NACECORR/proceedings-abstract/CORR06/All-CORR06/NACE-06156/118111 Accessed 25 August 2022
35. Craig BD, Anderson DS, Handbook of corrosion data. ASM International, 2002. ISBN 0-87170-518-4
36. Evaluation of measurement data–guide to the expression of uncertainty in measurement (2008). JCGM
37. Martini LJ. Practical seal design. Taylor and Francis. 1984. ISBN 0-8247-7166-4
38. Yasuda H, Rosengren KJ (1970) Isobaric measurement of gas permeability of polymers. J Appl Polym Sci. https://doi.org/10.1002/app.1970.070141117
39. Zhu L, Chiu F-C, Fu Q, Quirk RP, Cheng SZD. Physical constants of poly(ethylene), V/9 In: Brandrup J, Immergut EH, Grulke EA (eds.), Polymer Handbook, Wiley. 1999. ISBN 978-0471166283
40. Mark JE (ed.) Polymer data handbook. Oxford University Press. 2009. ISBN 978-0195181012
41. Comyn J (ed) (1985) Polymer permeability. Chapman and Hall. https://doi.org/10.1007/978-94-009-4858-7
42. Sears JK, Darby JR (1982) The technology of plasticizers. Wiley. https://doi.org/10.1002/pol.1982.130200810
43. Gladysz GM, Chawla KK. Intrinsic voids in polymers. In: Voids in materials: from unavoidable defects to designed cellular materials, Elsevier. 2015. ISBN 978-0-444-56367-5
44. Chinaglia CR, Correa CA. Análise de falhas em materiais através de técnicas avançadas de microscopia. Polímeros: Ciência e Tecnologia Jul/Set. 1997:19-23
45. Oka T, Jinno S, Fujinami M (2009) Analytical methods using a positron microprobe. Anal Sci. https://doi.org/10.2116/analsci.25.837

46. Yasuda H, Tsai JT (1974) Pore size of microporous polymer membranes. J Appl Polym Sci. https://doi.org/10.1002/app.1974.070180316
47. Permeameter N530, GBPI. 2022. https://www.gbpitester.com/gas-permeability-analyzer-for-testing-packaging-material-gtr-n530_p3.html Accessed 25 August 2022
48. Boyer HE, Gall TL (1984) Metals Handbook - Desk Edition. Am Soc Met. ISBN 978-0871701886

6. CONCLUSÃO

A comparação dos resultados apresentados no Artigo 3 com os dados presentes na literatura e no Artigo 2 indica a validade do referido equipamento que pode contribuir para a maior compreensão dos fenômenos de transporte de gás em polímeros e das interações gás-polímero em experimentos de longa duração em temperaturas e pressões mais próximas da realidade industrial.

O permeâmetro acima referido poderá ser empregado para indicar quantitativamente a permeabilidade de diferentes gases em materiais semipermeáveis, mostrar a diferença dos coeficientes de permeabilidade entre amostras de polímeros puros e de nanocompósitos poliméricos, indicar o teor de vazios ou verificar se o uso de aditivos provoca alterações na permeabilidade gasosa, por exemplo.

O permeâmetro apresentado pode determinar o coeficiente de permeabilidade do nitrogênio em membranas de polietileno de alta densidade puro com maior precisão que o equipamento apresentado no Artigo 2, comprovando que as melhorias implementadas foram adequadas além de possuir vantagens sobre os permeâmetros comerciais como baixo custo de produção e possibilidade de utilização de diferentes combinações de gases e polímeros ou outros materiais semipermeáveis.

A sugestão de trabalhos futuros é o desenvolvimento de um novo permeâmetro conforme descrito ao final do Artigo 3, visando reduzir eventuais erros operacionais, pois apesar dos avanços significativos realizados em relação ao equipamento descrito no Artigo 2 em termos de precisão e operacionalidade, o permeâmetro apresentado no Artigo 3 ainda requer o uso do torquímetro para fechamento do sistema RTJ, bem como um anel de vedação, cujo material tende a se desgastar ao longo do tempo, permitindo vazamentos,.

REFERÊNCIAS BIBLIOGRÁFICAS

1. Mark JE (ed.) (2007) *Physical Properties of Polymers Handbook*, Springer, ISBN 978-0387312354

2. Walter P, Heinemann J, Ebeling H, Mäder D, Trinkle S, Mülhaupt R (2001) *Correlations Between Chain Branching, Morphology Development and Polymer Properties of Polyethenes* In: Blom R, Follestad A, Rytter E, Tilset M, Ystenes M (eds) Organometallic Catalysts and Olefin Polymerization. Springer, https://doi.org/10.1007/978-3-642-59465- 6_27

3. Recommended Practice DNV-RP-J202, April 2010, Det Norske Veritas - https://rules.dnvgl.com/docs/pdf/DNV/codes/docs/2010-04/RP-J202.pdf. Acesso em 30 de outubro de 2022

4. Flaconnèche B, Martin J, Klopffer MH (2001) *Permeability, Diffusion and Solubility of Gases in Polyethylene, Polyamide 11 and Poly* (vinylidene fluoride). Oil & Gas Science and Technology - Revue d'IFP Energies nouvelles 56(3): 261-278, https://doi.org/10.2516/ogst:2001023

5. Flaconnèche B, Martin J, Klopffer MH (2001) *Transport Properties of Gases in Polymers: experimental methods*. Oil & Gas Science and Technology - Revue d'IFP Energies nouvelles 56(3): 245-259, https://doi.org/10.2516/ogst:2001022

6. Craster B, Jones TG (2019) *Permeation of a Range of Species through Polymer Layers under Varying Conditions of Temperature and Pressure* In: Situ Measurement Methods. Polymers, https://doi.org/10.3390/polym11061056

7. Baxter MR (1995) *Product Design - A Practical Guide to Systematic Methods of New Product Development*, CRC, ISBN 978-0748741977

8. *A Guide to the Project Management Body of Knowledge* - PMBOK Guides (2004) Project Management Institute, ISBN 1-930699-45-X

9. Permeameter GDP-C, Coesfeld Material Test - www.coesfeld.com Acesso em 30 de outubro de 2022

10. Permeameter GP-100A-B, Porous Materials Inc. - www.pmiapp.com Acesso em 30 de outubro de 2022

11. Permeameter QHV-4, Vinci Technologies - www.vinci-technologies.com Acesso em 30 de outubro de 2022

12. Martins GAS (1999) *Informações sobre Manuseio e Estocagem de Polietilenos e Polipropilenos,* Boletim Técnico n. 14, OPP Petroquímica S.A

13. Guitián R (1995) *Polietilenos*, Plástico Moderno, n. 275, pp. 45-48

14. Miles DC, Briston JH (1965) *Polymer Technology,* Temple Press Book, London, ISBN 978-0820602554

15. Doak KW (1986) *Ethylene Polymers* In: Mark HM, Bikales NM, Overberg CG, Menges G, *Encyclopedia of Polymer Science and Engineering*, John-Wiley & Sons, New York, v. 6, ISBN 978-0471800507

16. Domininghaus H (1993) Plastics for Engineers: materials, properties, applications. Munich: Hanser Publishers, ISBN 978-3446157231

17. Ward IM, Sweeney J (2004) *An Introduction to the Mechanical Properties of Solid Polymers*, 2 ed, Wiley, ISBN 978-0471496267

18. Vasile C (2000) *Handbook of Polyolefins*, 2 ed, CRC Press, ISBN 9780824786038

19. Neves CJA (1999) *Resistência Química de PE's a Vários Reagentes Químicos*, Boletim Técnico n. 13, OPP Petroquímica S.A.

20. Exxon - http://www.exxon.com Acesso em 30 de outubro de 2022

21. Vasile C (2005) *Practical Guide to Polyethylene*, Smithers Rapra Technology, ISBN 978-1859574935

22. Chanda M, Roy SK (2006) *Plastics Technology Handbook*, 4 ed, CRC Press, ISBN 978-0849370397

23. Coutinho FMB, Mello IL, Maria LCS (2003) *Polietileno: Principais Tipos, Propriedades e Aplicações*, Polímeros: Ciência e Tecnologia, v.13, n.1, pp.1-13, http://dx.doi.org/10.1590/S0104-14282003000100005

24. Cho JW, Paul DR (2001) *Nylon 6 nanocomposites by melt compounding*, Polymer 42:1083–94, https://doi.org/10.1016/S0032-3861(00)00380-3

25. McNally T, Murphy WR, Lew CY, Turner RJ, Brennan GP (2003) *Polyamide-12 layered silicate nanocomposites by melt compounding*, Polymer 44:2761–72, https://doi.org/10.1016/S0032-3861(03)00170-8

26. Solomon MJ, Almusallam AS, Seefeldt KF, Somwangthanaroj A, Varadan P (2001) Rheology of polypropylene/clay hybrid materials, Macromolecules 34:1864–72, https://doi.org/10.1021/ma001122e

27. Joly S, Garnaud G, Ollitrault R, Bokobza L, Mark JE (2002) *Organically Modified Layered Silicates as Reinforcing Fillers for Natural Rubber*, Chemistry Materials, American Chemical Society, https://doi.org/10.1021/cm020093e

28. Fischer H (2003) *Polymer nanocomposites: from fundamental research to specific applications*, Mater Sci Eng C, 23:763-72, https://doi.org/10.1016/j.msec.2003.09.148

29. Shunmugasamy VC, Xiang C, Gupta N (2015) Clay/Polymer Nanocomposites: Processing, Properties, and Applications, Hybrid and Hierarchical Composite Materials161-200, https://doi.org/10.1007/978-3-319-12868-9_5.

30. Sun L, Boo WJ, Clearfield A, Sue HJ.; Pham HQ (2008) Barrier properties of model epoxy nanocomposites, Journal of Membrane Science, v. 318, pp.129-136, https://doi.org/10.1016/j.memsci.2008.02.041

31. Yuan Q, Misra RDK (2006) Impact fracture behavior of clay-reinforced polypropylene nanocomposites, Polymer 47(12):4421-4433, https://doi.org/10.1016/j.polymer.2006.03.105

32. Manias E, Touny A, Wu L, Strawhecker K, Lu B, Chung TC (2001) Polypropylene/montmorillonite nanocomposites: review of the synthetic routes and materials properties, Chem Mater 13:3516–3523, https://doi.org/10.1021/cm0110627

33. Zanetti M, Lomakin S, Camino G (2000) Polymer layered silicate nanocomposites, Macromol Mater Eng 279:1–9, https://doi.org/10.1002/1439-2054(20000601)279:1<1:: AID- MAME1>3.0.CO;2-Q

34. Kornmann X, Lindberg H, Berglund LA (2001) Synthesis of epoxy–clay nanocomposites: influence of the nature of the clay on structure, Polymer 42:1303–1310, https://doi.org/10.1016/S0032-3861(00)00801-6

35. Kim CM, Lee DH, Hoffmann B, Kressler J, Stoppelmann G (2001) Influence of nanofillers on the deformation process in layered silicate/polyamide 12 nanocomposites, Polymer 42:1095–1100, https://doi.org/10.1016/S0032-3861(00)00468-7

36. Zerda AS, Lesser AJ (2001) Intercalated clay nanocomposites: morphology, mechanics and fracture behavior, J Polym Sci Polym Phys 39:1137–1146, https://doi.org/10.1002/polb.1090

37. Chin IJ, Thurn-Albrecht T, Kim HC, Russell TP, Wang J (2001) On exfoliation of montmorillonite in epoxy, Polymer 42:5947–5952, http://dx.doi.org/10.1016/S0032-3861(00)00898-3

38. Huang JC, Zhu ZK, Yin J, Qian XF, Sun YY (2001) Poly(etherimide)/ montmorillonite nanocomposites prepared by melt intercalation: morphology, solvent resistance properties and thermal properties, Polymer 42:873–877, https://doi.org/10.1016/S0032- 3861(00)00411-0

39. Wang KH, Choi MH, Koo CM, Choi CM, Chung IJ (2001) Synthesis and characterization of maleated polyethylene/clay nanocomposites, Polymer 42:9819–9826, https://doi.org/10.1016/S0032-3861(01)00509-2

40. Beyer G (2002) Nanocomposites: a new class of flame retardants for polymers, Plast Addit Compound 4(10):22–27, http://dx.doi.org/10.1016/S1464-391X(02)80151-9

41. Dennis HR, Hunter DL, Chang D, Kim S, White JL, Cho JW (2001) Effect of melt processing conditions on the extent of exfoliation in organoclay-based nanocomposites, Polymer 42:9513–9522, https://doi.org/10.1016/S0032-3861(01)00473-6

42. Varlot K, Reynaud E, Kloppfer MH, Vigier G, Varlet J (2001) Clay-reinforced polyamide: preferential orientation of the montmorillonite sheets and the polyamide crystalline lamellae, J Polym Sci Polym Phys 39:1360–70, https://doi.org/10.1002/polb.1108

43. Wu SH, Wang FY, Ma CCM, Chang WC, Kuo CT, Kuan HC, Chen WJ (2001) Mechanical, thermal and morphological properties of glass fiber and carbon fiber reinforced polyamide 6 and polyamide 6/clay nanocomposites, Mater Lett 49:327–33, https://doi.org/10.1016/S0167-577X(00)00394-3

44. Krishnamoorti R, Giannelis EP (1997) Rheology of end-tethered polymer layered silicate nanocomposites, Macromolecules 30:4097-4102, https://doi.org/10.1021/ma960550a

45. Koo JH (2006) Polymer Nanocomposites: processing, characterization and applications, McGraw-Hill, ISBN 978-0071458214

46. Paiva LB, Morales AR, Diaz FRV (2008) Argilas organofílicas: características, metodologias de preparação, compostos de intercalação e técnicas de caracterização, Cerâmica 54:213-226, https://doi.org/10.1590/S0366-69132008000200012

47. Paul DR, Robeson LM (2008) Polymer nanotechnology: nanocomposites, Polymer 49:3187–3204, http://dx.doi.org/10.1016/j.polymer.2008.04.017

48. Xiao J, Hu Y, Kong Q, Song L, Wang Z, Chen Z, Fan W (2005) Poly(butylene terephthalate)/Clay Nanocomposites directly Prepared from Pristine Montmorillonite (MMT), Polym Bull 54:271–278, https://doi.org/10.1007/s00289-005-0395-0

49. Nussbaumer RJ, Caseri WR, Smith P, Tervoort T (2003) Polymer-TiO2 Nanocomposites: A Route Towards Visually Transparent Broadband UV Filters and High Refractive Index Materials, Macromol Mater Eng 288:44–49, https://doi.org/10.1002/mame.200290032

50. Messersmith PB, Giannelis EP (1995) Synthesis and barrier properties of poly(ε-caprolactone)-layered silicate nanocomposites, J Polym Sci 33(7):104, https://doi.org/10.1002/pola.1995.080330707

51. Giannelis EP (1996) Polymer layered silicate nanocomposites, Adv Mater 8:29–35, https://doi.org/10.1002/adma.19960080104

52. Alexandre M, Dubois P (2000) Polymer–layered silicate nanocomposites: preparation, properties and uses of a new class of materials, Mater Sci Eng R 28:1–63, https://doi.org/10.1016/S0927-796X(00)00012-7

53. Mai YW, Yu ZZ (2006) Polymer nanocomposites, Woodhead Publishing Ltd., Cambridge, ISBN 978-1845691127

54. Le Baron PC, Wang Z, Pinnavaia TJ (1999) Polymer–layered silicate nanocomposites: an overview, Appl Clay Sci 15:11–29, https://doi.org/10.1016/S0169-1317(99)00017-4

55. Vaia RA, Wagner HD (2004) Framework for nanocomposites, Mater Today 7(11):32–37, https://doi.org/10.1016/S1369-7021(04)00506-1

56. Kannan M, Bhagawan SS, Jose T, Thomas S, Joseph K (2010) Effect of sequence of nanoclay addition in TPU/PP blends: thermomechanical properties, J Mater Sci 45:1078- 1085, https://doi.org/10.1007/s10853-009-4046-y

57. Nath DCD, Bandyopadhyay S, Rider J, Yu A, Blackburn D, White C (2011) Study of dynamic mechanical properties and morphological behaviours of fly ash reinforced polypropylene composites, Macromol. Res. 19, 338–344, https://doi.org/10.1007/s13233- 011-0408-9

58. Osman MA, Mittal V, Lusti HR (2004) The aspect ratio and gas permeation in polymer-layered silicate nanocomposites. Macromol Rapid Commun 25:1145–1149, https://doi.org/10.1002/marc.200400112

59. Modesti M, Lorenzetti A, Bon D, Besco S (2005) Effect of processing conditions on morphology and mechanical properties of compatibilized polypropylene nanocomposites, Polymer 46(23):10237–10245, http://dx.doi.org/10.1016/j.polymer.2005.08.035

60. Bharadwaj RK (2001) Modeling the Barrier Properties of Polymer-Layered Silicate Nanocomposites, Macromolecules 34(26):9189-9192, https://doi.org/10.1021/ma010780b

61. Kumar SA, Yuelong H, Yumei D, Le Y, Kumaran MG, Thomas S (2008) Gas Transport Through Nano Poly(ethylene-co-vinyl acetate) Composite Membranes, Ind Eng Chem Res 47(14):4898–4904, https://doi.org/10.1021/ie071624h

62. Choudalakis G, Gotsis AD (2009) Permeability of polymer/clay nanocomposites: a review, Euro Polymer J 45(4):967-984, https://doi.org/10.1016/j.eurpolymj.2009.01.027

63. De Paoli MA (2009) Degradação e Estabilização de Polímeros, Artliber, ISBN 978-8588098442

64. Fornes TD, Yoon PJ, Keskkula H, Paul DR (2001) Nylon 6 nanocomposites: the effect of matrix molecular weight, Polymer 42:9929–9940, https://doi.org/10.1016/S0032-3861(01)00552-3

65. Kim SW, Jo WH, Lee MS, Ko MB, Jho JY (2001) Preparation of clay-dispersed poly(styrene-co-acrylonitrile) nanocomposites using poly(α-caprolactone) as a compatibilizer, Polymer 42: 9837–9842, https://doi.org/10.1016/S0032-3861(01)00506-7

66. Lagaly G (1999) Introduction: from clay mineral-polymer interactions to clay mineral - polymer nanocomposites, Appl Clay Sci 15:1–9, ISSN: 0169-1317

67. Sun T, Garces JM (2002) High-performance polypropylene-clay nanocomposites by in-situ polymerization with metallocene/clay catalysts, Adv Mater 14:128–30, https://doi.org/10.1002/1521-4095(20020116)14:2%3C128::AID-ADMA128%3E3.0.CO; 2-7

68. Jin YH, Park HJ, Im SS, Kwak SY, Kwak S (2002) Polyethylene/clay nanocomposite by in-situ exfoliation of montmorillonite during Ziegler–Natta polymerization of ethylene, Macromol Rapid Commun 23:135–140, https://doi.org/10.1002/1521-3927(20020101)23:2%3C135::AID-MARC135%3E3.0.CO;2-T

69. Sepehr M, Utracki LA, Zheng X, Wilkie CA (2005) Polystyrenes with macrointercalated organoclay. Part I. Compounding and characterization, Polymer 46:11557–11568, http://dx.doi.org/10.1016/j.polymer.2005.10.014

70. Jiankun L, Yucai K, Zongneng Q, Xiao-Su Y (2001) Study on intercalation and exfoliation behavior of organoclays in epoxy resin, J Polym Sci Polym Phys 39:115–120, https://doi.org/10.1002/1099-0488(20010101)39:1%3C115::AID-POLB100%3E3 .0.CO;2-N

71. Liu X, Wu Q (2002) Polyamide 66/clay nanocomposites via melt intercalation, MacromolMater Eng 287:180–186, https://doi.org/10.1002/1439- 2054 (20020301) 287:3%3C180::AID-MAME180%3E3.0.CO;2-T

72. Vaia RA, Giannelis EP (2001) Liquid crystal polymer nanocomposites: direct intercalation of thermotropic liquid crystalline polymers into layered silicates, Polymer 42:1281–5, https://doi.org/10.1016/S0032-3861(00)00508-5

73. Porter D, Metcalfe E, Thomas MJK (2000) Nanocomposite fire retardants-a review, Fire Mater 24:45–52, http://dx.doi.org/10.1002/(SICI)1099-1018(200001/02)24:13.0.CO;2-S

74. Ashley RJ (1985) Permeability and Plastics Packaging In: Comyn J (ed) Polymer Permeability, Barking: Chapman & Hall, https://doi.org/10.1007/978-94-009-4858-7

75. Liu LM, Qi ZN, Zhu XG (1999) Studies on nylon-6 clay nanocomposites by melt-intercalation process, J Appl Polym Sci 71:1133–1138, https://doi.org/10.1002/(SICI)1097- 4628(19990214)71:7%3C1133::AID-APP11%3E3. 0.CO;2-N

76. Hotta S, Paul DR (2004) Nanocomposites formed from linear low density polyethylene and organoclays, Polymer 45:7639–7654, https://doi.org/10.1016/j.polymer.2004. 08.059

77. Harper CA, Petrie EM (2003) Plastics Materials and Processes: A Concise Encyclopedia, Wiley-Interscience, ISBN 978-0471459217

78. Zanetti M, Costa L (2004) Preparation and combustion behavior of polymer/layered silicate nanocomposites based upon PE and EVA, Polymer 45:4367–4373, https://doi.org/10.1016/j.polymer.2004.04.043

79. Zhai H, Xu W, Guo H, Zhou Z, Shen S, Song Q (2004) Preparation and characterization of PE and PE-g-MAH/montmorillonite nanocomposites, Eur Polym J 40:2539–2545, http://dx.doi.org/10.1016/j.eurpolymj.2004.07.009

80. Lu H, Hu Y, Xiao J, Kong Q, Chen Z, Fan W (2005) The influence of irradiation on morphology evolution and flammability properties of maleated polyethylene/clay nanocomposite, Mater Lett 59(6):648–651, http://dx.doi.org/10.1016/j.matlet. 2004.10.057

81. Morawiec J, Pawlak A, Slouf M, Galeski A, Piorkowska E, Kransnikowa N (2005) Preparation and properties of compatibilized LDPE/organo-modified montmorillonite nanocomposites, Eur Polym J 41:1115–1122, https://doi.org/10.1016/ j.eurpolymj. 2004.11.011

82. Barbosa R, Souza DD, Nóbrega KC, Araújo EM, Melo TJA (2009) Influência da Quantidade de Sal Quaternário de Amônio e do Tipo de Compatibilizante em Nanocompósitos PEAD/Argila Organofílica, 10o Congresso Brasileiro de Polímeros, Brasil

83. Fu C, Qutubuddin S (2001) Polymer-clay Nanocomposites: Exfoliation of Organophilic Montmorilonita Nanolayers in Polystyrene, Polymer 42:807-813, https://doi.org/10.1016/S0032-3861(00)00385-2

84. Strong AB (2005) Plastics-Materials and Processing, 3 ed, Prentice Hall, ISBN 978-0131145580

85. Sarantópulus CIGL, Teixeira F, Oliveira LM, Coltro L, Borges D, Soares B, Moreira C, Alves RMVO (2017) Embalagens plásticas flexíveis: principais polímeros e avaliação de propriedades, 2 ed, Campinas: CETEA/ITAL, ISBN 978-85-7029-140-0

86. Matteucci S, Raharjo RD, Kusuma VA, Swinnea S, Freeman BD (2008) Gas Permeability, Solubility and Diffusion Coefficients in 1,2-Polybutadiene Containing Magnesium Oxide, Macromolecules 41(6):2144-2156, https://doi.org/10.1021/ma702459k

87. Lei SG, Hoa SV, Ton-That MT (2006) Effect of Clay Types on the Processing and Properties of Polypropylene Nanocomposites, Compos Sci Technol 66(10):1274-1279, https://doi.org/10.1016/j.compscitech.2005.09.012

88. Lin H, Freeman B (2004) Gas solubility, diffusivity and permeability in poly(ethylene oxide), J Membr Sci 239(1):105–117, https://doi.org/10.1016/j.memsci.2003.08.031

89. Raharjo RD, Freeman BD, Paul DR, Sarti GC, Sanders ES (2007) Pure and mixed gas CH4 and n-C4H10 permeability and diffusivity in poly(dimethylsiloxane), J Membr Sci 306:75–92, http://doi.org/10.1016/J.Memsci.2007.08.014

90. Safari M, Ghanizadeh A, Montazer-Rahmati MM (2009) Optimization of membrane-based CO2-removal from natural gas using simple models considering both pressure and temperature effects, Int J Greenh Gas Control 3(1):3–10, https://doi.org/10.1016/j.ijggc.2008.05.001

91. Ghadimi A, Sadrzadeh M, Shahidi K, Mohammadi T (2009) *Ternary gas permeation* through a synthesized PDMS membrane: experimental and modeling, J Membr Sci 344:225–236, https://doi.org/10.1016/j.memsci.2009.08.001

92. Klopffer M, Flaconnèche B (2001) Transport Properties of Gases in Polymers: Bibliographic Review, Oil Gas Sci Technol Rev IFP 56(3):223–244, https://doi.org/10.2516/ogst:2001021

93. Picard E, Vermogen A, Gerard JF, Espuche E (2008) Influence of the compatibilizer polarity and molar mass on the morphology and the gas barrier properties of polyethylene/clay nanocomposites, J Polym Sci B Polym Phys 46(23):2593–2604, https://doi.org/10.1002/polb.21584

94. Utracki LA (2004) Clay-Containing Polymeric Nanocomposites, v. 1, Rapra Technology, England, ISBN 978-1859574379

95. Lange J, Wyser Y (2003) Recent innovations in barrier technologies for plastic packaging: a review, Packag Technol Sci 16(4):149–158, https://doi.org/10.1002/pts.621

96. Chafidz A, Ali MA, Elleithy R (2011) Morphological, thermal, rheological, and mechanical properties of polypropylene-nanoclay composites prepared from masterbatch in a twin-screw extruder, J Mater Sci 46:6075–6086, https://doi.org/10.1007/s10853-011- 5570-0

97. Becker LO, Varley RJ, Simon GP (2004) Thermal stability and water uptake of high performance epoxy layered silicate nanocomposites, Eur Polym J 40(1):187–195, https://doi.org/10.1016/j.eurpolymj.2003.09.008

98. Nielsen LE (1967) Models for permeability of filled polymer systems, J. Macromol. Sci. Part A. v.1, pp. 929-942, https://doi.org/10.1080/10601326708053745

99. Li, H. et al. (2018) Permeation Characteristic and Mechanism of CO2 in High Density Polyethylene. In: Han, Y. (eds) Advances in Materials Processing. CMC 2017. Lecture Notes in Mechanical Engineering. Springer, Singapore, https://doi.org/10.1007/978-981-13-0107-0_93

100. Salame M, Steingiser S (2008) Barrier Polymers, Polymer-Plastics Technology and Engineering 8(2):155-175, https://doi.org/10.1080/03602557708545034

101. Combellick WA (1990) Barrier Polymers In: Concise Encyclopaedia of Polymer Science and Engineering, Mark HF (ed), Bikales NM (ed), Overberger CG (ed), Menges G (ed), Kroschwitz JI (ed), 2 ed, Wiley-Interscience, ISBN 978-0471865193

102. Bousmina M (2005) Fundamental insight into polymer nanocomposites In: Abstracts of 21st Annual Meeting of Polymer Processing Society (PPS 21), Leipzig, Germany 219–219

103. Crawford RJ (1993) Rotational Molding, Rapra Technology, v. 6, n. 11, ISSN 0889-3144

104. Crawford RJ; Throne JL (2002) Rotational Molding Technology, Elsevier Science, ISBN 978-1884207853

105. Shen, F (1995) A filament-wound structure technology overview. Materials Chemistry and Physics, 42, 96-100, https://doi.org/10.1016/0254-0584(95)01554-X

106. Azeem M, Ya HH, Kumar M, Stabla P, Smolnicki M, Gemi L, Khan R, Ahmed T, Ma Q, Sadique MR, Mokhtar AA, Mustapha, M (2022) Application of Filament Winding Technology in Composite Pressure Vessels and Challenges: a review. Journal of Energy Storage, https://doi.org/10.1016/j.est.2021.103468

107. Nitrogen compressed - Safety Data Sheet - www.lindeus.com/-/media/corporate/praxairus/documents/sds/nitrogen/nitrogen-compressed-safety-data-sheet-sds-p4631.pdf ?la=en Acesso em 30 de outubro de 2022

108. Carbon dioxide compressed - Safety Data Sheet - www.lindeus.com/-/media/corporate/praxairus/documents/sds/carbon-dioxide/carbon-dioxide-medipure-co2-safety-data-sheet-sds-p4574.pdf?la=en Acesso em 30 de outubro de 2022

109. Methane compressed - Safety Data Sheet - www.lindeus.com/-media/corporate/praxairus/documents/sds/methane-ch4-safety-data-sheet-sds-p4618.pdf?la=en Acesso em 30 de outubro de 2022

110. Hydrogen sulfide - Safety Data Sheet - www.lindeus.com/-/media/corporate/praxairus/ documents/sds/hydrogen/hydrogen-sulfide-h2s-safety-data-sheet-sds-p4611.pdf?la= en Acesso em 30 de outubro de 2022

111. Speight JG (2015) Handbook of offshore oil and gas operations, Elsevier,

https://doi.org/10.1016/C2009-0-19144-4

112. Dow HDPE 35054L - Technical Data Sheet - https://materials.ulprospector.com/pt/ profile/default?e=141349 Acesso em 30 de outubro de 2022

113. Cloisite 20A - Technical Data Sheet - www.byk.com/en/additives/additives-by-name/ cloisite-20-a.php Acesso em 30 de outubro de 2022

114. Chemical Book - CAS DataBase List - Nitrogen - www.chemicalbook.com/ ChemicalProductProperty_EN_cb2159243.htm Acesso em 30 de outubro de 2022

115. The Engineering Toolbox - www.engineeringtoolbox.com/gases-solubility-water-d_1148.html Acesso em 30 de outubro de 2022

116. Alumínio naval ABNT 5052F - Tabela técnica - www.coppermetal.com.br/catalogos/ catalogo-aluminio.pdf Acesso em 30 de outubro de 2022

117. Aço inoxidável AISI 316 - Tabela técnica - https://favorit.com.br/tabelas/ acos_inoxidaveis.html Acesso em 30 de outubro de 2022

118. Minamata Convention on Mercury - http://www.mercuryconvention.org Acesso em 30 de outubro de 2022

119. Manufacturer's Rubber and Supply - www.manuf-rubber.com/news/buna-vs-viton- seals-whats-the-difference Acesso em 30 de outubro de 2022

120. Evaluation of measurement data - Guide to the expression of uncertainty in measurement - www.bipm.org/documents/20126/2071204/JCGM_100_2008_E.pdf Acesso em 30 de outubro de 2022

121. Talbot DEJ (ed.), Talbot JDR (ed.) (2018) Corrosion Science and Technology. CRC. https://doi.org/10.1201/9781351259910

122. Ammonia - Safety Data Sheet - www.lindedirect.com/docs/default-source/ brochures/industries/anhydrous-ammonia-safety-data-sheet.pdf?sfvrsn=83ec61a_0 Acesso em 30 de outubro de 2022

123. The Seak Man's O-Ring Handbook - Viton® - EPM, Inc. First edition, 2004

124. Martini LJ (1984) Practical Seal Design, Taylor & Francis, ISBN 0-8247-7166-4

125. Boyer HE (ed.), Gall TL (ed.) (1984) Metals Handbook - Desk Edition, American Society for Metals, ISBN 978-0871701886

126. Canevarolo SV et al. (2003) Técnicas de caracterização de polímeros, São Paulo: Artliber, ISBN 978-8588098190

127. TA Instruments - https://www.tainstruments.com Acesso em 30 de outubro de 2022

128. Brandrup J (ed.), Immergut EH (ed.), Grulke EA (ed.) (2003) Polymer Handbook, VI/546 - Permeability and Diffusion Data, 4 ed, John Wiley & Sons, ISBN 978-0-471-47936-9

129. Runt JP (1985) Crystallinity Determination In: Encyclopedia of Polymers Science and Engineering, 4, 482-519, John Wiley & Sons, New York. ISBN 978-0471800507

130. Vasile C (2018) Polymeric Nanocomposites and Nanocoatings for Food Packaging: a review. Materials, https://doi.org/10.3390/ma11101834

131. Guo F, Aryana S, Han Y, Jiao Y (2018) A Review of the Synthesis and Applications of Polymer-Nanoclay Composites. Appl Sci, https://doi.org/10.3390/app8091696

132. Chelladurai V, Jayas DS (2018) Nanoscience and Nanotechnology in Foods and Beverages. CRC, ISBN 978-1498760638

133. Kane RD, Trillo EA, Maligas MN, Coles M, Turbeville E (2006) Operational Limits for Austenitic Stainless Steels in H2S Containing Environments, Corrosion 2006, NACE-06156 - https://onepetro.org/NACECORR/proceedings-abstract/CORR06/All-CORR06/NACE- 06156 /118111 Acesso em 30 de outubro de 2022

134. Craig BD (ed.), Anderson DS (ed.) (2002) Handbook of Corrosion Data. ASM International, ISBN 0-87170-518-4

135. Yasuda H, Rosengren KJ (1970) Isobaric Measurement of Gas Permeability of Polymers, J Appl Polym Sci, https://doi.org/10.1002/app.1970.070141117

136. Zhu L, Chiu F-C, Fu Q, Quirk RP, Cheng SZD (1999) Physical Constants of Poly(ethylene), V/9 In Brandrup J (ed.), Immergut EH (ed.), Grulke EA (ed.), Polymer Handbook, Wiley, ISBN 978-0471166283

137. Mark JE (ed.) (2009) Polymer Data Handbook. Oxford University Press, ISBN 978- 0195181012

138. Comyn J (ed.) (1985) Polymer Permeability. Chapman & Hall, https://doi.org/10.1007/978-94-009-4858-7

139. Sears JK, Darby JR (1982) The technology of plasticizers, Wiley, https://doi.org/10.1002/pol.1982.130200810

140. Chinaglia CR, Correa CA (1997) Análise de Falhas em Materiais através de Técnicas Avançadas de Microscopia, Polímeros: Ciência e Tecnologia Jul/Set:19-23

141. Oka T, Jinno S, Fujinami M (2009) Analytical Methods Using a Positron Microprobe, Anal Sci, https://doi.org/10.2116/analsci.25.837

142. Yasuda H, Tsai JT (1974) Pore size of microporous polymer membranes. J Appl Polym Sci, https://doi.org/10.1002/app.1974.070180316

143. Gladysz GM, Chawla KK (2015) Intrinsic Voids in Polymers In: Voids in Materials: from unavoidable defects to designed cellular materials, Elsevier, ISBN 978-0-444-56367- 5

APÊNDICE

Os permeâmetros comerciais, geralmente, atendem à norma ASTM - D1434 que possibilita estimar a taxa de transmissão em estado estacionário de um gás através de plásticos sob a forma de filmes, folhas, laminados e papéis ou tecidos revestidos de plástico. O método de ensaio prevê a determinação da taxa de transmissão de gás (GTR), a permeância e, no caso de materiais homogêneos, a permeabilidade, devendo ser indicadas as condições de ensaio.

A taxa de transmissão de gás (*gas transmission rate* - GTR) é a quantidade de um dado gás que passa através de uma unidade das superfícies paralelas de um filme plástico em unidade de tempo sob as condições de teste cuja unidade SI é 1 mol/(m^2.s), sendo também usada a unidade 1 mL (STP)/(m^2.d) a um diferencial de pressão de uma atmosfera.

A permeância (P) é a razão entre a taxa de transmissão do gás e a diferença de pressão parcial do gás nos dois lados do filme cuja unidade SI é 1 mol/(m^2.s.Pa).

A permeabilidade (P) é o produto da permeância e da espessura de um filme. A permeabilidade é significativa apenas para materiais homogêneos nos quais é uma propriedade característica do material a granel. Esta quantidade não deve ser utilizada a menos que a constância da permeabilidade tenha sido verificada usando várias espessuras diferentes do material. A unidade SI de P é 1 mol/(m.s.Pa).

Em resumo, a amostra é montada numa célula de transmissão de gás de modo a formar uma semibarreira selada entre duas câmaras. Uma câmara contém o gás de teste a alta pressão específica enquanto a outra câmara, a uma pressão mais baixa, recebe o gás permeante, adotando-se um dos seguintes procedimentos:

- Procedimento Manométrico (M);
- Procedimento Volumétrico (V).

No Procedimento M, a câmara de pressão inferior é inicialmente evacuada e a transmissão do gás através do corpo de prova é indicada por um aumento de pressão enquanto no Procedimento V, a câmara de baixa pressão é mantida próxima à pressão atmosférica e a transmissão do gás através da amostra de ensaio é indicada por uma mudança de volume.

As medições fornecem estimativas semiquantitativas para a transmissão de gás de gases puros simples através de películas e chapas. A correlação dos valores medidos com qualquer utilização, como a protecção do conteúdo embalado, deve ser determinada pela experiência. A taxa de transmissão do gás é afetada por condições não especificamente previstas nos ensaios como teor de umidade, teor de plastificante e não homogeneidades.

Apesar dos permeâmetros comerciais apresentarem diferentes configurações conforme os exemplos a seguir dos equipamentos que obedecem à referida norma:

1. Testador de permeabilidade gasosa VAC-V2 (Labthink)

Figura 1 - Testador de permeabilidade gasosa VAC-V2 (Labthink)
Fonte: http://de.labthink.com/html/produkte/vac-v2-gasdurchlaessigkeitspruefgeraet.html

O equipamento VAC-V2 é baseado no método de pressão diferencial, atende à norma ASTM D1434 e aplica-se à determinação da permeabilidade ao gás, coeficiente de solubilidade, coeficiente de difusão e coeficiente de permeabilidade de filmes plásticos, filmes compostos, materiais de barreira e filmes de alumínio a diferentes temperaturas em filmes plásticos, películas, materiais aeroespaciais, papel, papelão e borrachas.

O equipamento apresenta as seguintes especificações técnicas:

- Faixa de medição: 0,05 ~ 50.000 $cm^3/m^2 \cdot 4h \cdot 0{,}1$ MPa;
- Resolução de vácuo: 0,1 Pa;
- Vácuo na câmara de teste: < 20 Pa;
- Faixa de temperatura: 5 a 95°C;
- Faixa de umidade: 0% RH, 2% RH - 98,5% RH, 100% RH;
- Pressão de teste: -0,1 MPa ~ +0,1 MPa (padrão);
- Dimensões: 760 mm (C) x 575 mm (L) x 450 mm (A);
- Peso líquido: 88 kg.

O equipamento apresenta as seguintes características:

- Teste de três amostras diferentes de modo independente;
- Controle de temperatura e umidade;
- Teste de diferentes gases;
- Controlado por computador;
- Folha de referência para calibração;
- Saída de dados para o computador via porta RS 232;
- Produção individual conforme as necessidades do cliente.

2) Analisador OX-TRAN 2/12 OTR (Mocon)

Figura 2 - Analisador OX-TRAN 2/12 OTR (Mocon)
Fonte: https://www.ametekmocon.com/products/permeationanalyzers/otr-permeation-analyzers/ox-tran-2-12-series

O modelo R da série OX-TRAN 2/12 é um analisador de permeação ao oxigênio que oferece ampla gama de detecção para barreiras de baixo a alto nível, medindo a taxa de transmissão de oxigênio de uma amostra em equilíbrio em um ambiente de controlado.

A amostra é montada à pressão atmosférica entre duas câmaras como uma barreira selada. Então, uma corrente de nitrogênio purga uma câmara enquanto a outra contém oxigênio. À medida que o oxigênio permeia o filme no gás transportador (nitrogênio), ele passa pelo detector, produzindo um sinal que representa a taxa de transmissão de oxigênio.

O equipamento apresenta as seguintes características:

- Teste da taxa de transmissão de oxigênio (OTR);
- Teste de filmes e pacotes;
- Sistema de cartucho com 2 (duas) células, permitindo que o teste de ampla variedade de tamanhos e tipos de amostras;
- Cartuchos de teste removíveis intercambiáveis com vários modelos, permitindo que diferentes tipos de barreiras e pacotes sejam testados;
- Cartuchos de teste com fixação pneumática;
- Tamanho padrão do filme: 4” x 4”;
- Área padrão de teste de filme: 50 cm^2;
- Níveis de detecção de 0,05 até 28.800 $cc/(m^2.dia)$;
- Controles automatizados de temperatura, vazão e umidade;
- Tela de toque gráfica intuitiva necessitando de pouco treinamento;
- Temperatura de operação: 22°C ± 2°C;
- Umidade de operação: 20% a 80% de umidade relativa (sem condensação);
- Pressão nominal de abastecimento do gás: 2,0 bar;
- Dimensões: 394 mm (C) x 304 mm (L) x 580 mm (A);
- Peso líquido: 43 kg.

3) Permeâmetro de gás PMI C-522

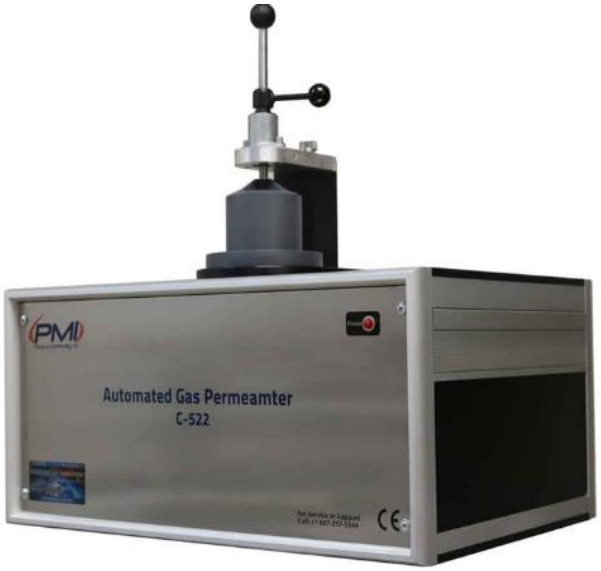

Figura 3 - Permeâmetro de gás PMI C-522 (Porous Materials Inc. EUA - PMI)
Fonte: https://pmiapp.com/products/gas-permeameter/

O permeâmetro de gás PMI C-522 fornece uma medição rápida e precisa da permeabilidade ao gás de amostras cilíndricas e de chapas sólidas ou ocas.

O equipamento apresenta as seguintes características:

- Faixa de permeabilidade: 1 x 10^{-3} - 50 Darcies;
- Resolução: 1 em 60.000;
- Precisão: 0,15% da leitura;
- Variação de pressão: 0 - 500 psi;
- Faixa de transdutor de fluxo de massa: 10 cc/minuto a 500 L/minuto;
- Gás pressurizado: ar limpo, seco e comprimido ou outro gás não inflamável e não corrosivo;
- Duração aproximada do teste: 10 minutos;
- Vasta gama de tipos e tamanhos de amostras;
- Câmaras de amostras múltiplas disponíveis;
- Manutenção mínima necessária;
- O software compatível com Windows trata com controle, medição, coleta de dados e geração de relatórios;
- A tela de teste gráfico em tempo real mostra o status e os resultados do teste durante toda a operação;
- Diâmetro da amostra: 1,75” - 2,5” (45 mm - 63,5 mm);
- Dimensões: 30” ou 76 mm (C) x 19” ou 483 mm (L) x 18,5” ou 470 mm (A);
- Peso: 100 lbs (45 kg).

4) Gas Permeability Tester GDP-C (Brugger)

Figura 4 - Analisador de permeabilidade gasosa GDP-C (Brugger)
Fonte: https://www.brugger-feinmechanik.com/en/products/permeation-testers/gdp-c-gas-permeability-tester/

O GDP-C determina a permeabilidade de gases secos para materiais de embalagem usando o método manométrico. As câmaras de pressão inferior e superior são inicialmente evacuadas. O computador calcula o tempo exigido pelo gás de teste para permear da câmara superior para a câmara inferior. Com este método, a permeabilidade ao gás pode ser determinada, bem como a constante de difusão e a solubilidade do gás (Time Lag).

A permeação na câmara inferior do corpo de prova é determinada pela análise do aumento da pressão no volume usando um computador externo. O método de medição manométrica é mencionado na norma ASTM D 1434-82.

O GDP-C possui as seguintes características:

- Teste de todos os gases não corrosivos;
- Faixa de medição: 0.5 a 30,000 ml/(m^2.dia.bar);
- Resolução: 0.1 cm^3/min;
- Faixa de temperatura: -20°C até 60°C;
- O teste é executado automaticamente após a definição do período de evacuação no intervalo de 10 segundos a 48 horas;
- Dimensões: 500 mm (C) x 310 mm (L) x 740 mm (A);
- Peso líquido: 20 kg.

Porém, ensaios interlaboratoriais revelam que as permeâncias medidas por estes procedimentos apresentam forte dependência do procedimento empregado, bem como, do laboratório que os realiza. A concordância com outros métodos, às vezes, é pobre e pode depender do material, pois os materiais que estão sendo testados muitas vezes afetam a precisão entre laboratórios. As causas dessas variações não são totalmente conhecidas.

ANEXO

Designation: D 1434 – 82 (Reapproved 2003)

Standard Test Method for Determining Gas Permeability Characteristics of Plastic Film and Sheeting[1]

This standard is issued under the fixed designation D 1434; the number immediately following the designation indicates the year of original adoption or, in the case of revision, the year of last revision. A number in parentheses indicates the year of last reapproval. A superscript epsilon (ε) indicates an editorial change since the last revision or reapproval.

1. Scope

1.1 This test method covers the estimation of the steady-state rate of transmission of a gas through plastics in the form of film, sheeting, laminates, and plastic-coated papers or fabrics. This test method provides for the determination of *(1)* gas transmission rate (GTR), *(2)* permeance, and, in the case of homogeneous materials, *(3)* permeability.

1.2 Two procedures are provided:

1.2.1 *Procedure M*— Manometric.

1.2.2 *Procedure V*— Volumetric.

1.3 The values stated in SI units are to be regarded as the standard.

1.4 *This standard does not purport to address all of the safety concerns, if any, associated with its use. It is the responsibility of the user of this standard to establish appropriate safety and health practices and determine the applicability of regulatory limitations prior to use.*

2. Referenced Documents

2.1 *ASTM Standards:* [2]

D 618 Practice for Conditioning Plastics for Testing

D 1898 Practice for Sampling of Plastics

3. Terminology

3.1 *Definitions of Terms Specific to This Standard:*

3.1.1 *gas transmission rate, GTR*— the quantity of a given gas passing through a unit of the parallel surfaces of a plastic film in unit time under the conditions of test. The SI unit of GTR is 1 mol/(m^2·s). The test conditions, including temperature and partial pressure of the gas on both sides of the film, must be stated. Other factors, such as relative humidity and hydrostatic pressure, that influence the transport of the gas must also be stated. The inch-pound unit of GTR, a commonly used unit of GTR, is 1 mL (STP)/(m^2·d) at a pressure differential of one atmosphere.

3.1.2 *permeance, P*—the ratio of the gas transmission rate to the difference in partial pressure of the gas on the two sides of the film. The SI unit of permeance is 1 mol/ (m^2·s·Pa). The test conditions (see 5.1) must be stated.

3.1.3 *permeability, $\underline{P}$*—the product of the permeance and the thickness of a film. The permeability is meaningful only for homogeneous materials, in which it is a property characteristic of the bulk material. This quantity should not be used unless the constancy of the permeability has been verified using several different thicknesses of the material. The SI unit of $\underline{P}$ is 1 mol/(m·s·Pa). The test conditions (see 3.1) must be stated.

NOTE 1—One millilitre (STP) is 44.62 μmol, one atmosphere is 0.1013 MPa, and one day is 86.4×10^3 s. GTR in SI units is obtained by multiplying the value in inch-pound units by 5.160×10^{-10}. Additional units and conversions are shown in Appendix X1.

3.1.4 *steady state*—the state attained when the amount of gas absorbed in the film is in equilibrium with the flux of gas through the film. For Method V this is obtained when the GTR is constant.

4. Summary of Test Method

4.1 The sample is mounted in a gas transmission cell so as to form a sealed semibarrier between two chambers. One chamber contains the test gas at a specific high pressure, and the other chamber, at a lower pressure, receives the permeating gas. Either of the following procedures is used:

4.1.1 *Procedure M*— In Procedure M the lower pressure chamber is initially evacuated and the transmission of the gas through the test specimen is indicated by an increase in pressure.

4.1.2 *Procedure V*— In Procedure V the lower pressure chamber is maintained near atmospheric pressure and the transmission of the gas through the test specimen is indicated by a change in volume.

5. Significance and Use

5.1 These measurements give semiquantitative estimates for the gas transmission of single pure gases through film and sheeting. Correlation of measured values with any given use, such as packaged contents protection, must be determined by

[1] This test method is under the jurisdiction of ASTM Committee F02 on Flexible Barrier Materials and is the direct responsibility of Subcommittee F02.30 on Test Methods.

Current edition approved July 30, 1982. Published November 1982. Originally published as D 1434 – 56 T. Last previous edition D 1434 – 75.

[2] For referenced ASTM standards, visit the ASTM website, www.astm.org, or contact ASTM Customer Service at service@astm.org. For Annual Book of ASTM Standards volume information, refer to the standard's Document Summary page on the ASTM website.

experience. The gas transmission rate is affected by conditions not specifically provided for in these tests, such as moisture content (Note 2), plasticizer content, and nonhomogeneities. These tests do not include any provision for testing seals that may be involved in packaging applications.

NOTE 2—The tests are run using gas with 0 % moisture changes.

5.2 Interlaboratory testing has revealed that permeances measured by these procedures exhibit a strong dependence on the procedure being used, as well as on the laboratory performing the testing. Agreement with other methods is sometimes poor and may be material-dependent. The materials being tested often affect the between-laboratory precision. The causes of these variations are not known at this time. It is suggested that this method not be used for referee purposes unless purchaser and seller can both establish that they are measuring the same quantity to a mutually agreed upon level of precision.

5.3 Use of the permeability coefficient (involving conversion of the gas transmission rate to a unit thickness basis) is not recommended unless the thickness-to-transmission rate relationship is known from previous studies. Even in essentially homogeneous structures, variations in morphology (as indicated, for example, by density) and thermal history may influence permeability.

6. Test Specimen

6.1 The test specimen shall be representative of the material, free of wrinkles, creases, pinholes, and other imperfections, and shall be of uniform thickness. The test specimen shall be cut to an appropriate size (generally circular) to fit the test cell.

6.2 The thickness of the specimen shall be measured to the nearest 2.5 μm (0.1 mil) with a calibrated dial gage (or equivalent) at a minimum of five points distributed over the entire test area. Maximum, minimum, and average values should be recorded. An alternative measure of thickness involving the weighing of a known area of specimens having a known density is also suitable for homogeneous materials.

7. Conditioning

7.1 *Standard Conditioning*—Condition all test specimens at 23 ± 2°C (73.4 ± 3.6°F) in a desiccator over calcium chloride or other suitable desiccant for not less than 48 h prior to test in accordance with Practice D 618, for those tests where conditioning is required. In cases of disagreement, the tolerances shall be ± 1°C (± 1.8°F).

7.2 *Alternative Conditioning*—Alternatives to 7.1 may be used for conditioning the specimens provided that these conditions are described in the report.

8. Sampling

8.1 The techniques used in sampling a batch of material to be tested by these procedures must depend upon the kind of information that is sought. Care should be taken to ensure that samples represent conditions across the width and along the length of rolls of film. Practice D 1898 provides guidelines for deciding what procedures to use in sampling a batch of material. Enough specimens must be tested to ensure that the information obtained is representative of the batch or other lot size being tested.

FIG. 1 Manometric Gas Transmission Cell

PROCEDURE M

(Pressure changes in the manometric cell may be determined by either visual or automatic recording.)

MANOMETRIC VISUAL DETERMINATION

9. Apparatus

9.1 The apparatus shown in Fig. 1 and Fig. 2 consists of the following items:[3]

9.1.1 *Cell Manometer System*—The calibrated cell manometer leg, which indicates the pressure of transmitted gas, shall consist of precision-bore glass capillary tubing at least 65 mm long with an inside diameter of 1.5 mm.

9.1.2 *Cell Reservoir System*, consisting of a glass reservoir of sufficient size to contain all the mercury required in the cell.

9.1.3 *Adapters*—Solid and hollow adapters for measurement of widely varying gas transmission rates. The solid adapter provides a minimum void volume for slow transmission rates. The hollow adapter increases the void volume by about a factor of eight for faster transmission rates.

9.1.4 *Cell Vacuum Valve*, capable of maintaining a vacuum-tight seal.[4]

9.1.5 *Plate Surfaces*, that contact the specimen and filter paper shall be smooth and flat.

9.1.6 *O-Ring*, for sealing the upper and lower plates.

9.1.7 *Pressure Gage*, mechanical or electrical type with a range from 0 to 333 kPa absolute. Used for measuring upstream gas pressure.

9.1.8 *Barometer*, suitable for measuring the pressure of the atmosphere to the nearest 133 Pa.

[3] The Dow gas transmission cell supplied by Custom Scientific Instruments, Inc., Whippany, NJ, has been found satisfactory for this purpose.

[4] The Dani-G Valve (¼-in. IPS) manufactured by G. W. Dahl Co., Inc., Bristol, RI, or a precision-ground glass stopcock, meets this requirement.

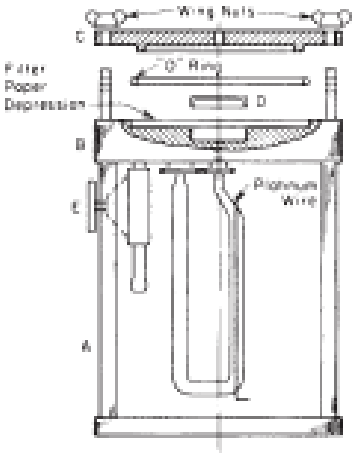

A—Supporting Legs
B—Lower Plate
C—Upper Plate
D—Adapter
E—Vacuum Valve

FIG. 2 Schematic View of Gas Transmission Cell

9.1.9 *Vacuum Gage*, to register the pressure during evacuation of the system to the nearest 13 Pa.

9.1.10 *Vacuum Pump*, capable of reducing the pressure in the system to 26 Pa or less.

9.1.11 *Needle Valve*, for slowly admitting and adjusting the pressure of the test gas.

9.1.12 *Cathetometer*, to measure the height of mercury in the cell manometer leg accurately. This instrument should be capable of measuring changes to the nearest 0.5 mm.

9.1.13 *Micrometer*, to measure specimen thickness, graduated to 2.5 μm (0.1 mil) or better.

9.1.14 *Elevated-Temperature Fittings*—Special cell fittings are required for high-temperature testing.

10. Materials

10.1 *Test Gas*—The test gas shall be dry and pure. The ratio of the volume of gas available for transmission to the volume of gas transmitted at the completion of the test shall be at least 100:1.

10.2 *Mercury*—Mercury used in the cell shall be triple distilled, checked regularly for purity, and replaced with clean mercury when necessary.

10.2.1 **Warning**—Very low concentrations of mercury vapor in the air are known to be hazardous. Guidelines for using mercury in the laboratory have been published by Steere.[5] Be sure to collect all spilled mercury in a closed container. Transfers of mercury should be made over a large plastic tray. Under normal daily laboratory-use conditions, the cells should be cleaned about every 3 months. Dirty mercury is indicated when the drop of the capillary becomes erratic or when mercury clings to the side of the capillary, or both. Whenever

[5] Steere, N. E. "Mercury Vapor Hazards and Control Measures" in Handbook of Laboratory Safety, N. V. Steere, Ed., CRC Press Inc., Boca Raton, FL, 1979.

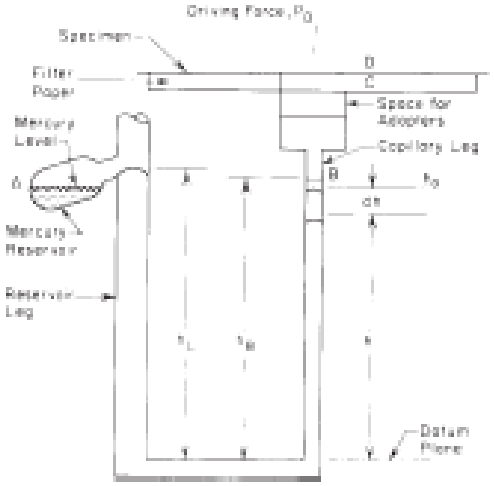

FIG. 3 Cell Manometer with Test Specimen in Place

such discontinuities occur, the mercury should be removed and the cell cleaned as follows:

(1) Wash with toluene (to remove greases and oils).

(2) Wash with acetone (to remove toluene).

(3) Wash with distilled water (to remove acetone).

(4) Wash with a 1 + 1 mixture of nitric acid and distilled water (to remove any mercury salts that may be present). This operation may be repeated if necessary in order to ensure complete cleaning of glassware.

(5) Wash with distilled water (to remove nitric acid).

(6) Wash with acetone (to remove water).

(7) Dry the cell at room temperature or by blowing a small amount of clean dry air through it.

11. Calibration

11.1 Each cell should be calibrated at the test temperature as follows (Fig. 3):

11.1.1 Determine the void volume of the filter paper from the absolute density of its fiber content (Note 3), the weight of the filter paper, and its apparent volume (Note 4). Express the void volume determined in this way in microlitres and designate as V_{CD}.

NOTE 3—Any high-grade, medium-retention qualitative noashing cellulosic filter paper, 90 mm in diameter will be satisfactory for this purpose. Cellulose fiber has an approximate density of 1.45 g/mL.

NOTE 4—The apparent volume may be calculated from the thickness and diameter of the filter paper.

11.1.2 Determine the volume of the cell manometer leg from *B* to *C*, Fig. 3, by mercury displacement. (Since the void volume of the adapters is included in this part of the calibration, the volume from *B* to *C* should be determined twice, once with the solid adapter in place, and once with the hollow.) This volume is obtained by dividing the weight of the mercury displaced by its density (Note 5). Determine this volume to nearest 1 μL and designate as V_{BC}.

NOTE 5—The density of mercury at 23°C is 13.54 g/mL.

11.1.3 Determine the volume, in microlitres, of the cell manometer leg from *A* to *B*, Fig. 3, by mercury displacement.

Determine the average cross-sectional area of the capillary by dividing this volume by the length (expressed to the nearest 0.1 mm) from *A* to *B*. Determine this area to the nearest 0.01 mm^2 and designate as a_c.

11.1.4 Determine the area of the filter paper cavity to the nearest 1 mm^2. Designate this area as *A*, the area of transmission.

11.1.5 Pour the mercury from the reservoir into the manometer of the cell by carefully tipping the cell. Record the distance from the datum plane to the upper calibration line *B* in the capillary leg as h_B. Record the distance from the datum plane to the top of the mercury meniscus in the reservoir leg as h_L. Determine h_B and h_L to the nearest 0.5 mm.

11.2 NBS Standard Reference Material 1470[6] is a polyester film whose permeance to oxygen gas has been certified for a range of experimental conditions. The calibration steps in 11.1 can be verified by comparing measurements obtained using this method of test in the user's laboratory with the values provided on the certificate accompanying the SRM.

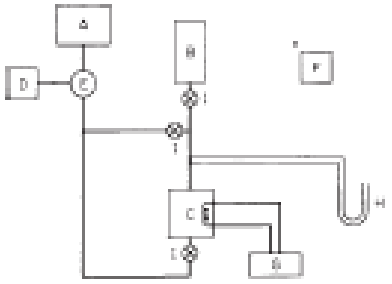

A—Vacuum Pump
B—Test Gas Cylinders
C—Gas Transmission Cell
D—Vacuum Gage
E—Trap
F—Barometer
G—Automatic Recorder (Optional)
H—Mercury Manometer
I—Needle Valve

FIG. 4 Component Arrangement of Gas Transmission Equipment

12. Procedure

12.1 Transfer all the mercury into the reservoir of the cell manometer system by carefully tipping the cell in such a way that the mercury pours into the reservoir.

12.2 Insert the appropriate adapter in the cell body.

12.3 Center a filter paper in the lower plate cavity.

12.4 Apply a light coating of vacuum grease on the flat metal that the surface of the specimen will contact. Avoid excessive grease.

12.5 Place the conditioned specimen smoothly on the lower lightly greased plate so that it covers the filter paper and the entire exposed face of the lower plate.

12.6 Locate the O-ring on the upper plate; then carefully position this plate over the specimen and fix the plate with uniform pressure to ensure a vacuum-tight seal.

12.7 Connect the line in which the test gas will be subsequently admitted to the upper plate. (The entire cell is now directly connected to the test gas line.)

12.8 Connect the vacuum source to the nipple attached to the cell vacuum valve. Evacuate the bottom of the cell; then, with the bottom still being evacuated, evacuate the top of the cell. Close off the vacuum line to the top of the cell; then close the line to the bottom (Fig. 4).

12.9 Flush the connecting line and the top of the chamber with test gas.

12.10 Reevacuate the system in the same manner as 12.8. The cell manometer system should be evacuated to a pressure of 26 Pa or less, as indicated on the vacuum gage.

12.11 Pour mercury from the reservoir into the manometer system of the cell by carefully tipping the cell. The height of the mercury in the capillary leg should be at approximately the same level as line *B* (Fig. 3) and stationary.

NOTE 6—A leak is indicated if the height of the mercury does not remain stationary. If such a leak occurs, discontinue the test and repeat the entire procedure. (If a leak occurs on a second trial, this may indicate a mechanical failure of the equipment.)

12.12 Record the height of the mercury in the capillary leg, h_o, at the start of each test, that is, immediately before the test gas has been admitted to the top of the cell.

12.13 After a suitable estimated time for attaining steady-state conditions, record the height of the mercury in the capillary leg, h_s, to the nearest 0.5 mm and the elapsed time, t_s, to the nearest 1 min.

12.14 Record the height of the mercury, *h*, in the capillary leg to the nearest 0.5 mm versus time, *t*, in hours, to the nearest 1 min. Take several readings (at least six are recommended) during the test. Calculate the function $g(h)$ for each *t* as defined in 13.1. Plot these values versus time, $(t-t_o)$, and construct the best straight line through these points. Use any observed values of *h* and *t* for h_s and t_s, respectively, if these values are within the steady-state region. A nonlinear plot of $g(h)$ versus $(t-t_o)$ that does not pass through the origin could indicate an improper selection of h_o and t_o; a new selection should then be made by using a larger mercury depression for the initial conditions.

NOTE 7—If, after all the mercury has been displaced from the capillary, any doubt exists as to the attainment of steady state, perform a check as follows:

(1) Return the mercury to the reservoir.

(2) Reevacuate the bottom of the cell only, leaving the top pressurized with test gas.

(3) Repeat 12.11, 12.13, and 12.14.

12.15 Return the mercury in the capillary leg to the reservoir by tipping the cell upon completion of the test and prior to opening the cell vacuum valve.

12.16 Remove the specimen from the cell and measure the thickness with a micrometer (Note 8). Record the average of five determinations made uniformly throughout the specimen to the nearest 2.5 μm (0.1 mil).

NOTE 8—If there is reason to believe that the specimen will expand or contract during transmission, the thickness should be measured prior to 12.5, as well as after transmission. If any change in thickness occurs, a

[6] This material is available from the Office of Standard Reference Materials, National Bureau of Standards, Washington, DC 20234.

note to this effect shall be included with the results.

12.17 Test three specimens with each gas.

12.18 If the requirements of 12.14 are not met in the normal atmospheric pressure test, repeat the procedure at a higher (up to 304 kPa) or lower (not less than 50 kPa) test pressure.

13. Calculation

13.1 Calculate the permeance, P, in SI units from the following relationship (Note 9):

$$P = g(h)/(t - t_o) \quad (1)$$

where:

$$g(h) = -\frac{1}{ART}\left[(V_f + a(p_u + h_B - h_o)] \ln\left\{1 - \frac{(h_o - h)}{P_u - (h_o - h_o)}\right\} + 2a(h_o - h)\right] \quad (2)$$

a_c = area of capillary $\overline{AB}$, mm^2,
A = area of transmission, cm^2,
h_o = height of mercury in the capillary leg at the start of the actual transmission run, after steady-state conditions have been attained, mm,
h = height of mercury in cell capillary leg at any given time, mm,
h_B = maximum height of mercury in the cell manometer leg from the datum plane to upper calibration line B, mm,
h_C = height of mercury in cell reservoir leg from datum plane to top of mercury meniscus, mm,
P_u = upstream pressure of gas to be transmitted,
R = universal gas constant 8.3143 × 10^3 L·Pa/(mol·K),
t_o = time at the start of the actual transmission run, h, after steady-state conditions have been attained,
t = time, h,
T = absolute temperature, K,
V_{BC} = volume from B to C, µL,
V_{CD} = void volume of depression, µL, and
V_f = $(V_{BC} + V_{CD})$, µL.

NOTE 9—The derivation of this equation is given in Appendix X2. Refer to Fig. 3 for location of symbols used in this equation.

13.2 A test result is defined as a single determination of the permeance of an individual sheet of material.

MANOMETRIC RECORDING DETERMINATION

14. Apparatus

14.1 The description of the apparatus is identical to that in Section 9, with the omission of 9.1.12, which does not apply in this procedure, and the addition of the following apparatus:

14.2 *Resistance-Recording Instrument*—A resistance-recording instrument suitably connected to a uniform-diameter platinum wire (Note 10) that runs the calibrated length of the cell manometer leg shall be employed to measure changes in height of the mercury in the cell manometer leg versus time. This instrument shall be capable of measuring such changes to the nearest 0.5 mm.

NOTE 10—A recommended automatic recording device (Fig. 4 shows a simplified schematic of a setup utilizing an automatic recorder) consists of No. 44 platinum wire (with a resistance of 0.8 Ω/cm) with No. 30 tungsten leads to the glass. These are connected by means of No. 16 gage three-conductor copper wire to a suitable ten-turn potentiometer in series with a resistance recorder whose full-scale range is 10 to 150 Ω.[7]

15. Materials

15.1 Same as Section 10.

16. Calibration

16.1 Same as Section 11, but should also include the following:

16.2 The recording instrument with the cell, lead wires, and external resistance (Note 11) in series as used in the test shall be calibrated at test temperature initially and every time after a cell has been cleaned or repaired.

NOTE 11—The external resistance should be so chosen to permit complete traverse of the chart by the pen when a change in the height of mercury equal to the height of A to B occurs (Fig. 3).

16.3 The recording system shall be calibrated as follows:

16.3.1 Allow the cell to come to constant temperature at test temperature.

16.3.2 With the top of the cell removed and the vacuum valve open, pour the mercury into the cell manometer leg such that the mercury is approximately at the same level as line B (Fig. 3) and relatively stationary. Adjust the external resistance of the recorder so that the pen indicates a chart position of zero.

16.3.3 Vary the height of the mercury column and note the position indicated by the chart pen so that a plot of chart position as ordinate versus mercury height as abscissa is obtained. A straight line should result.

16.3.4 Determine the rate of chart paper travel to the nearest 2.54 mm (0.1 in.)/h.

16.4 See 11.2 for the use of NBS Standard Reference Material 1470 in checking the calibration of the permeance measuring apparatus.

17. Procedure

17.1 Same as Section 12, with the following exceptions:

17.2 Adjust the pen of the resistance recording instrument by means of the external resistance so that the pen position corresponds with the height of mercury in the capillary leg as determined in Section 16.

17.3 For best results, set the chart to run at a speed that will plot the gas transmission curve at a slope of about 45° (Note 12). Once experience is gained, the proper chart speed is easily selected.

NOTE 12—This applies only to charts that have a variable-speed drive.

18. Calculation

18.1 For several values of t (at least six are recommended), read h from the recorder chart and plot the function $g(h)$ versus t as defined in 12.14.

[7] The Minneapolis-Honeywell Regulator Co. 60V Model 153X64978-X-41 resistance recorder has been found satisfactory for this purpose. It is recommended that a quick-change variable speed chart drive, such as that supplied by Inaco Co., Division of Barry Controls, Inc., Groton, MA, be installed in the recorder.

18.2 Calculate the permeance from the equations given in 13.1.

18.3 A test result is defined as the value of a single individual determination of permeance of a film.

19.2 *Precision Glass Capillaries* or manometers with various diameters (0.25, 0.50, and 1.0 mm are recommended). The glass capillaries should have a suitable U-bend to trap the manometer liquid and a standard-taper joint to fit into the cell.

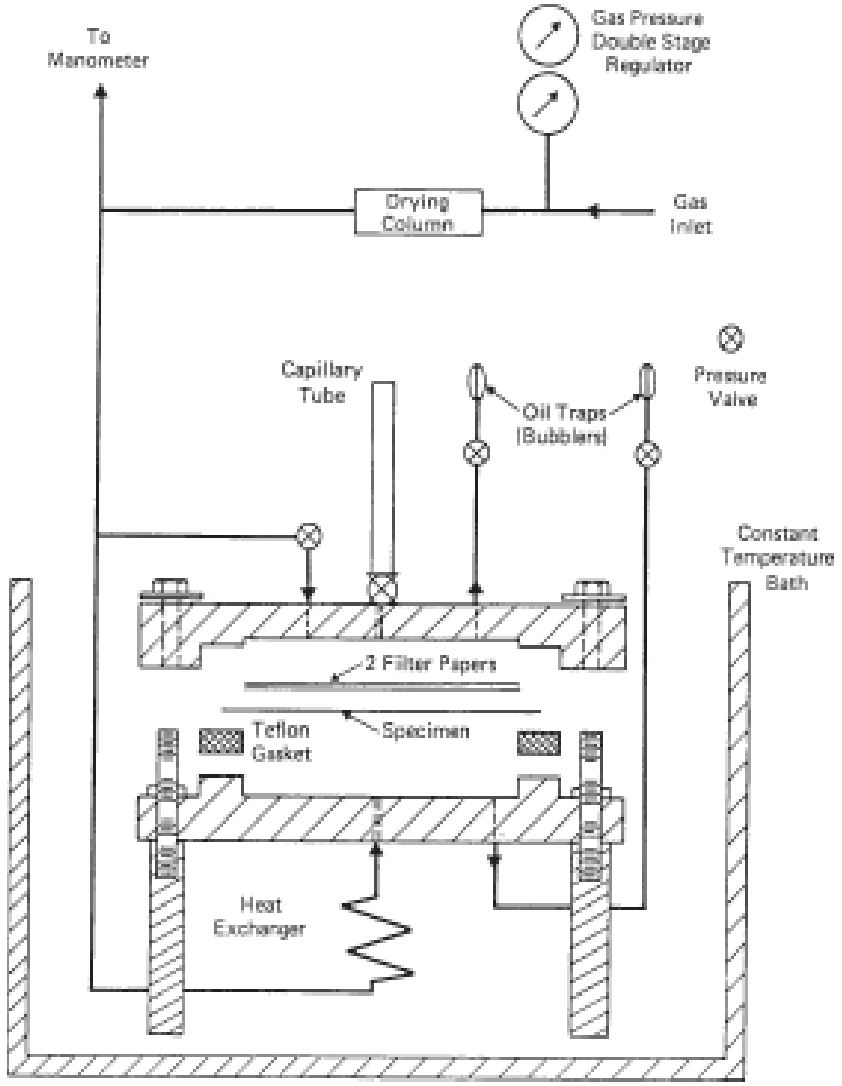

FIG. 5 Volumetric Gas Transmission Cell

PROCEDURE V

(Volumetric determinations may be made with several similar type apparatus.)

19. Apparatus

19.1 *Volumetric Gas Transmission Cell*[6], shown in Fig. 5.

19.3 *Cathetometer* or suitable scale for measuring changes in meniscus position to the nearest 0.5 mm.

19.4 *Temperature Control:*

19.4.1 A temperature-control liquid bath is recommended for controlling the temperature of the cell body to ± 0.1°C.

19.4.2 The apparatus should be shielded to restrict the temperature variations of the capillary to ± 0.1°C during the test.

19.5 *Micrometer*, to measure specimen thickness, to the nearest 2.5 μm (0.0001 in.) at a minimum of five points

[6] Suitable cells may be obtained from Custom Scientific Instruments, Whippany, NJ.

distributed over the entire test area. Maximum, minimum, and average values shall be recorded.

19.6 *Barometer*, suitable for measuring the pressure of the atmosphere to the nearest 133 Pa.

19.7 *Pressure Gage*, precision mechanical or electrical type for measuring absolute pressure over the range from 0 to 333 kPa.

20. Materials

20.1 *Cylinder of Compressed Gas*, of high purity equipped with pressure reducing valves.

20.2 *Capillary Liquid*— 4-Methyl-2-pentanone (methyl isobutyl ketone) (Note 13) or other appropriate liquid colored with a suitable dye[9] (Note 14).

NOTE 13—4-Methyl-2-pentanone has a vapor pressure of 933 Pa at 23°C. Erroneous results may be obtained in some cases, if the attainment of this equilibrium causes slug movement in the capillary. This may take an appreciable time, especially in small capillaries, and thereby lead to an erroneous answer. Also, the vapor of 4-methyl-2-pentanone may cause swelling of some materials, which will result in a change in the permeation rate.

NOTE 14—Mercury is not recommended for the capillary liquid except for use in calibrating cross-sectional areas because of contact angle hysteresis and resulting pressure errors (about 3 cm Hg in a 0.5-mm capillary), plus the much smaller readings resulting from the greater density of mercury as compared to 4-methyl-2-pentanone.

20.3 *Filter Paper*— Any high grade, medium-retention, nonashing cellulosic filter paper.

NOTE 15—Other porous filters such as sintered metal have been found to be satisfactory.

21. Calibration

21.1 **Warning**—Very low concentrations of mercury vapor in the air are known to be hazardous. Be sure to collect all spilled mercury in a closed container. Transfers of mercury should be made over a large plastic tray.

21.2 Place a column of clean mercury, approximately 70 mm (3 in.) long, in the capillary and measure its length with a cathetometer.

21.3 Transfer all of the mercury to a tared beaker and obtain the weight of the mercury on an analytical balance. Discard the mercury to be cleaned.

21.4 Since the density and weight of the column of mercury are known, its volume, V_M, in microlitres at room temperature (23°C), is given by the equation:

$$V_M = 10^3 \times W/13.54 \quad (3)$$

where:

W = weight of the mercury, g, and
13.54 g/mL = density of mercury at 23°C.

Since for a cylinder:

$$V_M = a_c l \quad (4)$$

where:

a_c = cross-sectional area, mm^2, and
l = length of mercury column, mm, then:

$$a_c = V_M/l \quad (5)$$

21.5 Calibrations shall be made at 23°C.

21.6 See 11.2 for the use of NBS Standard Reference Material 1470 in checking the calibration of permeance-measuring apparatus.

22. Procedure

22.1 Center a piece of filter paper in the upper portion of the test cell.

22.2 Place the conditioned specimen smoothly on the upper portion of the test cell.

22.3 Lightly grease[10] the rubber gasket, O-ring, or flat metal that the surface of the specimen will contact. Avoid excessive grease.

22.4 Place the upper half of the cell on the base and clamp it firmly to achieve a tight seal.

22.5 Apply positive test gas pressure to both sides of the cell, flushing out all air before closing the outlet vent. A recommended flushing time is at least 10 min at a flow rate of about 100 mL/min.

NOTE 16—The pressure differential is obtained by monitoring and adjusting the gage pressure on the high-pressure side of the cell so that it is the desired amount above the observed barometric pressure on the open (downstream) side.

22.6 Introduce an approximately 20-mm liquid slug (keep it intact) at the top of the capillary (Note 17) and close the upper outlet vent after the slug rests on the bottom of the capillary (Note 18). The capillary shall be clean and free of obstructions.

NOTE 17—It is convenient to add the liquid slug to the capillary with a syringe fitted with a long thin needle to aid proper insertion.

NOTE 18—After lowering the liquid slug into the capillary, sufficient time must be allowed for drainage down the inner wall of the capillary before beginning to take a series of readings.

22.7 Adjust the pressure across the specimen to maintain the exact pressure differential desired.

22.8 Small leaks around connections and joints can often be detected with soap solutions, but in some cases it may be necessary to immerse the cell in water while applying gas pressure, in order to observe bubbles at leak sites. Small leaks occurring on the high-pressure side of the cell should not be considered significant.

22.9 After a time interval estimated to be sufficient for attaining steady-state, begin measuring the displacement of the slug, using a stop watch (or clock) and distance scale maintained on the capillary or cathetometer. Take measurements at the top of the meniscus.

22.10 On completion of the run, return the slug to its starting position by slightly opening the low-pressure vent.

22.11 Repeat the measurement as necessary to assure the attainment of a steady-state condition.

NOTE 19—The time required to reach steady state will depend upon the nature of the specimen, its thickness, and the applied pressure differential. For specimens of low permeability, changes in ambient pressure may

[9] A suitable dye is Victoria Blue B, or Sudan Red available from chemical supply houses such as Pfaltz and Bauer, Inc.

[10] Stopcock grease available from Dow Corning Corp. has been found suitable.

TABLE 1 Results of Round-Robin Evaluation

Material	Gas	$\bar{P}$ (barrer)[A]	$\bar{P}$ (inch-pound units)[B]	(S_r) (barrer)	(S_L) (barrer)	(CV_r) (%)	(CV_R) (%)
Polyester film (100 A Mylar [C])	O_2	0.028	72.4	0.006	0.012	21	40
Polyester film (65 HS Mylar[C])	O_2	0.048	124	0.003	0.019	6	40
Polyester film (100 A Mylar [C])	CO_2	0.094	243	0.007	0.014	7	16
Polyester film (65 HS Mylar [C])	CO_2	0.16	466	0.009	0.026	5	16
Poly(propylene) film	O_2	1.29	3340	0.15	0.20	12	25
Poly(ethylene) film	O_2	1.94	5020	0.08	0.23	4	13
Poly(propylene) film	CO_2	4.85	12550	0.45	0.69	9	17
Poly(ethylene) film	CO_2	7.62	19710	0.40	0.94	5	13

(S_r) = the within-laboratory standard deviation of a single laboratory result for material i.
(S_L) = the square root of the between-laboratory component of variance.
(CV_r) = $100\,(S_r)/\bar{P}$.
(CV_R) = $100[(S_L)^2 + (S_r)^2]^{1/2}/\bar{P}$.

[A] One barrer equals 3.349×10^{-2} mol/m^2·s·Pa (see Table X1.1).
[B] Inch-pound units are mL (STP) mil/in^2·d·atm. See X1.1, X1.2, X1.3, and Appendix X2 for conversion factors.
[C] Registered trademark, E.I. duPont, Inc. for its polyester film.

interfere, particularly if long periods of test and repeated measurements are required to obtain reliable results.

23. Calculation

23.1 Plot the capillary slug position versus elapsed time and draw the best straight line through the points so obtained.

23.2 Calculate the volume-flow rate, V_r, in microlitres per second of transmitted gas from the slope of this line as follows:

$$V_r = \text{slope} \times a_c \tag{6}$$

where:
slope = rate of rise of capillary slug, mm/s, and
a_c = cross-sectional area of capillary, mm^2.

23.3 Calculate the gas transmission rate (GTR) in SI units as follows:

$$GTR = 10^{-6} \times p_a \times V_r A/(ART) \tag{7}$$

where:
A = transmitting area of specimen, mm^2,
p_a = ambient pressure, Pa,
R = universal gas constant ($R = 8.3143 \times 10^{3}$ L·Pa/(mol·K)), and
T = ambient temperature, K.

23.4 Calculate the permeance, P, in SI units as follows:

$$P = GTR/(p - p_a) \tag{8}$$

where p is the upstream pressure in pascals.

23.5 A test result is defined as the value obtained from an individual determination of the permeance of a specimen.

NOTE 20—The reliability of the measurements can be assessed to some extent by making measurements on SRM 1470 (see 11.2).

24. Report

24.1 The report shall include the following:

24.1.1 Procedure used,

24.1.2 Description of the sample, including identification of composition, presence of wrinkles, bubbles, or other imperfections, and manufacturer, if known,

24.1.3 Test gas used, and test gas composition, including purity,

24.1.4 Test temperature in degrees Celsius, and the pressure difference used,

24.1.5 Each thickness measurement made plus the average for each specimen. When five or more thickness measurements are made per specimen, the average, standard deviation and number of measurements made may be reported instead of each measurement, and

24.1.6 Each measurement obtained plus the appropriate averages in the units of choice. When five or more replicates are obtained the average, standard deviation, and number of replicates may be substituted for the above.

25. Precision

25.1 *General*—An interlaboratory evaluation of this method has been conducted.[11] Ten laboratories participated in determining the permeability, P, of four materials to oxygen and carbon dioxide. The results from the round robin are summarized in Table 1. The results demonstrate clearly that the precision of the results obtained depends strongly, but in an unpredictable manner, on the combination of material and gas being tested. Potential users of this method must, therefore, use their own experience in assessing the precision of the results being obtained.

25.1.1 The contribution arising from the between-laboratory component of the variance is larger than that from the within-laboratory component for all materials. This indicates that there are systematic differences between the procedures used in different laboratories. The magnitudes of these differences must be determined whenever two laboratories are comparing results for referee purposes.

25.2 *Repeatability*—Approximately 95 % of all test results will lie within $2(CV_r)$ % of the mean of all test results obtained within a given laboratory on a given material. Typical values of (CV_r) are given in Table 1.

25.3 *Reproducibility*—Approximately 95 % of all test results obtained in different laboratories will lie within $2(CV_R)$ %

[11] Supporting data are available from ASTM Headquarters. Request RR:D09-49.

TABLE X1.1 Factors for Converting Permeabilities from One System of Units to Another

Note 1—For instructions on using the table see X1.4.

Multiply ↓ \ To Obtain →	SI amol/m·s·Pa	Barrers 10^{-13} mL (STP) cm·s·cm Hg	Metric mL (STP) mil m²·d·atm	Inch-pound mL (STP) mil 100 in.²·d·atm
	Unit System (Dimensions of P_m)			
SI amol/m·s·Pa	1	2.986×10^{-3}	7.725	0.4884
Barrers 10^{-13} mL (STP) cm·s·cm Hg	0.3349×10^{3}	1	2.587×10^{3}	0.16991×10^{3}
Metric mL (STP) mil m²·d·atm	0.12945	0.3865×10^{-3}	1	64.52×10^{-3}
Inch-pound mL (STP) mil 100 in.²·d·atm	2.0094	5.991×10^{-3}	15.50	1

of the population mean of such values. Typical values of (CV_R) for the material examined in the round robin are shown in Table 1.

25.4 Users who wish to test materials other than those considered in the round robin must make their own assessment of the precision of their results. Variability between specimens is likely to be a dominant factor in such measurements.

APPENDIXES

(Nonmandatory Information)

X1. UNITS IN GAS TRANSMISSION MEASUREMENTS

X1.1 SI units for various quantities related to transmission of gases can be derived by recalling that the present standard defines the transmission rate, G, as the quantity of gas crossing a unit area of a barrier in unit time. Since the SI base unit for quantity of matter is the mole, the SI base unit for length is the metre, and the SI base unit for time is the second, the derived SI unit of transmission rate should be the mol/m²·s. Similarly, since the permeance, P, is defined as the ratio between the transmission rate and the partial pressure differential across the barrier, and since the SI unit of pressure is the pascal, appropriate SI units for permeances are mol/m²·s·Pa. Finally, for a homogeneous material, the permeability, P', is defined as the product of the permeance and the thickness of the film, which leads to the mol/m·s·Pa as the appropriate SI units.

X1.1.1 Appropriate unit prefixes must be attached to the SI units in order to bring the values that are actually observed onto a convenient scale for reporting or further manipulation. The following example will help to clarify this point: Consider a homogeneous film with a permeability of 1 amol/m·s·Pa (1 amol = 10^{-18} mol) and a thickness of 25.4 m. The permeance of this film would be 39.37 fmol/m²·s·Pa (1 fmol = 10^{-15} mol). If a pressure differential of one standard atmosphere (1 atm = 0.10132 MPa) were imposed across the barrier, the gas transmission rate would be 3.989 nmol/m²·s (1 nmol = 10^{-9} mol). Using the ideal gas law to convert this to inch-pound units yields a value of 7.725 mL(STP)/m²·d, which is a reasonable value for a good barrier.

X1.1.2 In these units the permeability of NBS Standard Reference Material to oxygen gas is approximately 7.8 amol/m·s·Pa.

X1.2 Table X1.1, Table X1.2, and Table X1.3 give conversion factors for converting measured permeabilities, permeances, and transmission rates between various unit systems. Considerable care must be taken in dealing with powers of 10 because transport coefficients can vary by as much as a factor of 10^{5} from one polymer to another.

X1.3 The major advantage of this proposed system of units over existing ones is that it essentially eliminates opportunities for incorrect dimensional calculations. It also affords a good basis for making comparisons when permeating substances are liquids or do not obey the ideal gas law. Modern coulometric and chromatographic detection systems are most readily calibrated in molar terms.

X1.4 In order to use the tables, proceed as follows: (*1*) label the measured quantity (G, P, or P') by X_i, where i is the number of the row in the table corresponding to the system of units in

TABLE X1.2 Factors for Converting Permeances from One System of Units to Another

Note 1—See X1.4 for instructions on using this table.

Multiply ↓ \ To Obtain →	SI $mol/m^2 \cdot s \cdot Pa$	Barrer-type $\frac{10^{-10}\ mL\ (STP)}{cm^2 \cdot s \cdot cm\ Hg}$	Metric $\frac{mL\ (STP)}{m^2 \cdot d \cdot atm}$	Inch-pound $\frac{mL\ (STP)}{100\ in.^2 \cdot d \cdot atm}$
SI $mol/m^2 \cdot s \cdot Pa$	1	29.88×10^{-3}	0.19621	12.659×10^{-3}
Barrer-type $\frac{10^{-10}\ mL\ (STP)}{cm^2 \cdot s \cdot cm\ Hg}$	33.49	1	6.571	0.4240
Metric $\frac{mL\ (STP)}{m^2 \cdot d \cdot atm}$	5.097	0.15218	1	64.52×10^{-3}
Inch-pound $\frac{mL\ (STP)}{100\ in.^2 \cdot d \cdot atm}$	79.00	2.359	15.50	1

TABLE X1.3 Factors for Converting Gas Transmission Rates from One System of Units to Another

Note 1—See X1.4 for instructions on using this table.

Multiply ↓ \ To Obtain →	SI $mol/m^2 \cdot s$	Barrer-type $\frac{10^{-10}\ mL\ (STP)}{cm^2 \cdot s}$	Metric $\frac{mL\ (STP)}{m^2 \cdot d}$	Inch-pound $\frac{mL\ (STP)}{100\ in.^2 \cdot d}$
SI $mol/m^2 \cdot s$	1	22.414	1.9355	0.12494
Barrer-type $\frac{10^{-10}\ mL\ (STP)}{cm^2 \cdot s}$	44.62×10^{-3}	1	86.40×10^{-3}	5.574×10^{-3}
Metric $\frac{mL\ (STP)}{m^2 \cdot d}$	0.5164	11.574	1	64.52×10^{-3}
Inch-pound $\frac{mL\ (STP)}{100\ in.^2 \cdot d}$	8.004	179.40	15.50	1

which X was measured, (*2*) extract Y_{ij} from the appropriate table as the value at the intersection of the *i*th row and the *j*th column where *j* labels the column corresponding to the units in which X is to be expressed after conversion, and (*3*) obtain X_j from $X_j = X_i Y_{ij}$.

X2. ADDITIONAL CONVERSION FACTORS FOR VARIOUS PERMEABILITY UNITS

Note X2.1—To obtain unit in left-hand vertical column multiply unit in top horizontal column by figure opposite both units.

To Obtain \ Multiply	$\frac{cm^3 \cdot cm}{cm^2 \cdot s \cdot cm\ Hg}$	$\frac{cm^3 \cdot mil}{m^2 \cdot 24\ h \cdot atm}$	$\frac{cm^3 \cdot mil}{100\ in^2 \cdot 24\ h \cdot atm}$	$\frac{cm^3 \cdot mm}{m^2 \cdot 24\ h \cdot atm}$
$\frac{cm^3 \cdot cm}{cm^2 \cdot s \cdot cm\ Hg}$	1.00	3.87×10^{-14}	6.00×10^{-13}	1.52×10^{-17}
$\frac{cm^3 \cdot mil}{m^2 \cdot 24\ h \cdot atm}$	2.58×10^{13}	1.00	15.5	39.4
$\frac{cm^3 \cdot mil}{100\ in^2 \cdot 24\ h \cdot atm}$	1.67×10^{12}	6.45×10^{-2}	1.00	2.54
$\frac{cm^3 \cdot mm}{m^2 \cdot 24\ h \cdot atm}$	6.57×10^{11}	2.54×10^{-2}	0.394	1.00

X3. DERIVATION OF EQUATION FOR PERMEANCE USING THE MANOMETRIC GAS CELL

X3.1 The following symbols are used in the derivations of the equation used in Section 13 to calculate the permeance.

a = area of capillary $\overline{AB}$, mm^2,
A = area of transmission, mm^2,
dP = dh = differential pressure change of transmitted gas, mm Hg,
dV = $a d\ h$ = differential volume change of transmitted gas, µL,
h_o = initial height of mercury in the capillary leg at the start of the actual transmission run with steady-state conditions attained, mm,
h = height of mercury in cell capillary leg at any given time, mm,
h_B = maximum height of mercury in the cell manometer leg from the datum plane to upper calibration line B, mm,
h_L = height of mercury in cell reservoir leg from datum plane to top of mercury meniscus, mm,
n_o = quantity of gas transmitted at the start of the actual transmission run after steady-state conditions have been attained, mol,
n = quantity of gas transmitted, at any given time, mol,
P = permeance of the film, the SI unit of permeance is 1 mol ($m^2 \cdot s \cdot Pa$),
p_t = $(h_L - h)$ = pressure of transmitted gas at time t, mm Hg,
p_o = pressure of gas to be transmitted, mm Hg,
R = universal gas constant, 8.314×10^{-3}, L·Pa/(mol·K),
t = time, h,
t_o = time at start of the actual transmission run after steady-state conditions have been attained, h,
T = absolute temperature, K,
V_{BC} = volume from B to C, µL,
V_{CD} = void volume of depression, µL,
V_f = $(V_{BC} + V_{CD})$, µL, and
V_t = $[V_f + a(h_B - h)]$ = volume of transmitted gas, µL at time t.

X3.2 The number of mols of gas transmitted, n, may be determined from the ideal gas law (which is valid at the low pressure involved) as follows:

$$n = p_t V_t / RT \tag{X3.1}$$

For differential changes in p_t and V_t Eq X3.1 can be differentiated as follows:

$$nRT = p_t V_t$$
$$RTdn = d(p_t V_t) \tag{X3.2}$$
$$RTdn = p_t dV + V_t dp \text{ (Note X3.1)}$$

NOTE X3.1—This differentiation is the form $d(uv) = udv + vd\ u$. Substitute into Eq X3.2 the values for $d\ V$ and dP given in the definition of symbols.

$$RTdn = -p_t a dh - V_t dh, \text{ or} \tag{X3.3}$$
$$dn = (-ap_t dh - V_t dh)/RT$$

By definition,

$$p_t = (h_L - h), \text{ and}$$
$$V_t = [V_f + a(= h_B - h)]$$

Therefore, substituting into Eq X3.3 and collecting terms,

$$dn = [-a(h_L - h)dh - [V_f + a(h_B - h)]\ dh]/RT$$
$$dn = [(-ah_L + ah)dh - (V_f + ah_B - ah)dh]/RT \tag{X3.4}$$
$$dn = [dh(-ah_L + ah - V_f - ah_B + ah)]/RT$$
$$dn = [dh(2ah - a(h_L + h_B) - V_f)]/RT$$

X3.3 The permeance (P) expressed in $cm^3/(m^2 \cdot 24\ h \cdot atm)$ can be obtained by integrating Eq X3.4 and using the following conversion factors:

$$\int_{t_o}^{t} P\,dt = \int_{n_o}^{n} dn\ \text{mol} \times \frac{24}{24/t}$$
$$\times\ 22.415 \frac{cm^3}{mol} \times \frac{760 \frac{mm}{atm} \times 10\,000 \frac{cm^2}{m^2}}{P_a(mm) \times A\ (mm^2)}$$

The term P_a, which is the driving force, and A, the area of transmission, must be included in this equation in order to

obtain the permeance in the desired units. Collecting terms and substituting for the following:

$$P_e = (p_u - p_l)$$

$$\int_o^t dt = \int_{h_o}^{h} \frac{dv}{(p_u - p_l)A}(24 \times 22\ 415 \times 760 \times 10\ 000)$$

or substituting for dv from Eq X3.4 and $p_l = (h_L - h)$:

$$\int_o^t P\,dt = \frac{1}{ART}\int_{h_o}^{h}\frac{[2ah - a(h_L + h_a) - V_f]dh}{p_u - (h_L - h)} \quad \text{(X3.5)}$$

X3.4 To find an expression that applies over an extended period of time, Eq X3.5 must be integrated as described by Evans.[12]

$$\int_o^t P\ dt = \frac{1}{ART}\left[2a\int_{h_o}^{h}\frac{h\,dh}{p_u a - (h_L - h)} - a(h_L + h_a)\right.$$
$$\left.\int_{h_o}^{h}\frac{dh}{h_o p_u - (h_L - h)} - V_f\int_{h_o}^{h}\frac{dh}{h_o p_u - (h_L - h)}\right]$$

The first term can be integrated by parts or found in standard integration tables. The remaining terms are straightforward. The following result is obtained for steady-state gas transmission:

$$P(t - t_o) = \frac{-1}{ART}\left\{2a(h_o - h) + [V_f + a(2p_u - h + h_a)]\ln\left[\frac{p_u - (h_L - h)}{p_u - (h_L - h_o)}\right]\right\}$$

This can be written in the form:

$$P(t - t_o) = \frac{-1}{ART}\left\{2a(h_o - h) + [V_f + a(2p_u - h_L + h_a)]\ln\left[1 - \frac{(h_o - h)}{S}\right]\right\} \quad \text{(X3.6)}$$

where:

$$S = p_u - (h_L - h_a).$$

Eq X3.6 is the exact relationship for calculating steady-state permeance over an extended period of time.

X3.5 If we assume that time-lag effects are not important, Eq X3.6 takes proper account of the fact that the driving force for permeation is decreasing continuously during a manometric permeation experiment. If one assumes that the rate of pressure rise is constant with time in the downstream cell volume, thereby failing to correct for the decrease in driving force, the resulting permeance values are too low. If we denote the permeance value obtained from uncorrected data by P', we can say that the true permeance, P, is given by

$$P = \frac{P'}{1 - \epsilon}$$

X3.6 It can be demonstrated, by computer simulation or by series expansion methods, that

$$\epsilon = (h_L - h_f)\left[\frac{a}{V_f + a(h_a - h_L)} + \frac{1}{2p_u}\right] \text{ for } \epsilon < 0.3$$

where h_f is the depression of the mercury column at the end of the experiment. Evans has demonstrated[12] that ϵ can become as large as 0.2 in realistic situations.

X3.7 If the function $g(h)$, as given by the right-hand side of Eq X3.6, exhibits curvature when plotted as a function of time one or more of the assumptions used in deriving Eq X3.6 is not being met, and further studies are needed to establish the causes of this behavior.

X3.7.1 Possible sources of error include *(1)* failure to achieve steady-state conditions, *(2)* the presence of time-lag effects, and *(3)* viscoelastic processes.

[12] Evans, R. E. "The Calculation of Gas Transmission Rates Using Manometric Methods", *Journal of Testing and Evaluation*, ASTM, Vol 2, No. 6, pp. 529–532.